The Finnish Environment 644

INTERNATIONAL COOPERATION

Kimmo Ruosteenoja, Timothy R. Carter,
Kirsti Jylhä and Heikki Tuomenvirta

Future climate in world regions: an intercomparison of model-based projections for the new IPCC emissions scenarios

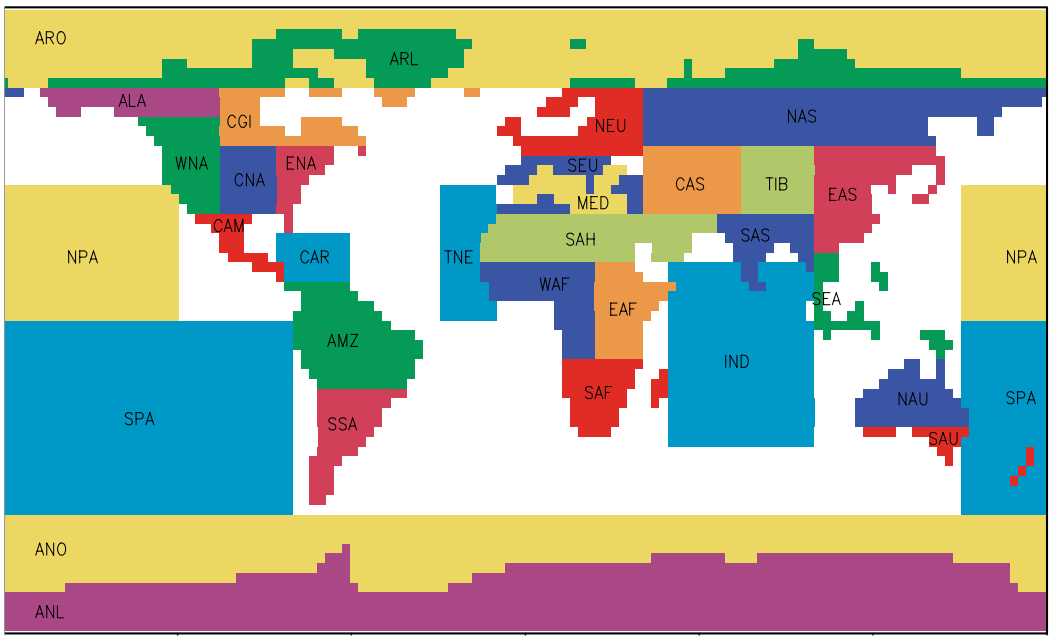

Kimmo Ruosteenoja[1], Timothy R. Carter[2], Kirsti Jylhä[1] and Heikki Tuomenvirta[1]

Future climate in world regions: an intercomparison of model-based projections for the new IPCC emissions scenarios

[1] Finnish Meteorological Institute, Box 503, FIN-00101 Helsinki, Finland
[2] Finnish Environment Institute, Box 140, FIN-00251 Helsinki, Finland
*Corresponding author email:tim.carter@ymparisto.fi

HELSINKI 2003

FINNISH ENVIRONMENT INSTITUTE

Painotuote

ISBN 952-11-1463-0 (nid.)
ISBN 952-11-1464-9 (PDF)
ISSN 1238-7312

Page layout: DTPage Oy
Printer: Tummavuoren Kirjapaino, Vantaa 2003
Helsinki 2003
Finland

Preface

In 2000, the Intergovernmental Panel for Climate Change (IPCC) released a new set of scenarios describing projected emissions of greenhouse gases and aerosols into the global atmosphere during the 21st century. The estimates span a range of emissions arising from different assumptions of socio-economic and technological development up to 2100.

Changes in atmospheric composition caused by these emissions alter the radiative balance of the atmosphere and hence affect the global climate. Preliminary estimates of the implications of these scenarios for climate in 32 world regions were presented in a previous report (The Finnish Environment 433). Those estimates were extrapolated from existing climate model simulations that assumed earlier IPCC emissions scenarios.

This report presents an intercomparison of climate changes projected for the same 32 regions, but this time using new climate model results from simulations that are based directly on the latest IPCC emissions scenarios. Results are presented for seasonal temperature and precipitation changes between 1961–1990 and three time periods in the future centred on the 2020s, 2050s and 2080s.

In common with the previous report, a major objective is to provide quantitative guidance on the range of uncertainty in future regional climate changes. The report seeks to identify regions showing apparent agreement in the direction of future climate change as well as regions where projected changes are more uncertain. Information on the statistical significance of projected changes in relation to modelled natural climate variability is also provided.

The report may be of assistance to researchers wishing to select climate scenarios for assessing the potential impacts of climate change. It may also provide useful background information for evaluating the climate scenarios already applied in published impact studies, especially in the context of the IPCC Fourth Assessment Report (AR4).

We are grateful to Dr. David Viner at the University of East Anglia and Drs. Francis Zwiers and Slava Kharin at the Canadian Centre for Climate Modelling and Analysis for providing data from AOGCM control simulations. Valuable comments were received from the following: E. Barrow, M. Hulme, L. Mearns, J. Mitchell, T. Mitchell, C. Rosenzweig, R. Stouffer and T. Wigley. Financial assistance for this work was provided by the Ministry for Foreign Affairs of Finland, the Government of Canada and the Intergovernmental Panel for Climate Change Trust Fund.

Contents

Introduction

In its Third Assessment Report, the Intergovernmental Panel on Climate Change concluded that the global average surface air temperature has increased by 0.6 ± 0.2 °C during the 20th century, which is likely to be the largest rise of any century during the past 1000 years (IPCC, 2001a). Moreover, it presented convincing new evidence that most of the observed warming over the last 50 years is attributable to increases in atmospheric greenhouse gas concentrations.

Without concerted actions to cut emissions, global climate change is expected to accelerate in the future. The IPCC presented climate change projections based on the new IPCC emissions scenarios (Nakićenović et al., 2000 – see Box on the next page), which assume no explicit climate policies. Global mean surface temperature is projected to increase by 1.4 to 5.8 °C between 1990 and 2100, which is a much more rapid rate of warming than during the 20th century and very likely to be unprecedented in at least the last 10,000 years.

The IPCC concluded that recent regional changes in temperature have had discernible impacts on the natural environment (e.g., shrinkage of glaciers, thawing of permafrost, and earlier flowering of trees and egg-laying in birds). There is also emerging evidence that some social and economic systems have been affected by a recent increased frequency of floods and droughts in some areas (IPCC, 2001b). With the prospect of accelerating climate change in the future, impacts on natural and human systems are likely to become profound. In order to improve our understanding of the likely regional distribution of these impacts, information on projected future climate is therefore needed at a regional scale.

The tools most commonly adopted for projecting future climate are coupled atmosphere-ocean general circulation models (AOGCMs). These numerical models provide a comprehensive three-dimensional representation of the climate system, describing the main dynamical and physical processes, their interactions and feedbacks. They can generate regional estimates of climate in response to given changes in greenhouse gas and aerosol concentrations; an increase of greenhouse gases tends to warm the Earth, while most aerosols have a cooling effect.

The ability of the models to simulate climate is best at large horizontal scales and is severely restricted as the scale is decreased. Therefore, any intercomparison of regional climate change from such models is likely to be most meaningful when conducted for sub-continental scale (10^6–10^8 km^2) regions. This is the scale of analysis adopted in this report. An equivalent regional subdivision has been employed by Giorgi et al. (2001) and Giorgi and Mearns (2002).

At smaller spatial scales (i.e., the scale of many national or local impact studies), AOGCMs may still provide useful information on climate change. However, they are not capable of capturing many features of changes in local climate, such as storms, orographic rainfall and heavy precipitation events. Other techniques are commonly adopted to obtain such high resolution information, including dynamical and statistical downscaling approaches (Giorgi et al., 2001).

There are two key sources of uncertainty in projections of future regional climate that should be considered in determining the impacts of climate change:

1. Uncertainties in future emissions, which affect the radiative forcing[1] of the climate system. Climate modellers have recently begun to apply a number of different emissions scenarios reported in the IPCC Special Report on Emissions Scenarios (SRES, Nakićenović et al., 2000, see box) to represent the emission-related range of uncertainty.

The Special Report on Emissions Scenarios

The Special Report on Emissions Scenarios (SRES) was formally approved by the IPCC in April 2000 (Nakićenović et al., 2000). However, a preliminary set of four "marker" emissions scenarios and their associated socio-economic driving forces were already available in 1998, to provide inputs for AOGCM simulations. It is these scenarios (labelled SRES98), which in most respects differ little from the final versions, that have been used in the AOGCM outputs presented here. The SRES scenarios were constructed quite differently from the previous emissions scenarios developed by the IPCC (the IS92 scenarios – Leggett et al., 1992). They are reference scenarios for the 21st century that seek specifically to exclude the effects of climate change and climate policies on society and the economy ("non-intervention"). They are based on a set of four narrative storylines labelled A1, A2, B1 and B2. The storylines combine two sets of divergent tendencies: one set varying its emphasis between strong economic development and strong environmental protection, the other set between increasing globalization and increasing regionalization (Nakićenović et al., 2000). They are briefly described as follows:

A1: A future world of very rapid economic growth, low population growth and rapid introduction of new and more efficient technology. Major underlying themes are economic and cultural convergence and capacity building, with a substantial reduction in regional differences in per capita income. In this world, people pursue personal wealth rather than environmental quality.

A2: A differentiated world. The underlying theme is that of strengthening regional cultural identities, with an emphasis on family values and local traditions, high population growth, and less concern for rapid economic development.

B1: A convergent world with rapid change in economic structures, "dematerialization" and introduction of clean technologies. The emphasis is on global solutions to achieving environmental and social sustainability, including concerted efforts for rapid technology development, dematerialization of the economy, and improving equity.

B2: A world in which the emphasis is on local solutions to achieving economic, social, and environmental sustainability. It is a heterogeneous world with less rapid, and more diverse technological change but a strong emphasis on community initiative and social innovation to find local, rather than global solutions.

The storylines were quantified to provide families of scenarios for each storyline. In all 40 scenarios were quantified, six of which are used as illustrative scenarios by the IPCC. Three alternative technological futures are used as illustrations for the A1 storyline: A1FI (fossil intensive), A1T (predominantly non-fossil) and A1B (balanced across energy sources). One illustrative scenario represents each of the A2, B1 and B2 storylines. In descending order of radiative forcing by 2100, the illustrative scenarios rank: A1FI, A2, A1B, B2, A1T, B1.

Although these are all non-intervention scenarios, it can be difficult to distinguish between scenarios that envisage stringent environmental policies (e.g. B1) and scenarios that include direct climate policies (e.g. CO_2 stabilization scenarios). Emissions scenarios leading to stabilization and their climatic consequences are discussed in more detail by Morita et al. (2001), Cubasch et al. (2001) and Swart et al. (2002), but are not considered in this report.

[1] Radiative forcing is the aggregate effect of greenhouse gas and aerosol concentrations on the radiation balance of the Earth.

2. Uncertainties in the global mean climate sensitivity and in the regional pattern of climate change simulated by climate models. Due to the different ways in which AOGCMs represent physical processes and feedbacks in the climate system, each climate model simulates a different global mean and regional pattern of change in climatic variables such as temperature, precipitation, cloudiness and atmospheric circulation.

An additional source of uncertainty relates to the natural variability of climate. Part of this variability is unforced, due to internal perturbations in the climate system. Another part is due to external forcing from natural phenomena such as variations in solar activity or volcanic eruptions.

Climate scenarios have been applied in impact and adaptation assessments conducted in all parts of the world during the past few decades. However, the selection of regional climate scenarios has often been arbitrary, and there is little consistency in the scenarios applied in various studies. Moreover, the scenarios rarely capture the entire range of uncertainties in projections (IPCC, 2001b). These inadequacies in scenario selection can hamper the intercomparison and interpretation of results of impact studies.

The work reported here builds upon, and largely supersedes, an earlier intercomparison study of AOGCM climate change patterns for the same regional scale (Carter et al., 2000). That study was based on AOGCM simulations assuming the IS92a emissions scenario, but pattern-scaled to represent a preliminary set of SRES emissions scenarios. That report also contained information on the SRES scenarios themselves, including the demographic and economic driving factors assumed in the scenarios, directly comparable atmospheric composition scenarios, and global sea-level rise projections, as well as information on past regional temperature and precipitation trends. In assessing the impact of future climate change, in addition to climate scenarios information is also required about other concurrent environmental and socio-economic changes (Carter et al., 2001).

The present study also complements work by Giorgi et al. (2001), who presented AOGCM estimates of temperature and precipitation change for the SRES A2 and B2 scenarios over 23 continental land areas (similar to those adopted in this report) for the December-February and June-August seasons. Giorgi and Mearns (2002) extended that analysis by introducing a method to calculate sub-continental scale climate change as a weighted average of changes simulated by various models. These studies did not attempt to embrace the wider range of SRES emissions scenarios using pattern-scaling techniques.

This report provides a comprehensive intercomparison of recent, readily available AOGCM simulations of future climate for different sub-continental regions of the world. Such a large-scale intercomparison may offer useful guidance on the selection of a representative range of climate scenarios for regional impact studies. This procedure often precedes a further "regionalization" exercise to obtain higher resolution scenarios at the scale of the impact study. The report does not pass judgment on the merits of alternative model projections; rather it presents a selection of available projections in a form that may assist impact analysts in making informed selections of their own.

The main scope of this study is the following:

- Outputs from seven different AOGCMs are represented (see section 2), all of which are available for downloading from the IPCC Data Distribution Centre (DDC).
- AOGCM simulations are based on the SRES emissions scenarios (in most cases, these are the A2 and B2 emissions scenarios, see box). Since simulations corresponding to the highest (A1FI) and lowest (B1) SRES emissions

scenarios have been conducted with few AOGCMs, most estimates for these scenarios are obtained by "pattern-scaling" the available AOGCM outputs. The version of the pattern-scaling technique employed in this study and its applicability are discussed in section 3.2.

- Projections of future changes in surface air temperature and precipitation are given as averages over 32 large world regions (see section 3).
- Climate changes, averaged over four seasons (December-February, March-May, June-August and September-November), are presented for three 30-year time slices in the future, centred on the 2020s, 2050s and 2080s, each relative to the 1961–1990 climatological baseline period.
- Climate changes are compared with model estimates of inter-tridecadal natural variability, based on long AOGCM simulations performed without increased radiative forcing (section 3.1).

The information on changes in temperature and precipitation for each season, time slice and region is presented in the form of scatter diagrams. These diagrams are designed to provide a consistent overview of the range of AOGCM projections in different regions of the world. Analysts in a given region can use this information to select scenarios that suit their particular needs. They can also compare these results with other sub-continental scale projections obtained from AOGCMs (e.g., earlier model runs), from high resolution models or using statistical methods. Guidance for the use of the scatter diagrams is given in Appendix A and the complete set of diagrams is presented in Appendix B.

The following section describes the AOGCM outputs used in the analysis and gives a few examples of how the model output compares with observed climate data. Section 3 outlines the techniques applied to construct the scatter diagrams, including estimation of natural climate variability and a description of the pattern-scaling method. The concluding section discusses the results and their interpretation, including uncertainties captured or m̨isse̩d and signal-to-noise issues. There is also discussion on the applicability of the pattern-scaling method.

2 Climate model data

In this study, we analyzed 17 SRES scenario runs performed with seven coupled atmosphere-ocean GCMs. Only data available from the IPCC Data Distribution Centre (DDC) were used (http://ipcc-ddc.cru.uea.ac.uk/dkrz/dkrz_index.html; this site contains links to brief model descriptions). All models supplying data fulfil a minimum set of four criteria required for inclusion in the DDC (Parry, 2002), such that they are full three-dimensional coupled AOGCMs, are documented in the peer reviewed literature, have performed a multi-century control run (for stability reasons) and have participated in CMIP2 (second Coupled Model Intercomparison Project). If there were two models or model versions from the same research centre, only the most recent model was included in this study.

The main properties of the models are summarized in Table 1. For more detailed information and references to model documentation (e.g., resolution in the oceanic component of the model), the reader is referred to McAvaney et al. (2001), especially Table 8.1 and related discussion. As a measure of the sensitivity of the model to radiative forcing, Table 1 gives the global mean temperature response to the A2 forcing scenario for each model. We find that the CCSR/NIES model produces a significantly larger and the NCAR DOE PCM a much smaller temperature response than the remaining models. This is in good agreement with the model climate sensitivities reported in Table 9.1 of Cubasch et al. (2001).

Table 1. Coupled AOGCMs analyzed in the present report. Column 1 gives the model acronym and column 2 the country where the model was developed. For horizontal resolution, truncation in spherical harmonics space (TRUNC.) and the grid distance in grid-point space (GRID) as well as the total number of points in the horizontal grid (N) are given. HadCM3 is a grid point model, and therefore spectral truncation cannot be defined for that model. Vertical resolution is expressed by the number of model levels (L). The next column tells whether flux adjustment is employed. ΔT_{glob} is the simulated change of the global mean temperature from 1961–1990 to 2070–2099 as a response to the A2 forcing scenario.

MODEL	COUNTRY	TRUNC.	GRID	N	L	ADJ.	ΔT_{glob}
CCSR/NIES	Japan	T21	5.6 × 5.6°	2048	20	Yes	4.4°C
CGCM2	Canada	T32	3.8 × 3.8°	4608	10	Yes	3.5°C
CSIRO Mk2	Australia	R21	3.2 × 5.6°	3584	9	Yes	3.4°C
ECHAM4/OPYC3	Germany	T42	2.8 × 2.8°	8192	19	Yes	3.3°C
GFDL R30	U.S.A.	R30	2.2 × 3.8°	7680	14	Yes	3.1°C
HadCM3	United Kingdom	-	2.5 × 3.8°	7008	19	No	3.2°C
NCAR DOE PCM	U.S.A.	T42	2.8 × 2.8°	8192	18	No	2.4°C

There are marked variations in horizontal resolution among the models (Table 1); models with the highest horizontal resolution have four times the number of grid points compared to the lowest-resolution model. The number of model levels in the vertical varies between 9 and 20.

All models except for two employ flux adjustment. This implies that heat and freshwater are artificially added to or removed from those areas in which unrealistic sea surface temperature or salinity is produced by the model. Flux adjustment improves the simulation of present-day climate, but might bring about problems in the simulation of climate change, for example, producing spurious multiple equilibrium states of the ocean circulation. Conversely, without flux adjustment model projections may include a component of climate drift in addition to the response to anthropogenic forcing.

For all models in Table 1, we analyzed the response to the middle forcing scenarios A2 and B2. The low-forcing scenario B1 was available from the DDC for the CCSR/NIES and CSIRO Mk2 models and the high forcing scenario A1FI for the CCSR/NIES model only. At the time of the study, no ensemble runs for any of these simulations were available.

Most of the AOGCM datasets analyzed included monthly mean surface air temperatures and precipitation totals for the period beginning in 1960 or 1961 and ending in 2099. However, in some simulations the few first decades of this period were missing. As advised by the contact persons in the corresponding modelling centres (Hans Luthard and Jerry Meehl, pers. comm.), in those cases the time series were completed by utilizing previous simulations performed with the same model. This is justified by the fact that in all the simulations available in the IPCC DDC, radiative forcing up to 1990 was derived from historical emission and concentration data.

It is not the purpose of the present work to rank the quality of the climate models used. However, for a deeper understanding of the results presented later in this report, it is beneficial for the reader to have some idea of the accuracy at which the models are able to simulate present climate. Figure 1 gives two examples of this. In general, models are more successful at simulating the annual cycle of present-day temperatures than precipitation. For example, the course of simulated mean temperature in Northern Europe (Fig. 1a) is qualitatively correct. In winter, three of the seven models have a cold bias of 2 to 5°C. In summer, some models slightly overestimate, others underestimate the temperature, the deviation being at most ~ 5°C.

In most cases, simulations for precipitation are far less successful than those for temperature. For instance, the annual course of monthly precipitation in Central America is given in Fig. 1b. In the dry winter season all models but one severely overestimate precipitation. In the wet summer season there are three models with excessive and another three with deficient rain, one of the models giving estimates close to observed precipitation. Admittedly, in all models the division of the year into dry and wet seasons is qualitatively correct, but none is able to simulate the course of precipitation with quantitative accuracy throughout the year.

There are two factors that must be borne in mind in comparing the modelled present-day climate with observations. Firstly, there is natural interdecadal variability both in the models and in the real world. This variability is stronger for precipitation than for temperature, and may partly explain the model vs. observed differences in Fig. 1b. Secondly, due to the low horizontal resolution of the models, orography is represented fairly crudely. Thus the area-mean elevation in a model may deviate from the real elevation, biasing the temperature. Precipitation is sensitive to small-scale orographic features, which are poorly represented in present-day models.

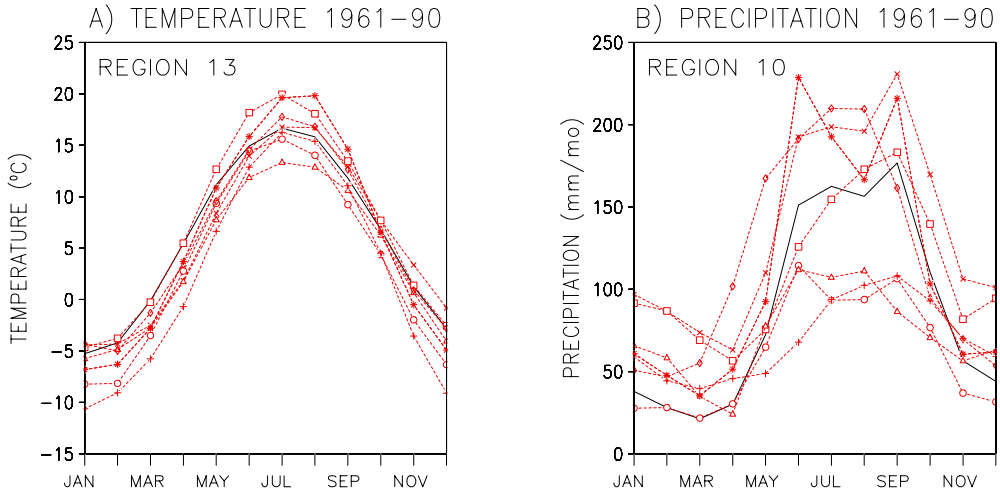

Fig. 1. Annual course of a) surface air temperature in Northern Europe and b) precipitation in Central America during 1961–1990. Red dashed curves depict the model simulation: CCSR/NIES (pluses), CSIRO Mk2 (squares), CGCM2 (crosses), ECHAM4/OPYC3 (diamonds) GFDL-R30 (snowflakes), HadCM3 (circles) and NCAR DOE PCM (triangles). The solid black curve depicts area means inferred from observations. Observational data were obtained from the IPCC DDC (http://ipcc-ddc.cru.uea.ac.uk/cru_data/datadownload/download_index.html) — for documentation, see New et al. (1999). The area averages were calculated over land areas defined for each region in Table 2.

3 Construction of the scatter diagrams

An effective method of condensing the model-derived information on sub-continental scale climate change is to represent it as spatial averages over a number of discrete world regions. The 32 regions employed in this study are defined in Table 2, and the subdivision is illustrated in Fig. 2 for one model grid. The regions cover all land areas of the Earth and those ocean areas where most of the populated islands are located. In addition, polar ocean areas, where several models simulate significant climate change, are included in the subdivision. Essentially the same subdivision of the world has previously been used by Carter et al. (2000), and a similar classification by Giorgi and Francisco (2000) for continental regions. Henceforth, all the results presented are area-weighted spatial means over the land or ocean grid boxes within the borders of a given region. For precipitation, regionally averaged changes are expressed as percentages relative to the mean for the baseline period.

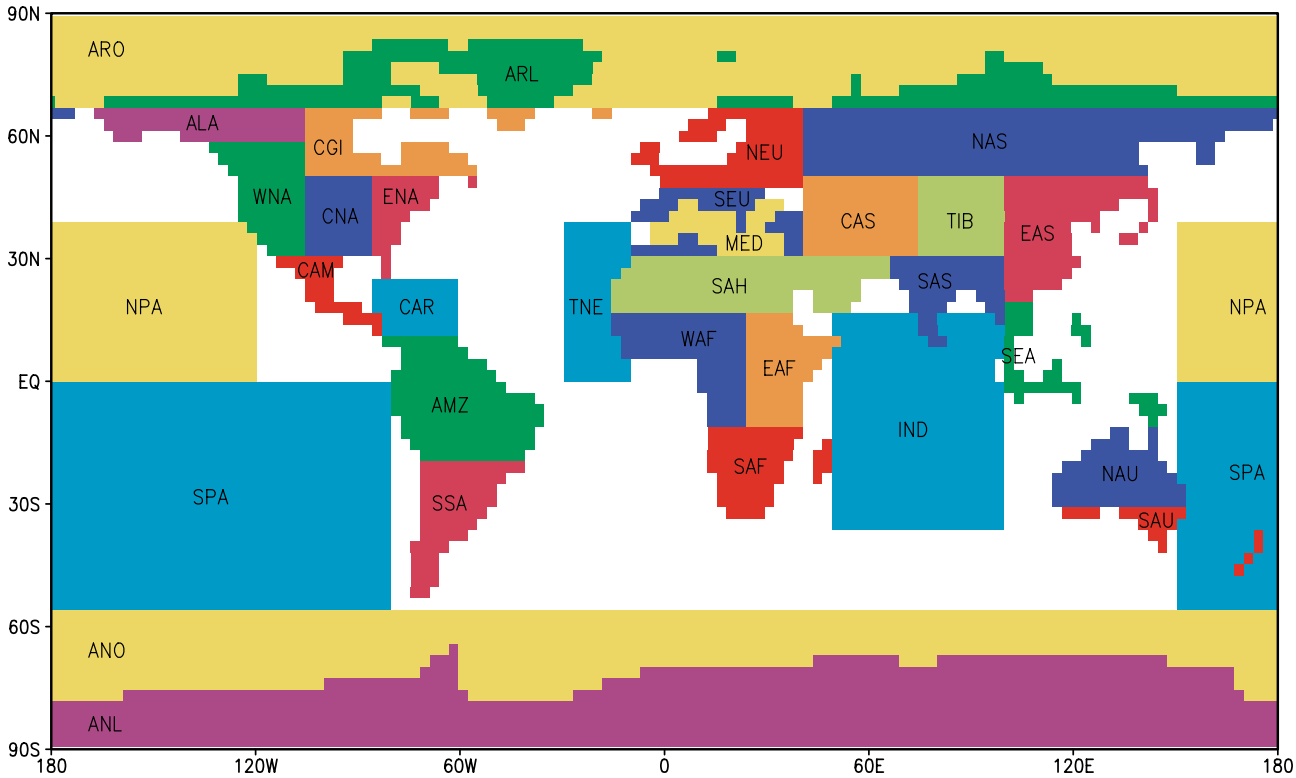

Fig. 2. The 32 world regions defined in Table 2 shown on the ECHAM4 model grid (resolution 2.8° × 2.8°).

Table 2. Latitude and longitude limits of the 32 world regions employed in reporting sub-continental climate change. The first four columns of the table state the number, name and code of the region and whether the region consists of land (L) or ocean (O). The four remaining columns define the southern (S), northern (N), western (W) and eastern (E) boundary of the region in degrees of latitude/longitude. Region 6 (CGI) consists of Eastern Canada, Southern Greenland and Iceland.

	Subregion	Code	L/O	S Lat	N Lat	W Lon	E Lon
1	Arctic land	ARL	L	67.5	90.0	-180.0	180.0
2	Arctic ocean	ARO	O	67.5	90.0	-180.0	180.0
3	Antarctic land	ANL	L	-90.0	-55.0	-180.0	180.0
4	Antarctic ocean	ANO	O	-90.0	-55.0	-180.0	180.0
5	Alaska, NW Canada	ALA	L	57.5	67.5	-170.0	-105.0
6	E Canada etc.	CGI	L	50.0	67.5	-105.0	-10.0
7	Western N America	WNA	L	30.0	57.5	-135.0	-105.0
8	Central N America	CNA	L	30.0	50.0	-105.0	-85.0
9	Eastern N America	ENA	L	25.0	50.0	-85.0	-50.0
10	Central America	CAM	L	10.0	30.0	-115.0	-82.5
11	Amazonia	AMZ	L	-20.0	10.0	-82.5	-35.0
12	Southern S America	SSA	L	-55.0	-20.0	-75.0	-40.0
13	Northern Europe	NEU	L	47.5	67.5	-10.0	40.0
14	S Europe, N Africa	SEU	L	30.0	47.5	-10.0	40.0
15	Sahara	SAH	L	17.5	30.0	-20.0	65.0
16	Western Africa	WAF	L	-10.0	17.5	-20.0	25.0
17	Eastern Africa	EAF	L	-10.0	17.5	25.0	55.0
18	Southern Africa	SAF	L	-35.0	-10.0	10.0	50.0
19	Northern Asia	NAS	L	50.0	67.5	40.0	-170.0
20	Central Asia	CAS	L	30.0	50.0	40.0	75.0
21	Tibetan Plateau	TIB	L	30.0	50.0	75.0	100.0
22	Eastern Asia	EAS	L	20.0	50.0	100.0	150.0
23	Southern Asia	SAS	L	5.0	30.0	65.0	100.0
24	Southeast Asia	SEA	L	-10.0	20.0	100.0	150.0
25	Northern Australia	NAU	L	-30.0	-10.0	110.0	155.0
26	Southern Australia	SAU	L	-47.5	-30.0	110.0	180.0
27	Mediterranean	MED	O	30.0	45.0	-5.0	35.0
28	Caribbean	CAR	O	10.0	25.0	-85.0	-60.0
29	Tropic. NE Atlantic	TNE	O	0.0	40.0	-30.0	-10.0
30	Northern Pacific	NPA	O	0.0	40.0	150.0	-120.0
31	Indian Ocean	IND	O	-35.0	17.5	50.0	100.0
32	Southern Pacific	SPA	O	-55.0	0.0	150.0	-80.0

Figure 3 illustrates how the greenhouse gas and aerosol forced changes in region-averaged climate variables are calculated. The spatial mean surface air temperature varies from year to year, but besides these variations there is a distinct warming trend. For the baseline period 1961–1990, the mean temperature for region 22 inferred from this time series is +20.2 °C. For the periods 2010–2039, 2040–2069 and 2070–2099 the corresponding mean temperatures are +21.8 °C, +23.2 °C and +25.6 °C, implying a temperature rise of 1.6 °C, 3.0 °C and 5.4 °C, respectively. Accordingly, the temperature rise in this region exceeds the corresponding global mean (see Table 1). Such simulated changes in temperature and precipitation for all regions are depicted in the form of scatter diagrams in Appendix B. Of course, in utilizing these regionally-averaged results one must realize that changes can vary quite significantly within individual regions.

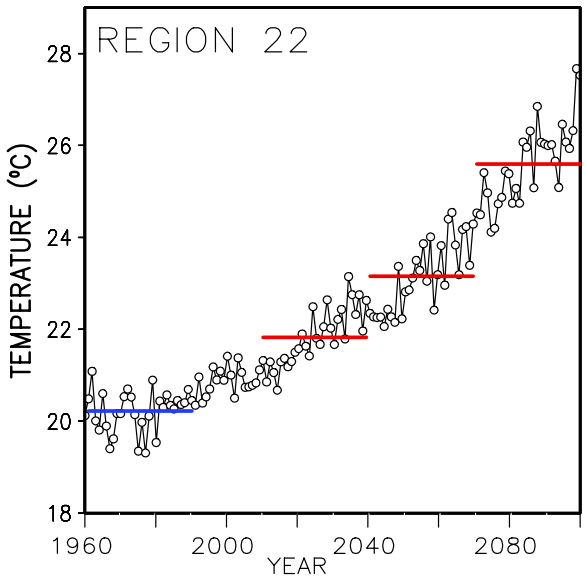

Fig. 3. Time series of the spatial mean surface air temperature in region 22 (Eastern Asia) in June-August over the period 1960–2099 (black curve with open circles). Values are from the HadCM3 simulation forced by the SRES A2 scenario. The blue line shows the time mean of the series for years 1961–1990, the red lines indicate means for periods 2010–2039, 2040–2069 and 2070–2099.

Due to the varied horizontal grid resolution in various models, the location of coastlines also varies among the models. Consequently, the actual borders between the regions are model-dependent. The difference is generally non-systematic and at the most ~ 2° latitude/longitude. An exception is NCAR DOE PCM, in which the land-sea mask differs notably from that in other models, the coastlines being located systematically much further offshore. Therefore, in this model land regions are wider and ocean regions smaller than in other models, typically by a few hundred kilometres. The difference manifests itself most dramatically in the Mediterranean region, which in the ECHAM4 grid (Fig. 2) covers 45 oceanic grid boxes but in applying the NCAR land-sea mask covers only 6 boxes. These figures are directly comparable, since in both models the sizes of the grid boxes are exactly the same (see Table 1).

In order to assess the influence of the divergent definition of regions, we calculated the region-averaged climate changes derived from the NCAR model output by applying the subdivision based on both the NCAR and on the ECHAM4

land-sea masks. In most cases, the magnitude of the temperature rise differed by much less than 10%. Even for the sensitive Mediterranean case, the difference was typically between 10 and 20%. The precipitation changes were fairly robust as well. These results indicate that the projected regionalized climate change is not very sensitive to the details of the subdivision. All subsequent analyses make use of regional subdivisions based on the original horizontal grid and land-sea distributions defined for each model.

3.1 Approximating the natural variability

In addition to externally-forced changes, the climate system produces unforced internal variability at various time scales. This part of natural variability is induced by interactions between various components of the climate system, i.e., the atmosphere, ocean, cryosphere, soil, vegetation, etc. In order to assess the significance of the model-simulated response to changes in the atmospheric composition, we have to compare the climate change signal to the noise caused by internal variability.

Time series of meteorological observations are not long enough to give an adequate picture of the character of natural variability at the multi-decadal and century time-scale. Moreover, they are likely themselves to be affected by radiative forcing from historical changes in atmospheric composition. Therefore, the statistical properties of the variability of climate were inferred from two 1000-year AOGCM simulations, in which the composition of the atmosphere and other external forcing agents (e.g., solar radiation) were kept constant. The models analyzed were CGCM2 and HadCM3. In the analysis of the statistical significance of model-simulated forced time-averaged climate change, one needs an estimate of internal natural variability at an equivalent temporal scale. Accordingly, we computed a series of 30-year temporal averages of regional-mean precipitation and temperature from the unforced model simulations. In practice, we used temporally overlapping averages, so that a 1000-year model simulation yields 970 such averages (non-overlapping averages were also examined, and the results inferred from these did not systematically deviate from those inferred from overlapping averages).

From these sets of tridecadal averages, standard deviations of temperature (°C) and precipitation (mm/d) and the correlation between these two variables were calculated. For precipitation, the standard deviation was normalized by the time mean, giving a percentage coefficient of variation for this variable. These three parameters define a two-dimensional normal distribution (Hald, 1952, p. 600), for which the 95% contour ellipse can be determined:

$$\frac{1}{1-\rho^2}\left\{\frac{T'^2}{\sigma_T^2}-2\rho\frac{T'}{\sigma_T}\frac{R'}{\sigma_R}\frac{R'^2}{\sigma_R^2}\right\}=\chi^2\left(df=2,p=0.95\right)=5.99 \qquad (1)$$

In (1), T′ and R′ are the anomalies and σ_T and σ_R the standard deviations of the temperature and normalized precipitation. ρ stands for the correlation between temperature and precipitation anomalies. On the right-hand side, the 95 percentile of the χ^2 distribution with degrees of freedom df = 2 is given, with a numerical value of 5.99.

The contour ellipse encloses an area centred on the origin within which 95% of the probability density of the two-dimensional normal distribution is concentrated. In the scatter diagrams illustrating model-projected climate changes (sec-

tion 3.3), we plotted such contour ellipses for both millennial GCM simulations, to give a measure of the model-generated internal variability. If a scatter point in the diagram is located distinctly outside these ellipses, we can consider the climate change represented by this point statistically significant. If the point falls inside or close to the ellipse, the signal is of the same order of magnitude as internal multi-decadal variability and thus not statistically robust.

Figure 4 depicts the distribution of temperature and normalized precipitation anomalies, as well as the 95% contour ellipse of the Gaussian distribution, for two regions. In Antarctic land areas during the southern hemisphere summer (Fig. 4, left panel), temperature and precipitation anomalies in the unforced CGCM2 simulation are strongly positively correlated. The contour ellipse is accordingly highly asymmetric, the major axis being directed from bottom-left to top-right. In the other example (Southern Africa in the southern hemisphere winter; Fig. 4, right panel), the correlation is fairly small and negative, and the major axis of the close-to-symmetric contour ellipse is directed from top-left to bottom-right.

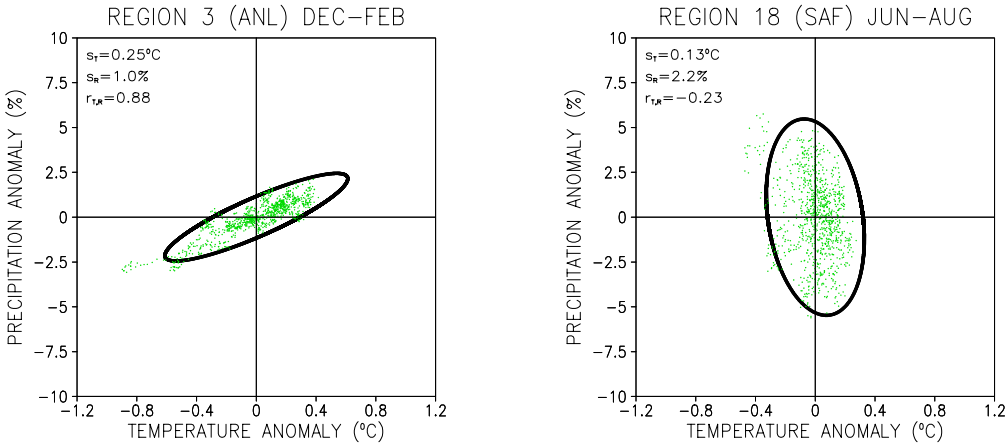

Fig. 4. The two-dimensional joint distribution of surface air temperature (°C) and normalized precipitation (%) anomalies in an unforced 1000 year simulation performed with CGCM2 for December-February over Antarctic land areas (Reg. 3, left panel) and for June-August over Southern Africa (Reg. 18, right panel). The regions are defined in Table 2. Small green dots depict the temperature and precipitation anomalies in individual overlapping 30 year periods. The thick black curve is the 95% contour ellipse of the two-dimensional normal distribution adjusted to the anomaly data. On the top-left corner of the panel are shown the parameters defining this normal distribution: standard deviations of the temperature and precipitation and their correlation.

In Fig. 4, a large majority of the scatter points representing unforced tridecadal anomalies lie inside the ellipse, and most of the remainder fairly close to the ellipse. However, in the Antarctic region in particular, the distribution of the points is not quite normal, there being points in the bottom-left sector much further from the origin than in the top-right sector, and correspondingly the density of the points is largest slightly to the right and above the origin. In the Southern Africa region skewness is much less remarkable.

We studied the joint distribution of temperature and precipitation in several regions. In many cases the distribution was somewhat skewed, but generally to a much lesser extent than in the above-discussed example of Antarctic summer. Thus, in most cases the normal distribution can be used as a reasonable first approximation for the internal temperature and precipitation variability.

The segment of a line defined by the projection of the contour ellipse on the x-axis (i.e., representing temperature) falls between the points $\pm 2.45\sigma_T$. Thus, this range is somewhat broader than the corresponding one-dimensional 95% confidence interval $\pm 1.96\sigma_T$. However, when comparing a modelled temperature change to natural variability, one has to consider that there is internal variability both in the baseline and in the future climate. We do not know quantitatively how this variability alters during climate change. One possibility is to assume that the standard deviation of tridecadal temperature variability would remain unchanged. Applying this approximation, the 95% confidence interval of temperature variability should be multiplied by $\sqrt{2}$ in order for the temperature change to be statistically significant. Accordingly, the 95% confidence interval for temperature change is $\pm 2.77\sigma_T$, so that the projection of the ellipse on the x-axis actually approximates the 92% confidence interval. By analogy, the confidence interval of precipitation change can be inferred from the projection of the ellipse on the y-axis. These confidence intervals should be used if one is interested to study the significance of modelled changes of temperature and precipitation *alone* rather than the joint distribution (see section 3.3). This argumentation also implies that a scatter point must be located distinctly outside the ellipse in order for the joint temperature/precipitation change to be considered significant.

In seasons with the temperature close to 0 °C, the CGCM2 model has a strong tendency to favour temperatures between 0 °C and +1 °C. This feature has been noted by Huth et al. (2001), for instance. This bias is evidently caused by the soil thermodynamic parameterization, which overestimates the energy consumed and released by phase transitions of water. Consequently, in cool climate regions the CGCM2-estimated natural variability may be too weak in certain seasons. The temperature variability in the millennial HadCM3 run has been analyzed by Collins et al. (2001). They reported that the simulated spatial pattern of surface temperature variability is qualitatively similar to that observed, although there is an overestimation of the land temperature variability and regional errors in ocean temperature variability. Owing to the shortness of the observational time series, that study focused on somewhat shorter time-scales than those examined in the present work.

The contour ellipses derived from the two millennial runs, conducted with CGCM2 and HadCM3, were fairly dissimilar in some regions, although the order of magnitude of the standard deviations was the same. This topic will be discussed further in sections 3.3–3.4.

3.2 Pattern scaling method

For most of the GCMs analyzed in this work, only model responses to the A2 and B2 forcing scenarios were available in the IPCC DDC at the time of the study. The B1 response had only been calculated by two models (CCSR/NIES and CSIRO) and the A1FI response by one model (CCSR/NIES). In order to form projections corresponding to these scenarios for other models, we applied a simple version of the pattern-scaling method introduced by Santer et al. (1990). The idea in this technique is that the geographical pattern of the response is assumed to be independent of the forcing, while the amplitude of the response at every location is linearly proportional to the global mean change in the surface air temperature. Consequently, the response to arbitrary forcing can be calculated from an existing AOGCM response by multiplying that pattern pointwise (or, in this work, region by region) by the ratio of the global mean changes. For example, if the temperature/precipitation response to forcing scenario B2 has been calculated by a GCM, the response to scenario B1 is found by scaling the pattern at all grid points:

$$\Delta T_{B1,s} = \left\langle \frac{\Delta T_{B1}}{\Delta T_{B2}} \right\rangle \Delta T_{B2,g}; \quad \Delta R_{B1,s} = \left\langle \frac{\Delta T_{B1}}{\Delta T_{B2}} \right\rangle \Delta R_{B2,g} \tag{2}$$

where ΔT and ΔR are the regional changes of temperature and precipitation. ⟨ ⟩ denotes a global mean, and subscripts B1 and B2 refer to the forcing scenarios. The temperature/precipitation change denoted by subscript *g* is simulated by a GCM, changes with subscript s are pattern-scaled. The projection for each scenario was always scaled by the nearest scenario for which an GCM run exists, i.e., an A1FI projection was derived from the A2, a B1 projection from the B2 simulation.

In practice, the global mean temperature changes were calculated with a simple climate model system, which had been calibrated to be consistent with each AOGCM to be emulated. Such models require few computational resources, and can readily be used to calculate global mean temperature changes for all relevant forcing scenarios. In this study, we employed the global temperature changes obtained with the TAR version of MAGICC (Model for the Assessment of Greenhouse-gas Induced Climate Change), a set of coupled gas-cycle, climate and ice-melt models (IPCC, 2001a, Appendix 9.1; Raper et al., 2001). The model has been utilized to emulate climate responses of four coupled AOGCMs, namely CSIRO Mk2, ECHAM4, HadCM3 and NCAR PCM, for which SRES simulations are readily available. The MAGICC-emulated time series of global annual mean temperature changes for these four models were supplied to us by Dr. Sarah Raper.

On the basis of these time series, we calculated the MAGICC-derived changes of the global mean temperature for time slices 2010–2039, 2040–2069 and 2070–2099, relative to the climatological baseline period 1961–1990, for forcing scenarios A1FI, A2, B1 and B2. Ratios of the global mean temperature changes corresponding to different forcing scenarios, i.e., the scaling coefficients employed in (2) and (3), are given in Table 3.

Table 3. The ratios of the global mean temperature changes induced by various forcing scenarios for periods 2010–2039 (~ 2020s), 2040–2069 (~ 2050s) and 2070–2099 (~ 2080s), relative to the baseline period 1961–1990. The temperature changes were calculated by the simple climate model MAGICC.

	$\left\langle \frac{\Delta T_{B1}}{\Delta T_{B2}} \right\rangle$			$\left\langle \frac{\Delta T_{A1F1}}{\Delta T_{A2}} \right\rangle$			$\left\langle \frac{\Delta T_{A2}}{\Delta T_{B2}} \right\rangle$		
PERIOD	2020s	2050s	2080s	2020s	2050s	2080s	2020s	2050s	2080s
CSIRO Mk2	0.88	0.86	0.81	1.08	1.26	1.25	0.86	1.03	1.27
ECHAM4	0.86	0.85	0.81	1.10	1.29	1.26	0.83	1.03	1.29
HadCM3	0.87	0.86	0.81	1.09	1.28	1.25	0.84	1.04	1.29
NCAR PCM	0.86	0.85	0.80	1.10	1.29	1.25	0.84	1.05	1.31

We tested the ability of the pattern-scaling procedure by comparing the approximate pattern-scaled and the actual AOGCM-simulated temperature responses to scenario A2. In this case, the pattern-scaled response was derived from the GCM response to the B2 forcing scenario:

$$\Delta T_{A2,s} = \left\langle \frac{\Delta T_{A2}}{\Delta T_{B2}} \right\rangle \Delta T_{B2,g} \qquad (3)$$

The value of the scaling coefficient $\left\langle \frac{\Delta T_{A2}}{\Delta T_{B2}} \right\rangle$ for period 2070–2099 depends on the model, varying between 1.27 and 1.31 (see Table 3). The spatial mean temperature changes for the 32 world regions for period 2070–2099 are depicted in Fig. 5. For all four models, at this horizontal scale the pattern-scaled temperature changes agree well with the AOGCM-derived ones, the correlation between the two being in the order of 0.99 and rms difference at least one order of magnitude smaller than the projected temperature changes themselves (these statistical variables were calculated directly from the set of region means in Fig. 5). In other seasons the correlations are of the same order of magnitude, being in general lowest in March-May and highest in December-February.

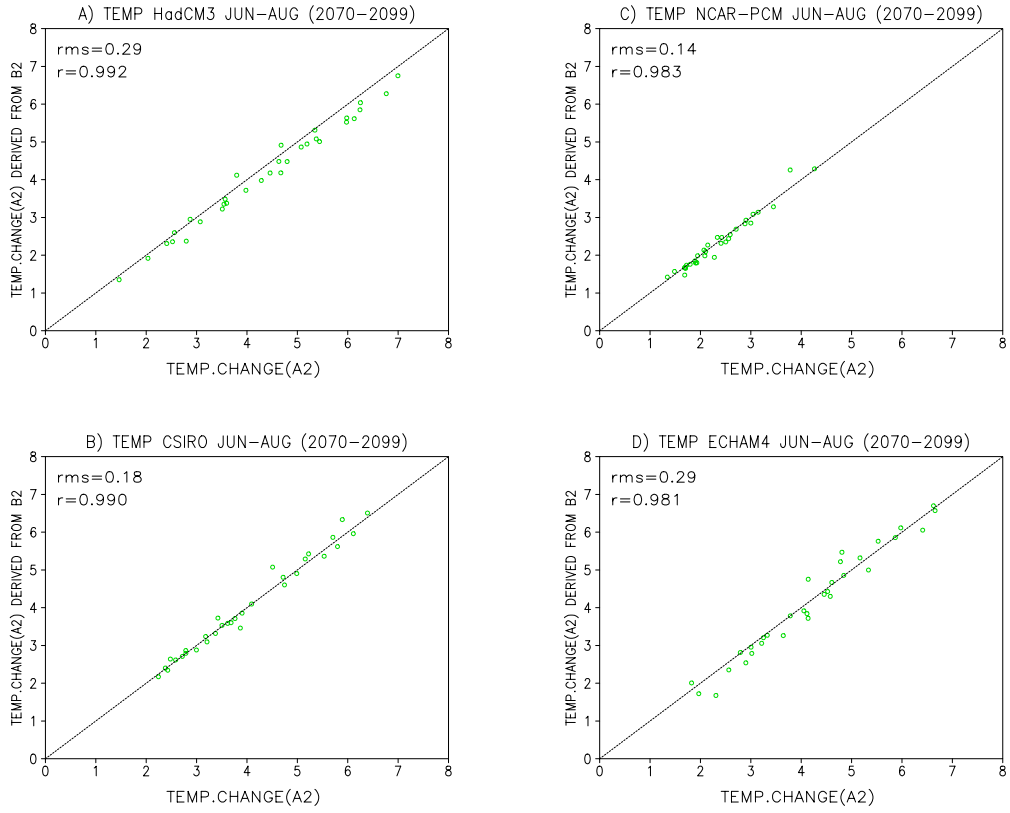

Fig. 5. Scatter plots showing the comparison between the pattern-scaled and AOGCM-simulated temperature changes (in °C) for period 2070–2099 relative to 1961–1990 for 32 world regions in the June-August season. Comparisons are shown for a) HadCM3, b) CSIRO Mk2, c) NCAR PCM and d) ECHAM4. The horizontal axis gives the AOGCM-simulated temperature response to forcing scenario A2, the vertical axis the corresponding change scaled up from the B2 simulation applying eq. (3). If the two projections are identical, the point falls on the black line. The correlation coefficient and rms difference are given in the top-left corner.

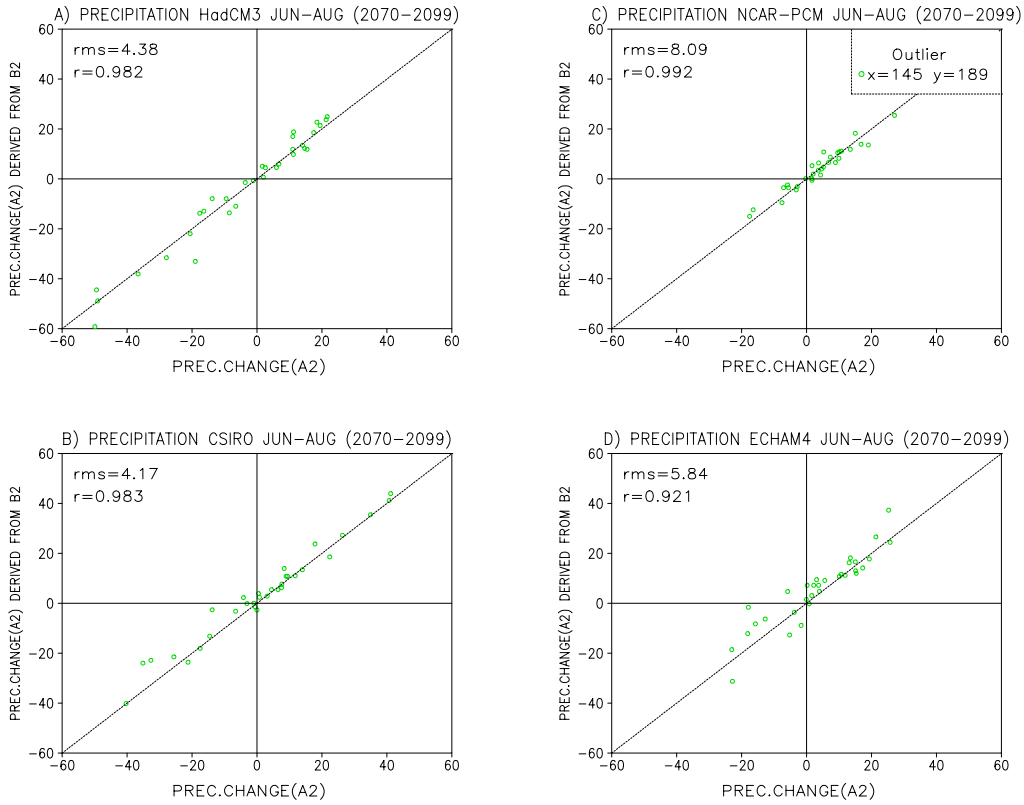

Fig. 6. As Fig. 5, but for percentage precipitation changes.

In assessing temperature changes for less distant periods 2010–2039 and 2040–2069, the pattern-scaling as employed in this study proved somewhat less successful. For period 2040–2069, the correlation between the pattern-scaled and directly GCM-simulated temperature changes mostly varied between 0.96 and 0.99; for period 2010–2039 between 0.87 and 0.98. During these time slices, the global scale greenhouse gas forcing is weaker, and therefore the contributions of horizontally inhomogeneous aerosol forcing and stochastic noise are more important than for the more distant periods. This evidently explains why the spatial distributions of temperature change do not correlate as strongly.

We also compared the patterns of temperature change obtained with various models against one another. The rms differences between the changes obtained with different models applying the same forcing scenario were typically 3–5 times larger than the above-discussed rms differences between the GCM-simulated and pattern-scaled responses. The correlations were likewise substantially lower. This indicates that the temperature change obtained with an individual model is generally a fairly linear function of the amplitude of the forcing, the patterns simulated by different models being qualitatively far less similar.

The applicability of the pattern-scaling technique was also studied for precipitation. Note that the change in precipitation is scaled by the ratio of the global mean *temperature* changes, in a similar way to temperature (see eqs. (2) and (3)). Figure 6 shows that the method works fairly well, in accordance with the findings of Mitchell (2003), although the correlations are slightly smaller than for temperature. Nevertheless, in areas with small present-day precipitation, the proportion of noise in simulated precipitation change may be large. In that case,

scaling of the noise-related part of the precipitation change can potentially result in unreasonable total changes. In Fig. 6c, the large increase of precipitation in the Sahara region (+145% in the A2 GCM simulation, the scaled increase being +189%) appears to be an example of such a phenomenon. Note also that an outlier such as this in the joint distribution produces a spuriously high correlation.

Giorgi and Mearns (2002, Fig. 6) studied the linearity of the response in the same horizontal scale as discussed here. However, they did not deal with various models separately, but studied a weighted average of a set of changes simulated by various models. They found that the scaling technique works excellently for the temperature, being somewhat less good for precipitation.

Very commonly the response patterns are scaled, in contrast to what is done above, from a stronger response to a weaker one. The advantage of that approach is the higher signal-to-noise ratio in the scaled response. We employed this method in inferring B1-forced changes from B2-forcing. However, for the purpose of testing the method it is unimportant in which direction the scaling is performed; the correlation between the scaled and the reference patterns is exactly the same irrespective of the scaling direction.

We could not evaluate the pattern-scaling method for scenario A1FI, since global mean change of temperature from the energy balance model were not available for the only GCM (CCSR/NIES) in the IPCC DDC with which the A1FI run had been made. It is possible that in that case the method does not work as well as for the pair A2/B2, since after 2040 the A1FI scenario produces the strongest radiative forcing (IPCC, 2001a), and the response may behave more nonlinearly as a function of the forcing amplitude. On the other hand, the relatively small climate change induced by scenario B1 is likely to conform to the linearity assumption, and a pattern-scaled response should be reasonable. The present study confines itself to assessing the pattern-scaling method for SRES scenarios; applications to stabilization scenarios are evaluated in Mitchell et al. (1999) and Mitchell (2003).

The above discussion concerns the applicability of the pattern-scaling method (2)–(3) in constructing climate changes for the 32 world regions. Our conclusions do not hold for any particular horizontal scale, because the area of the regions varies. In the future evaluation of the method, it might be appropriate to decompose the geographical distribution of temperature change etc. into various horizontal scales, for example, by applying spherical harmonics functions. In addition, it would be interesting to extend the evaluation to variables other than temperature and precipitation, such as surface pressure, humidity or radiation.

3.3 An example of a scatter diagram

An example of how the climate changes simulated by various models are represented by a scatter diagram is given in Fig. 7. The figure illustrates climate change in the Southern Australia region in the southern hemisphere summer. The range of internal natural variability of temperature and precipitation, inferred from millennial AOGCM runs (section 3.1), is depicted by contour ellipses centred on the origin. The figure indicates that there is a 95% probability that the internal 30-year average temperature and precipitation anomalies are smaller than ~ 0.3°C and ~ 10%, respectively. In this region HadCM3 produces slightly less internal variability than CGCM2. Moreover, the unforced precipitation and temperature anomalies simulated by HadCM3 tend to be negatively correlated, there being little correlation in the unforced CGCM2 simulation.

The climate responses to the four forcing scenarios as simulated by various models are depicted with scatter points. For scenario A1FI, only one of the pro-

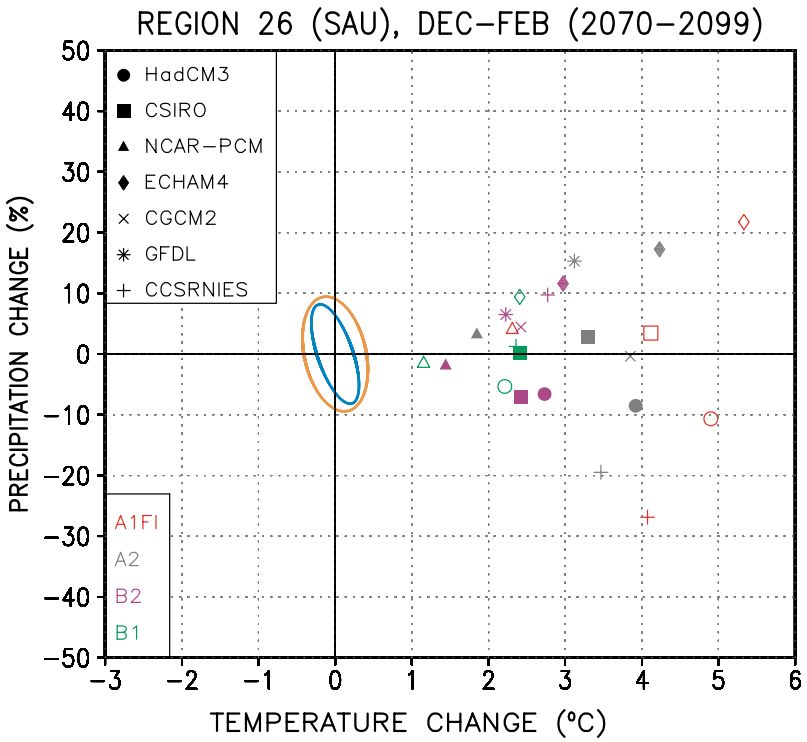

Fig. 7. Projected climate change by 2070–2099 (relative to the baseline period 1961–1990) in the Southern Australia region (Reg. 26) during December-February as illustrated by a scatter diagram. The x-axis shows temperature changes in °C, the y-axis precipitation changes in percent. Each scatter point represents the temperature and precipitation response to one of the forcing scenarios simulated by a coupled AOGCM. The scenario is depicted by the colour of the point, see legend at the bottom-left. The shape of the symbol defines the model, legend at the top-left. Solid symbols correspond to responses directly inferred from AOGCM runs; open symbols are those calculated by the pattern-scaling method. Ovals centred on the origin are the 95% Gaussian contour ellipses of the natural tri-decadal variability of temperature and precipitation, derived from the unforced 1000-year AOGCM runs performed by CGCM2 (orange) and HadCM3 (blue); for further information, see section 3.1.

jections is directly calculated from a GCM simulation (by CCSR/NIES), while the four other projections (HadCM3, NCAR-PCM, ECHAM4 and CSIRO Mk2) are found by applying the pattern-scaling technique described in section 3.2. The pattern-scaled responses are shown by open symbols. For the B1 scenario, there are three pattern-scaled (HadCM3, NCAR-PCM and ECHAM4) and two directly GCM-derived (CSIRO Mk2 and CCSR/NIES) assessments. For the A2 and B2 scenarios, GCM simulations were available for all models included in the study.

In Fig. 7, all the scatter points representing model-simulated human-induced climate change at the end of the 21th century are located far outside the 95% contour ellipses of internal natural variability. Accordingly, the joint temperature/precipitation responses can be considered statistically significant. However, this result mainly reflects the large, positive temperature changes predicted by all models. Modelled precipitation changes, considered on their own, are predominantly *not* statistically significant relative to modelled natural variability

(compare the points with the projection of the ellipses along the y-axis – see section 3.1). In this region and season for precipitation, positive and negative changes are almost equally common. When one studies every model separately, the warming simulated appears to be a monotonic function of the intensity of forcing, i.e., the B1 scenario yields the smallest, the A1FI the largest warming. For precipitation, in contrast, such a relation does not hold: several models even simulate precipitation changes of opposite sign with various forcing scenarios. This may be due to the large proportion of noise in the simulated precipitation changes. In this example, the ECHAM4 and GFDL models produce a climate wetter than at present for all scenarios, while in the HadCM3 simulation precipitation invariably decreases. The most modest temperature rise is simulated by NCAR-PCM, the most severe by ECHAM4.

3.4 Seasonal scatter diagrams: a brief summary

A complete set of climate change scatter diagrams is given in Appendix B and instructions on their interpretation provided in Appendix A. Diagrams are presented for all the 32 regions (regions are defined in Table 2 and Fig. 2), four seasons (December-February, March-May, June-August and September-November) and three time periods (2010–39, 2040–69 and 2070–99). Accordingly, there are 384 scatter diagrams altogether. For period 2010–2039, scaled points have been omitted from the figures. For that period, due to the low signal-to-noise ratio, the pattern-scaling technique was less applicable than for more distant time slices (section 3.2), and various scenarios deviated little from one another. Consequently scaled points would not introduce any significantly new information. GCM responses for that period are considerably affected by noise.

The character of the internal variability (ellipses centred on the origin) inferred from the two 1000-year GCM runs is by no means identical. The standard deviation of the temperature does not seem systematically larger in either of the models, although in individual regions these may differ substantially. The normalized variability of the precipitation, by contrast, is larger in the unforced HadCM3 simulation in the majority of regions.

In most cases the anthropogenically-forced simulated climate change is statistically significant, i.e., it falls distinctly outside the contour ellipses of unforced natural variability. The robustness is caused either by the statistically significant change in both variables or by the confidence of the temperature change alone. In all simulations and regions, the temperature shows a warming tendency. For precipitation, changes of both sign are found, increasing precipitation totals being more common than decreasing ones. In most regions, confidence in the precipitation change is less than for the temperature change. An exception is region 4 (Antarctic ocean), where the increase of precipitation is more robust than the warming.

It is important to emphasize that the lack of statistical significance of the precipitation change in several regions does not exclude the possibility of practically important changes in the future. The low significance may be caused by large natural variability, resulting in a low signal-to-noise ratio even with large precipitation changes.

Except for a few regions situated close to the poles, the NCAR DOE PCM simulates the most modest rise of temperature. In a large number of regions, this model predicts fairly small changes of precipitation as well. The largest warming for most of the regions is given by the CCSR/NIES model. Note that in the CCSR/NIES model the global mean temperature change is larger than in other models,

while in our set NCAR PCM is the model that produces smallest global warming (Table 1). For precipitation, in some regions the HadCM3 simulates markedly larger seasonal increases (Regs. 22, 29, 30) or decreases (Regs. 11, 12, 18, 28) than do other models.

In all areas, there are marked inter-model differences in projected climate changes, the differences being similar in magnitude to the differences in the responses to various scenarios. In the scatter diagrams, this is represented by the mixing of different coloured points. However, in some regions the model simulations agree qualitatively. For example, all models predict increasing precipitation in high latitudes (Regs. 1–6 and 19 in all seasons; Reg. 13 in all seasons except summer). Likewise, the Asian (Regs. 22–23) summer monsoon precipitation invariably tends to intensify. In Southern Africa (Reg. 18), all models show a tendency towards reduced precipitation in the second half of the year.

In the Sahara region (Reg. 15), some models simulate large relative increases (up to five-fold) of precipitation. However, in this area the present-day precipitation is so sparse that such an immense percentage change is not especially large in the absolute sense.

In the scatter diagrams, it is sometimes hard to discern individual points, because the points frequently cover one another. Therefore, the information included in the diagrams is also available in numerical form from the IPCC DDC (http://ipcc-ddc.cru.uea.ac.uk/asres/scatter_plots/scatterplots_home.html).

4 Discussion and conclusions

In anticipating future climate change, there are three main sources of uncertainty. Firstly, we do not know the future anthropogenic emissions and resulting atmospheric concentrations of greenhouse gases and aerosols. Secondly, the response to greenhouse gas and aerosol forcing differs between various models, simulated regional climate changes being particularly model-dependent. Thirdly, in addition to anthropogenic forcing, climate changes are induced by natural forcing (e.g., volcanoes and variations in solar activity) as well as by unforced internal variability in the climate system.

Forced and unforced natural climatic fluctuations cannot be forecasted at present in a deterministic sense. The uncertainty associated with future anthropogenic forcing can be tackled by constructing a number of emission scenarios, four of which are used in the present paper. Scenario B1 represents a low level, scenario A1FI a high level of emissions, and on the basis of present knowledge, we can expect it to be very likely that future emissions will fall between these extreme scenarios. Compared with these extremes, the other two scenarios, A2 and B2, produce moderate increases in the anthropogenic forcing, A2 being the stronger of the two. Of course, future emissions are highly dependent on the evolution of technology and human behaviour, factors that are almost unforeseeable.

In the models there are several processes that are treated fairly crudely. These include, for instance, coupling between the oceans and atmosphere and the influence of clouds on radiative transfer. Model uncertainty is considered by examining simulated climate changes from several models. For scenarios A2 and B2, the number of model simulations viewed was seven. For scenarios A1FI (B1) only one (two) AOGCM simulations were available, and consequently projections associated with these scenarios were mainly inferred from the middle-range scenarios A2 and B2, applying a pattern-scaling technique.

Climate models are evolving all the time, and we can anticipate that their ability to simulate the response to anthropogenic climate forcing will improve further. The sub-continental scale regional climate projections given in this report are based on existing climate models. In the future, new more accurate models are likely to alter our picture of expected climate change, and the present account will thus have to be updated.

The model-simulated regional-mean temperature changes were almost invariably statistically significant, i.e., they clearly exceed the magnitude of natural multi-decadal variability occurring in long unforced coupled AOGCM runs, whereas the significance of precipitation changes was generally lower. However, as also found in Chapter 9 of IPCC (2001a), the climate change projections obtained with various models differed substantially from one another. In fact, even in the most distant period 2070–2099, when the difference between the forcing scenarios is largest, the inter-model differences were of the same order of magnitude as the differences between the responses to various forcing scenarios, even accounting for the contribution of natural variability. After year 2100, the responses to various scenarios would diverge more rapidly, but that era is beyond the scope of this report.

For a given model, at the horizontal scales studied, the geographical pattern of the simulated response to various forcing scenarios proved to be very similar. Only the amplitude of the response varied, as a function of the forcing. For example, the correlation between temperature changes from 1961–1990 to 2070–2099 under scenarios A2 and B2 was as high as ~ 0.99 (four GCMs were analyzed). Even for precipitation changes the agreement was surprisingly good, with correlations generally much higher than 0.9.

The high similarity in response patterns from a given AOGCM under different forcings provided a good justification for deriving sub-continental scale climate change projections under other forcing scenarios not explicitly modelled by AOGCMs. Using this pattern-scaling method, the temperature (or precipitation) response to an arbitrary forcing scenario can be found by multiplying the GCM-simulated response to some other forcing scenario by the ratio of the global mean temperature change induced by these two scenarios. The global mean change can be determined by a simple climate model that is calibrated to agree with the AOGCM in question. In this study we applied the pattern-scaling technique to construct A1FI and B1 projections of temperature and precipitation for those models with which these full AOGCM runs had not been conducted or were not available in the IPCC DDC.

Owing to the success of the pattern-scaling technique for the levels of forcing studied, we conclude that it may not be necessary to make a large number of fully coupled AOGCM runs for different forcing scenarios in order to characterize sub-continental scale climate change. Rather, in accord with the conclusions presented by Mitchell et al. (1999), we find that it is reasonable to perform only a few full simulations and to derive the results for other scenarios with the pattern-scaling method. Possible exceptions to this general conclusion have been noted by Mearns et al. (2001), including scenarios in which the forcing stabilizes and the climate approaches an equilibrium at different rates in different parts of the world, and scenarios of heterogeneous aerosol forcing, where the regional climate response may vary strongly over both space and time. Nevertheless, where the forcing is fairly uniform, pattern-scaling appears to be a useful device for limiting the number of time-consuming coupled model runs, and hence releasing resources for the purposes of model development.

References

Carter, T.R., M. Hulme, J.F. Crossley, S. Malyshev, M.G. New, M.E. Schlesinger, and H. Tuomenvirta, 2000: Climate change in the 21st century – interim characterizations based on the new IPCC emissions scenarios. *The Finnish Environment* 433, Finnish Environment Institute, Helsinki, 148 pp.

Carter, T.R., E.L. La Rovere, R.N. Jones, R. Leemans, L.O. Mearns, N. Nakićenović, A.B. Pittock, S.M. Semenov, and J. Skea, 2001: Developing and applying scenarios. In: *Climate Change 2001: Impacts, Adaptation, and Vulnerability. Contribution of Working Group II to the Third Assessment Report of the Intergovernmental Panel on Climate Change* [McCarthy, J.J., O.F. Canziani, N.A. Leary, D.J. Dokken, and K.S. White (eds)]. Cambridge University Press, Cambridge and New York, pp. 145-190.

Collins, M., S. F. B. Tett and C. Cooper, 2001: The internal climate variability of HadCM3, a version of the Hadley Centre coupled model without flux adjustment. *Climate Dyn.*, **17**, 61-81.

Cubasch, U., G.A. Meehl, G.J. Boer, R.J. Stouffer, M. Dix, A. Noda, C.A. Senior, S. Raper, and K.S. Yap, 2001: Projections of future climate change. In: *Climate Change 2001: The Scientific Basis. Contribution of Working Group I to the Third Assessment Report of the Intergovernmental Panel on Climate Change* [Houghton, J.T., Y. Ding, D.J. Griggs, M. Noguer, P.J. van der Linden, X. Dai, K. Maskell, and C.A. Johnson (eds.)]. Cambridge University Press, Cambridge and New York, pp. 525-582.

Giorgi, F. and R. Francisco, 2000: Evaluating uncertainties in the prediction of regional climate change. *Geophys. Res. Lett.*, **27**, 1295-1298.

Giorgi, F., B. Hewitson, J. Christensen, M. Hulme, H. von Storch, P. Whetton, R. Jones, L. Mearns, and C. Fu, 2001: Regional climate information – evaluation and projections. In: *Climate Change 2001: The Scientific Basis. Contribution of Working Group I to the Third Assessment Report of the Intergovernmental Panel on Climate Change* [Houghton, J.T., Y. Ding, D.J. Griggs, M. Noguer, P.J. van der Linden, X. Dai, K. Maskell, and C.A. Johnson (eds.)]. Cambridge University Press, Cambridge and New York, pp. 583-638.

Giorgi, F. and L.O. Mearns, 2002: Calculation of average, uncertainty range, and reliability of regional climate changes from AOGCM simulations via the "reliability ensemble averaging" (REA) method. *J. Climate*, **15**, 1141-1158.

Hald, A., 1952: *Statistical Theory with Engineering Applications*. Wiley International Edition, New York. 783 p.

Huth, R., J. Kysely and M. Dubrovsky, 2001: Time structure of observed, GCM-simulated, downscaled, and stochastically generated daily temperature series. *J. Climate*, **14**, 4047–4061.

IPCC, 2001a: *Climate Change 2001: The Scientific Basis. Contribution of Working Group I to the Third Assessment Report of the Intergovernmental Panel on Climate Change* [Houghton, J.T., Y. Ding, D.J. Griggs, M. Noguer, P.J. van der Linden, X. Dai, K. Maskell, and C.A. Johnson (eds.)]. Cambridge University Press, Cambridge and New York, 881 pp.

IPCC, 2001b: *Climate Change 2001: Impacts, Adaptation, and Vulnerability. Contribution of Working Group II to the Third Assessment Report of the Intergovernmental Panel on Climate Change* [McCarthy, J.J., O.F. Canziani, N.A. Leary, D.J. Dokken, and K.S. White (eds)]. Cambridge University Press, Cambridge and New York, 1032 pp.

Leggett, J., W.J. Pepper, and R.J. Swart, 1992: Emissions scenarios for IPCC: an update. In: *Climate Change 1992. The Supplementary Report to the IPCC Scientific Assessment* [Houghton, J.T., B.A. Callander and S.K. Varney (eds.)]. Cambridge University Press, Cambridge, UK, pp. 71-95.

McAvaney, B.J., C. Covey, S. Joussaume, V. Kattsov, A. Kitoh, W. Ogana, A.J. Pitman, A.J. Weaver, R.A. Wood, and Z.-C. Zhao, 2001: Model evaluation. In: *Climate Change 2001: The Scientific Basis. Contribution of Working Group I to the Third Assessment Report of the Intergovernmental Panel on Climate Change* [Houghton, J.T., Y. Ding, D.J. Griggs, M. Noguer, P.J. van der Linden, X. Dai, K. Maskell, and C.A. Johnson (eds.)]. Cambridge University Press, Cambridge and New York, pp. 471-523.

Meehl, G.A., G.J. Boer, C. Covey, M. Latif, and R.J. Stouffer, 2000: The Coupled Model Intercomparison Project (CMIP). *Bull. Am. Met. Soc.*, **81**, 313-318.

Mearns, L.O., M. Hulme, T.R. Carter, R. Leemans, M. Lal and P. Whetton, 2001: Climate scenario development. In: *Climate Change 2001: The Scientific Basis. Contribution of Working Group I to the Third Assessment Report of the Intergovernmental Panel on Climate Change* [Houghton, J.T., Ding, Y., Griggs, D.J., Noguer, M., van der Linden, P.J., Dai, X., Maskell, K. and Johnson, C.A. (Eds.)]. Cambridge University Press, Cambridge and New York, pp. 739-768.

Mitchell, J. F. B., T. C. Johns, M. Eagles, W. J. Ingram and R. A. Davis, 1999: Towards the construction of climatic change scenarios. *Climatic Change*, **41**, 547-581.

Mitchell, T.D., 2003: Pattern scaling. An examination of the accuracy of the technique for describing future climates. *Climatic Change*, in press.

Morita, T., J. Robinson, A. Adegbulugbe, J. Alcamo, D. Herbert, E.L. La Rovere, N. Nakićenović, H. Pitcher, P. Raskin, K. Riahi, A. Sankovski, V. Sokolov, B. de Vries, D. Zhou, 2001: Greenhouse gas emission mitigation scenarios and implications, In: *Climate Change 2001: Mitigation. Contribution of Working Group III to the Third Assessment Report of the Intergovernmental Panel on Climate Change* [Metz, B., O. Davidson, R. Swart, and J. Pan (eds)]. Cambridge University Press, Cambridge and New York, pp. 115-166.

Nakićenović, N., J. Alcamo, G. Davis, B. de Vries, J. Fenhann, S. Gaffin, K. Gregory, A. Grübler, T.Y. Jung, T. Kram, E.L. La Rovere, L. Michaelis, S. Mori, T. Morita, W. Pepper, H. Pitcher, L. Price, K. Raihi, A. Roehrl, H.-H. Rogner, A. Sankovski, M. Schlesinger, P. Shukla, S. Smith, R. Swart, S. van Rooijen, N. Victor, and Z. Dadi, 2000: *Emissions Scenarios. A Special Report of Working Group III of the Intergovernmental Panel on Climate Change*. Cambridge University Press, Cambridge, UK and New York, USA, 599 pp.

New, M., M. Hulme and P. Jones, 1999: Representing twentieth-century space-time climate variability. Part I: Development of a 1961-90 mean monthly terrestial climatology. *J. Climate*, **12**, 829-856.

Parry, M.L., 2002: Scenarios for climate impact and adaptation assessment. *Global Environmental Change*, **12**, 149-153.

Raper, S.C.B, J.M. Gregory and T.J. Osborn, 2001: Use of a upwhelling-diffusion energy balance climate model to simulate and diagnose A/OGCM results. *Clim. Dyn.*, **17**, 601-613.

Santer, B. D., T. M. L. Wigley, M. E. Schlesinger and J. F. B. Mitchell, 1990: Developing climate scenarios from equilibrium GCM results. *Rep. No. 47, Max-Planck-Institut-für-Meteorologie*, Hamburg, 29 pp.

Swart, R., J. Mitchell, T. Morita and S. Raper, 2002: Stabilisation scenarios for climate impact assessment. *Global Environmental Change*, **12**, 155-165.

Appendix A. Instructions for the users of scatter diagrams

Explanation of the diagrams

The scatter diagrams depict projected changes in seasonal surface air temperature and precipitation for three 30-year periods (2010–2039, 2040–2069 and 2070–2099) relative to the baseline period 1961–1990 in 32 sub-continental scale regions (defined in Table 2 of the report). The climate changes have been simulated by seven coupled atmosphere-ocean general circulation models (AOGCMs; see Table 1 of the report), the greenhouse gas and aerosol forcing being inferred from the SRES emission scenarios A1FI, A2, B1 and B2. Responses to the A2 and B2 scenarios are based on AOGCM simulations; projections for other scenarios were mainly derived from available runs applying a pattern-scaling technique (for a description of the technique and its applicability, see section 3.2 of the report). As we have dealt with 32 regions, three projection periods and four seasons, there are 384 scatter diagrams altogether.

In the scatter diagrams, the x-axis shows temperature changes in °C, the y-axis precipitation changes in percent. Each scatter point represents a single model-simulated temperature/precipitation response to one forcing scenario. The scenario is depicted by the colour of the point (A1FI - red, A2 - grey, B1 - green and B2 - violet). The shape of the symbol defines the model: CCSR/NIES (pluses), CSIRO Mk2 (squares), CGCM2 (crosses), ECHAM4/OPYC3 (diamonds), GFDL-R30 (snowflakes), HadCM3 (circles) and NCAR DOE PCM (triangles). Solid symbols correspond to responses directly inferred from AOGCM runs; open symbols are those calculated by the pattern-scaling method. Scaled points have been omitted from the diagrams for the earliest projection period 2010–2039. Since it is difficult to determine the exact locations of points depicted in the scatter diagrams, this information is available in numerical format, alongside the report, from the IPCC Data Distribution Centre (http://ipcc-ddc.cru.uea.ac.uk/asres/scatter_plots/scatterplots_home.html).

The ovals centred on the origin indicate the 95% Gaussian contour ellipses of the natural internal tridecadal variability of temperature and precipitation, derived from unforced 1000-year AOGCM runs performed by CGCM2 (orange) and HadCM3 (blue); for further information see section 3.1 of the report. If a scatter point falls distinctly outside the ellipses, the model-simulated joint temperature/precipitation change is statistically significant. Note that inspection of the diagrams indicates statistically significant changes in the large majority of cases analyzed. This is due to strong temperature changes which usually lie well outside the range of natural variability. In contrast, precipitation changes exceed natural variability in far fewer cases. To assess the statistical significance of the temperature and precipitation changes *separately*, the dimensions of the contour ellipses on the x- and y-axes should be employed as described in section 3.1.

One must bear in mind that, in addition to the response to human-induced forcing, the modelled climate change includes contributions due to noise and, perhaps also, to climate drift. The influence of noise is strongest in the short-term projections, which is why pattern-scaling has not been applied for the earliest projection period. Moreover, present climate models are far from complete, and there are components of the climate system that we do not yet understand properly. Therefore, it is not impossible that the response of the real climate system could fall outside the range projected by the model simulations discussed in the report.

Possible uses of the diagrams

The scatter diagrams are designed to offer guidance to analysts who wish to assess the likely range of future climate change in a region. For instance, the diagrams can be used to define the limits of temperature/precipitation change to be employed in climate impact sensitivity studies. The data may also assist an analyst in selecting a representative set of model-based projections to be employed as scenarios. However, it is recommended that further study of the AOGCM outputs be undertaken to establish their suitability for application in regional impact studies, preferably in co-operation with experienced climatologists.

For instance, one possible criterion for judging model suitability is its skill at reproducing present-day observed climate (see section 2 of the report). Confidence in a model is enhanced further if the model is able to capture regional phenomena such as the Asian monsoon, the El Niño – Southern Oscillation and seasonal ice and snowcover, which are important for many impact applications. Nevertheless, model performance varies widely at regional scale, and it should be remembered that a model that performs well in one region or for one variable might perform less well in another region or for a different variable. Moreover, even though a good simulation of present-day regional climate is an encouraging result, it is still no guarantee of reliable projections of climate change (Mearns et al., 2001). General information on the performance of AOGCMs, including the seven models used in this exercise, is presented in McAvaney et al. (2001), which draws extensively on the results of the Coupled Model Intercomparison Project (Meehl et al., 2000).

Appendix B. Scatter diagrams

Region 1: Arctic Land (2010–2039)

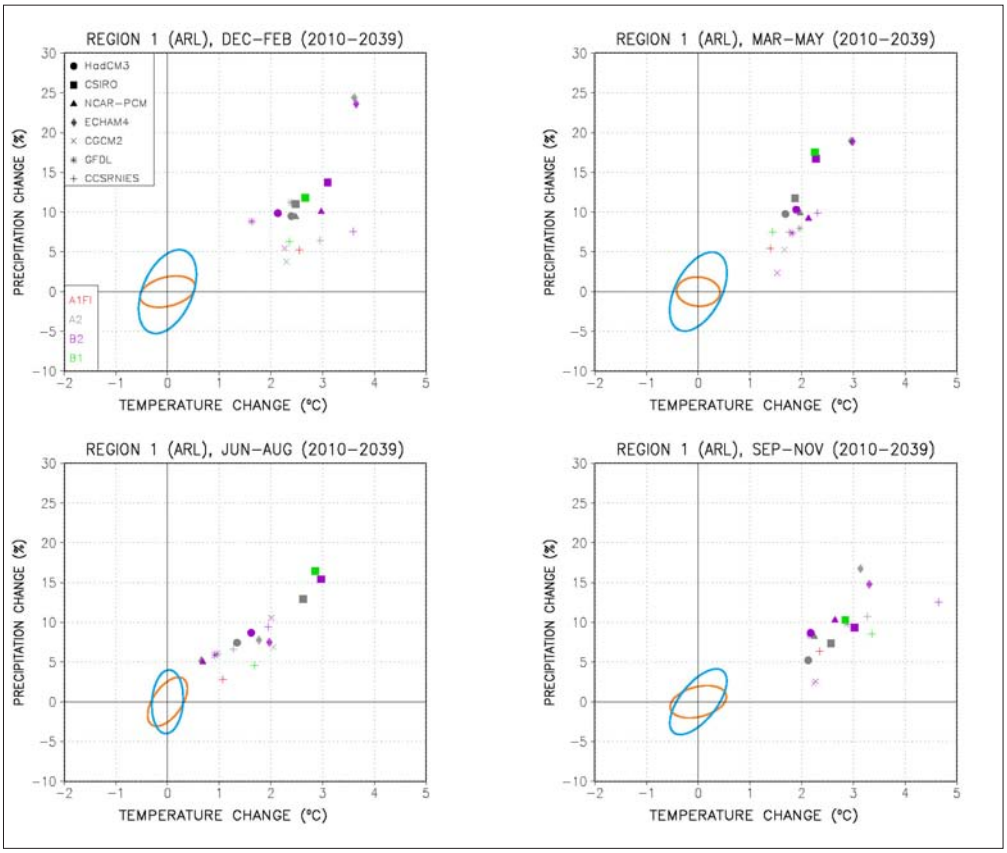

Region 1: Arctic Land (2040–2069)

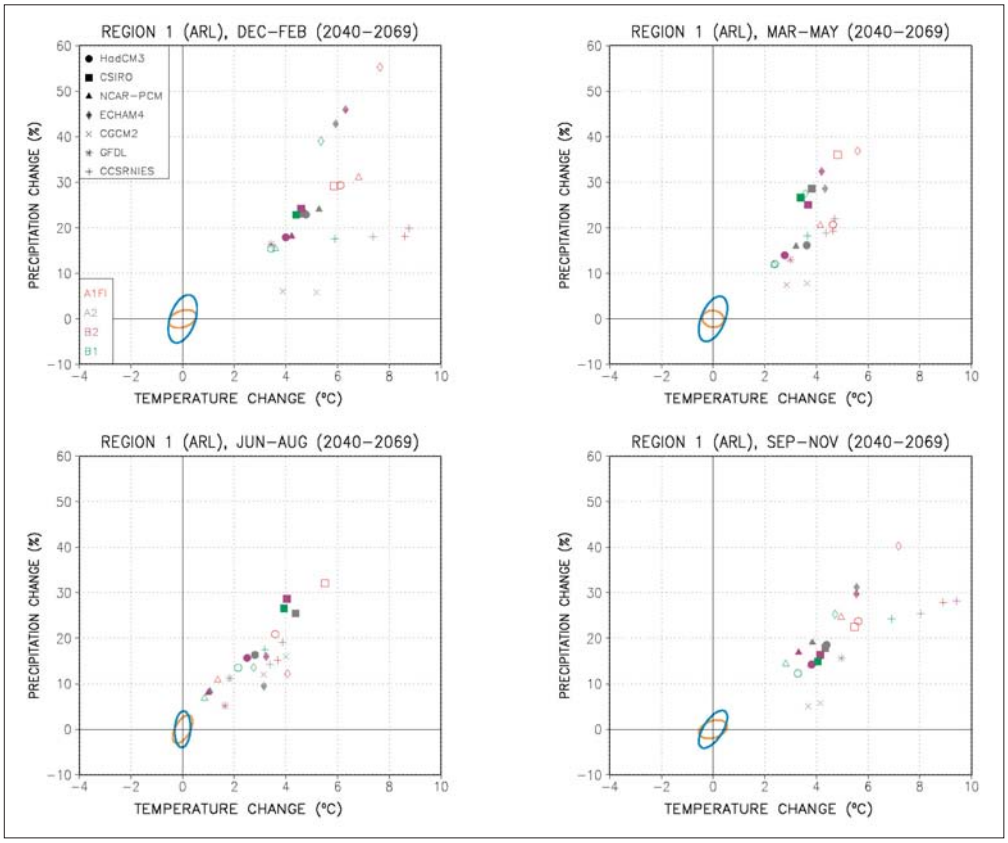

Region 1: Arctic Land (2070–2099)

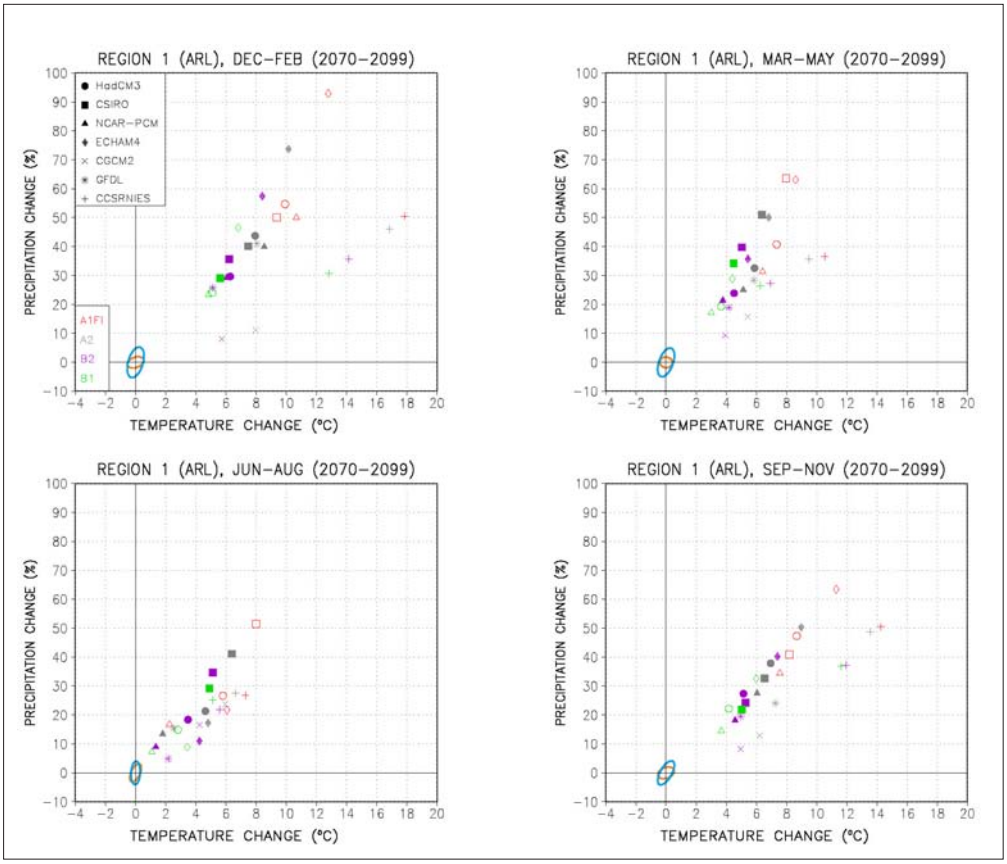

Region 2: Arctic Ocean (2010–2039)

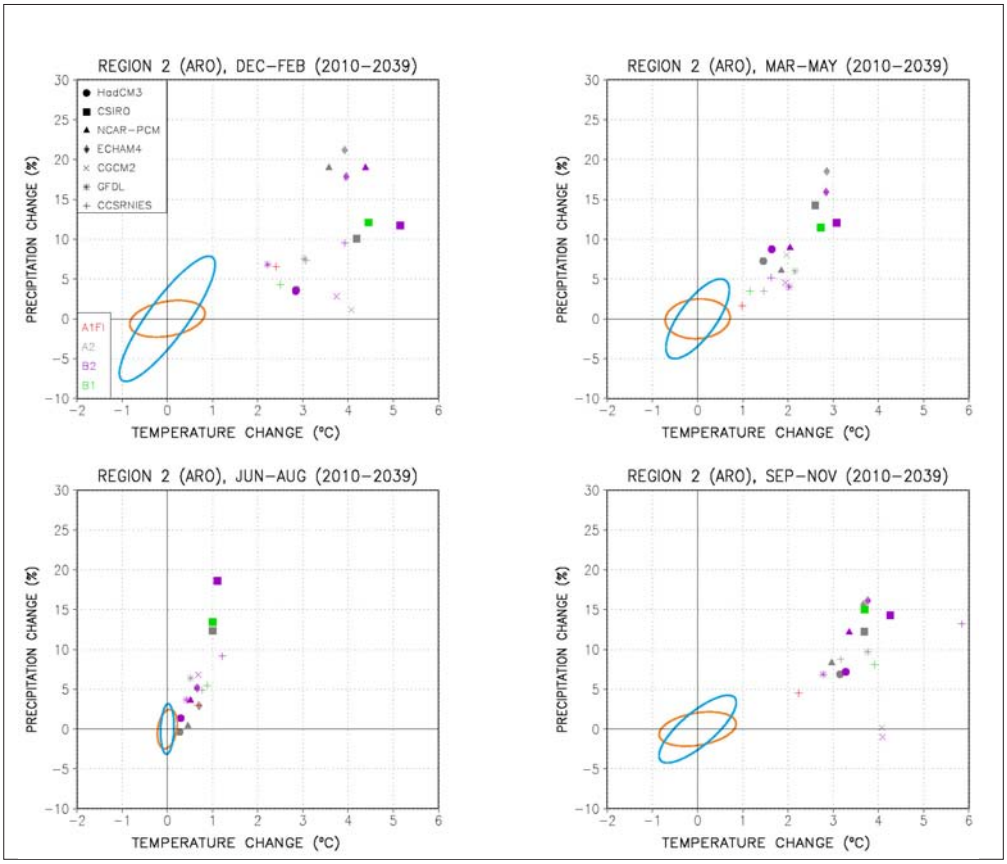

Region 2: Arctic Ocean (2040–2069)

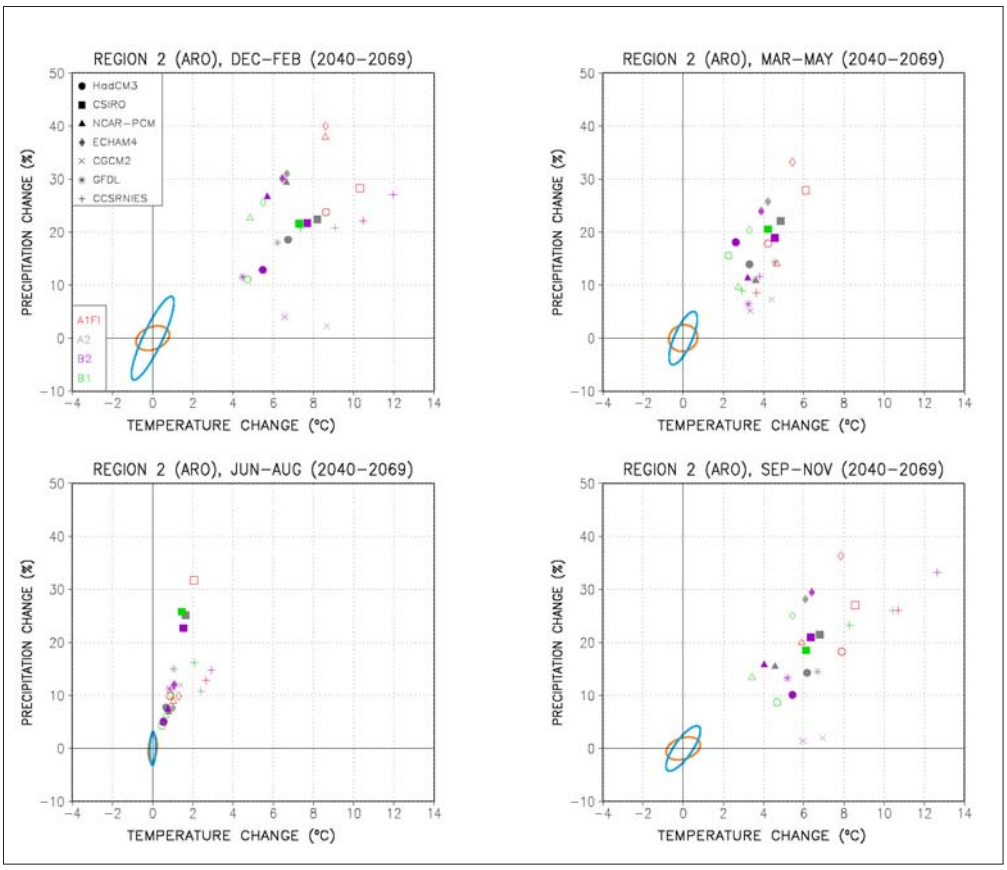

Region 2: Arctic Ocean (2070–2099)

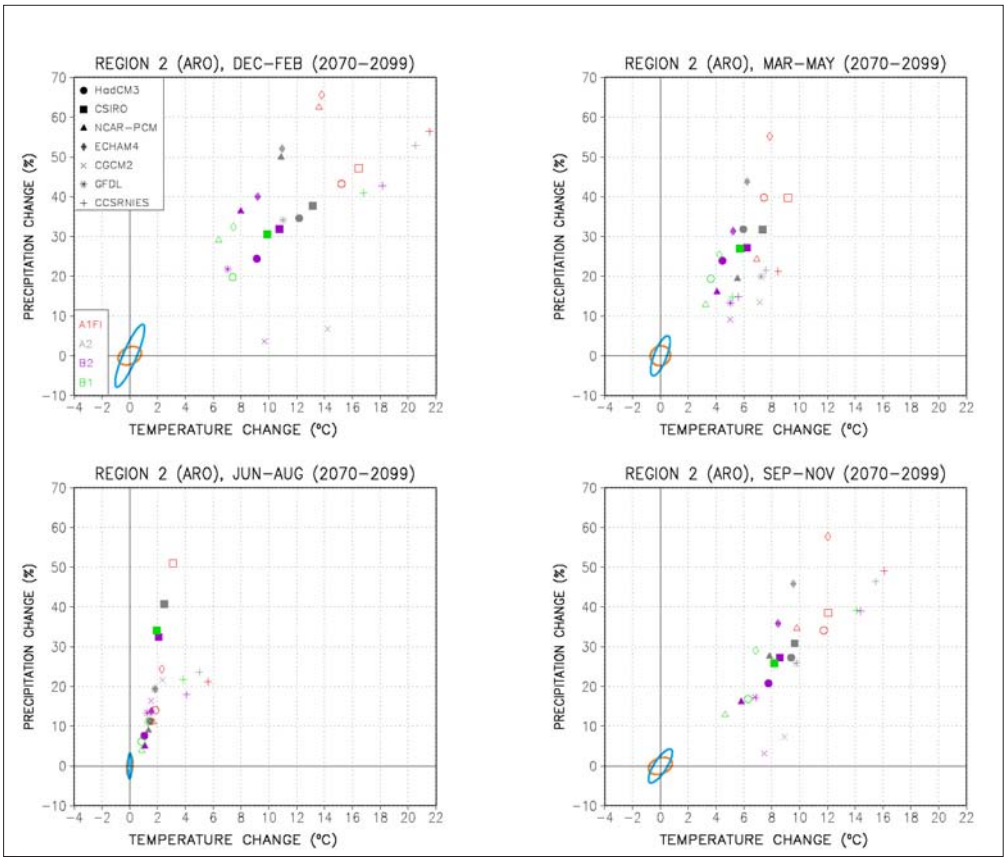

Region 3: Antarctic Land (2010–2039)

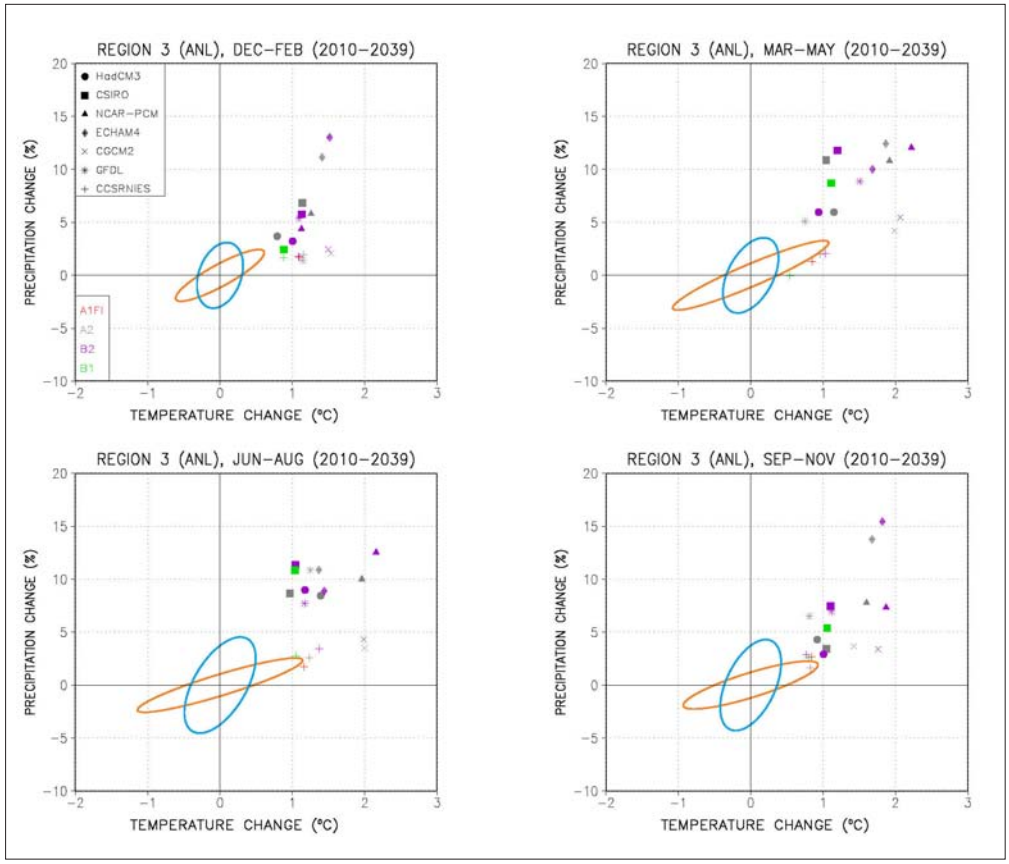

Region 3: Antarctic Land (2040–2069)

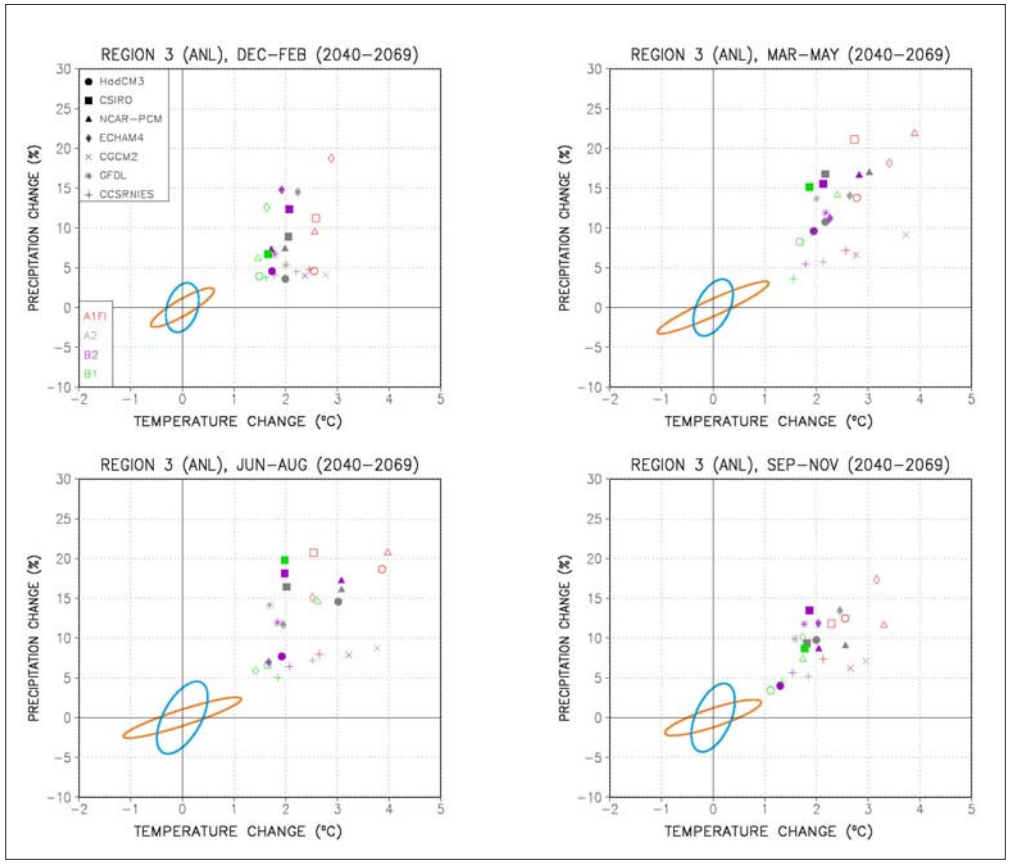

Region 3: Antarctic Land (2070–2099)

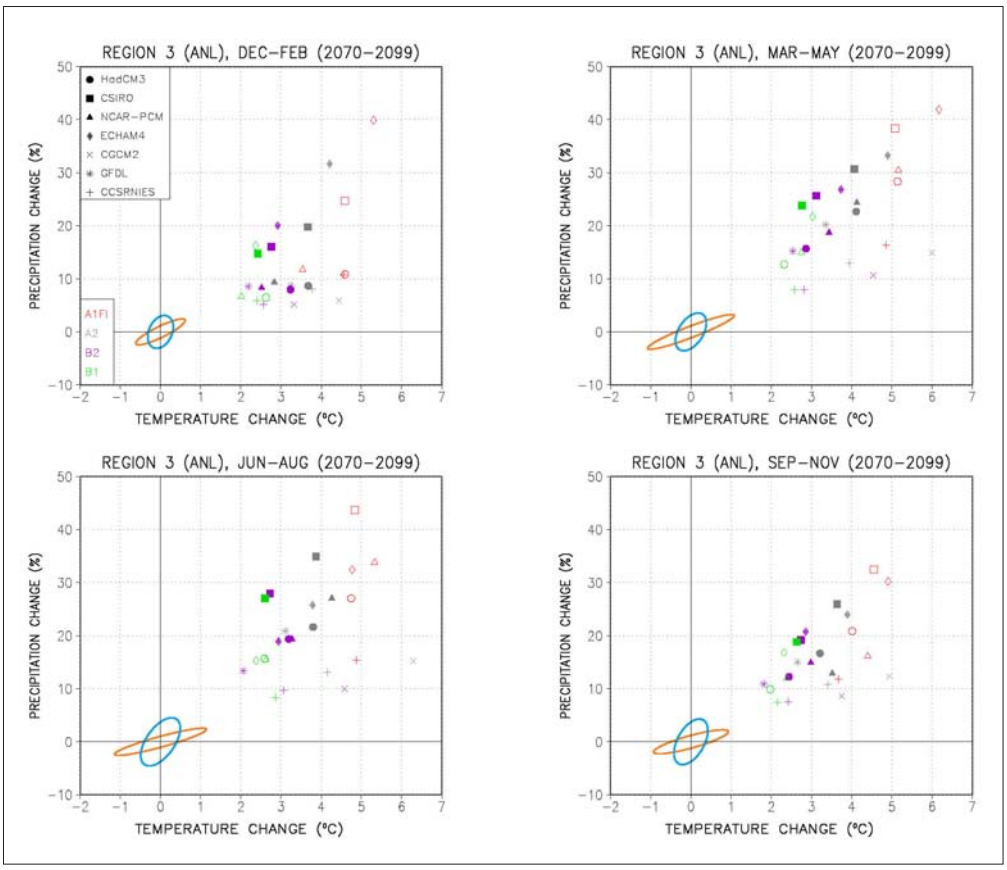

Region 4: Antarctic Ocean (2010–2039)

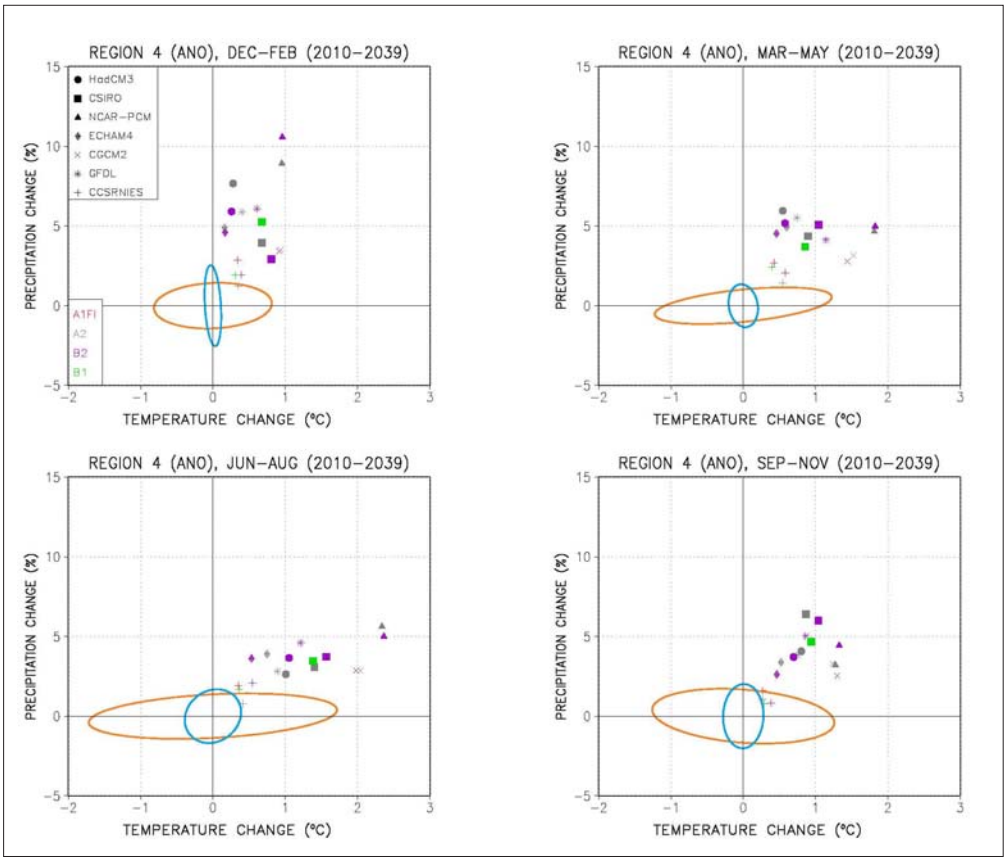

Region 4: Antarctic Ocean (2040–2069)

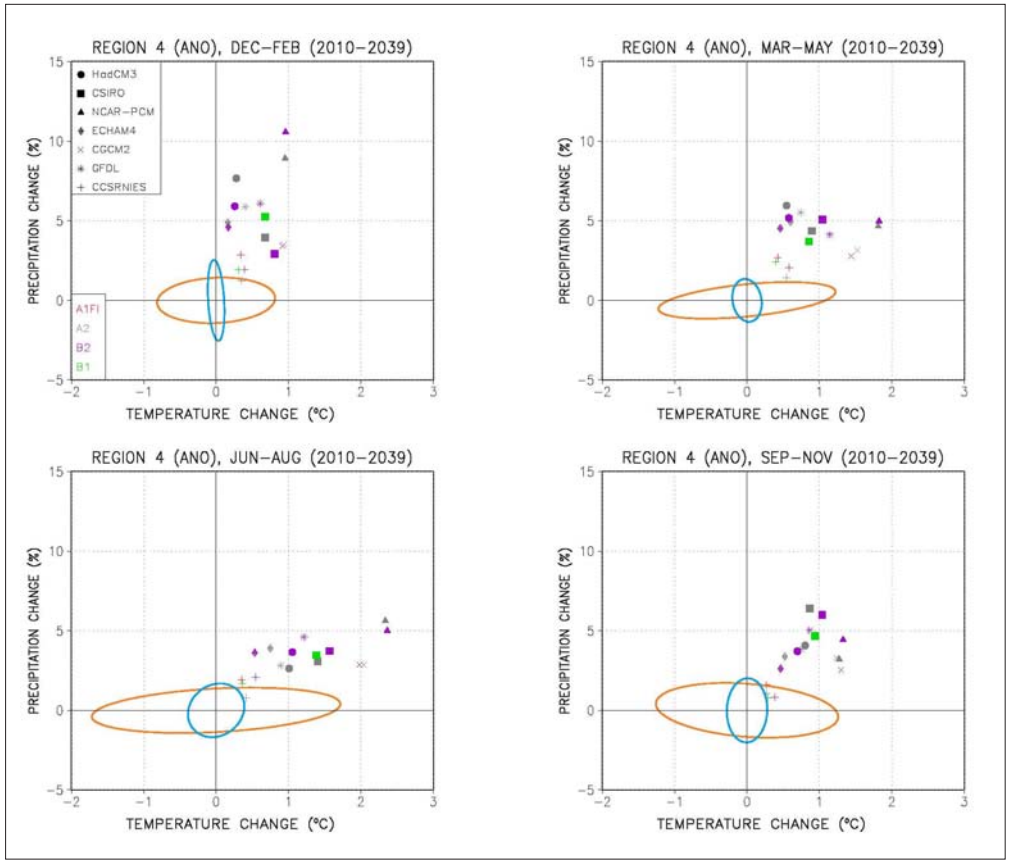

Region 4: Antarctic Ocean (2070–2099)

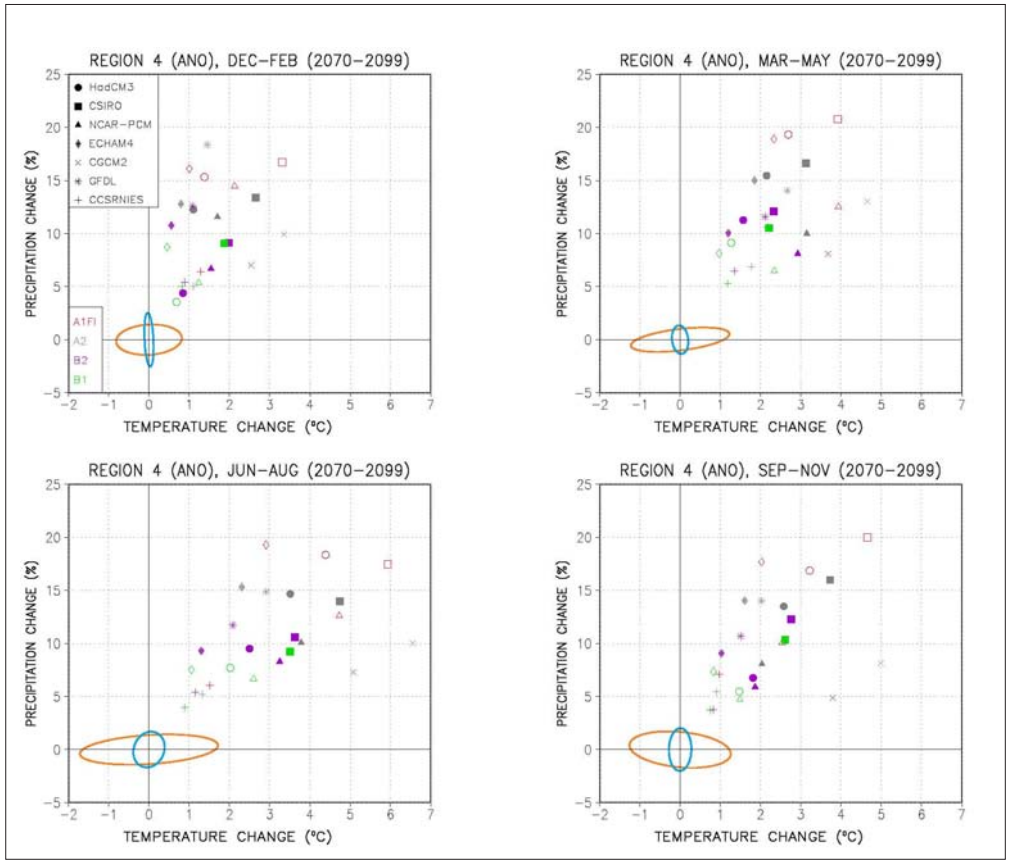

Region 5: Alaska, NW Canada (2010–2039)

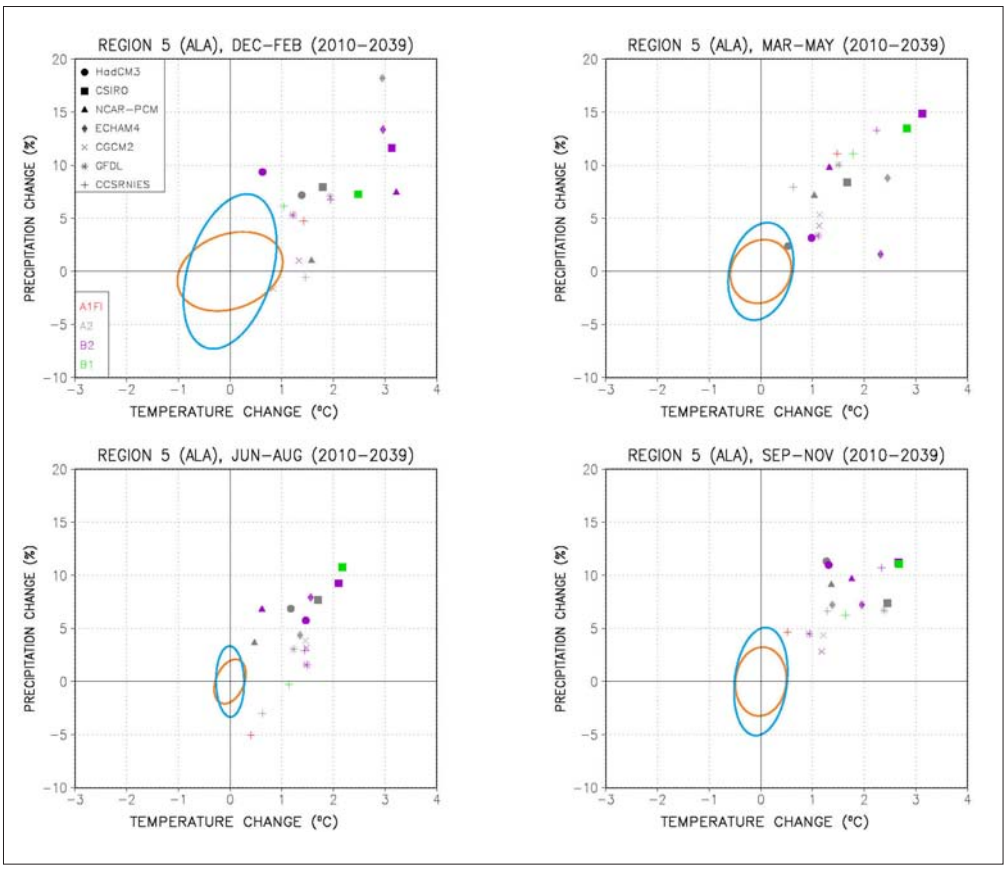

Region 5: Alaska, NW Canada (2040–2069)

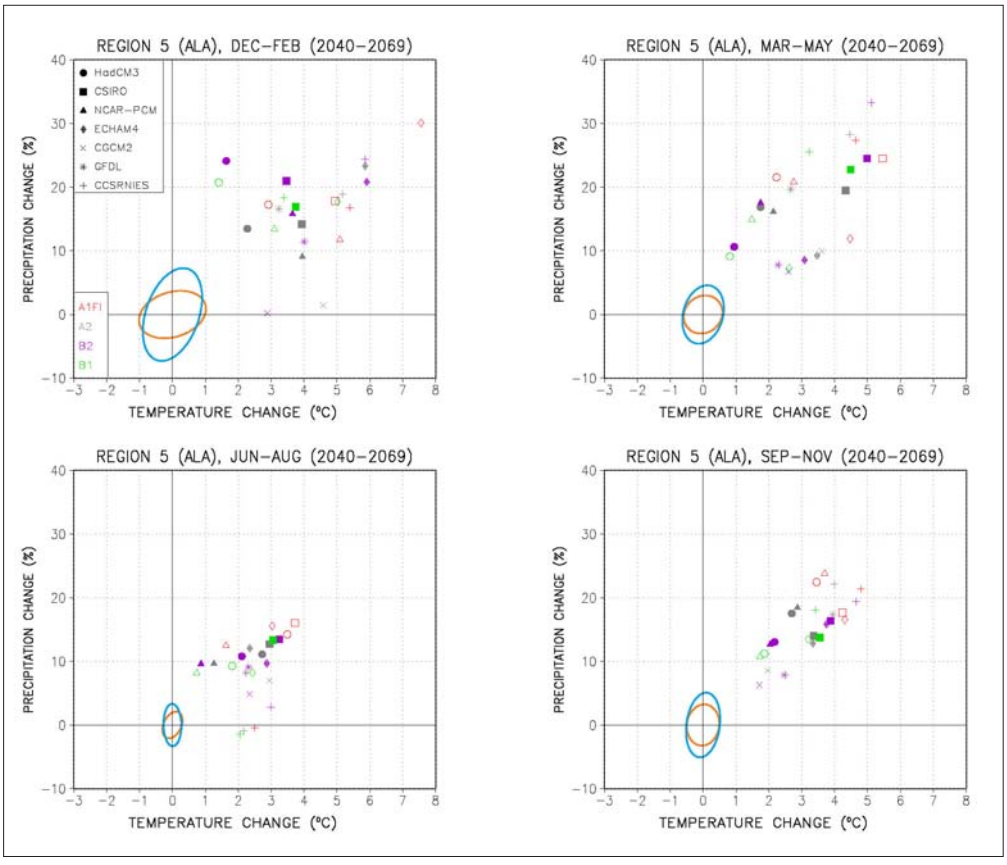

Region 5: Alaska, NW Canada (2070–2099)

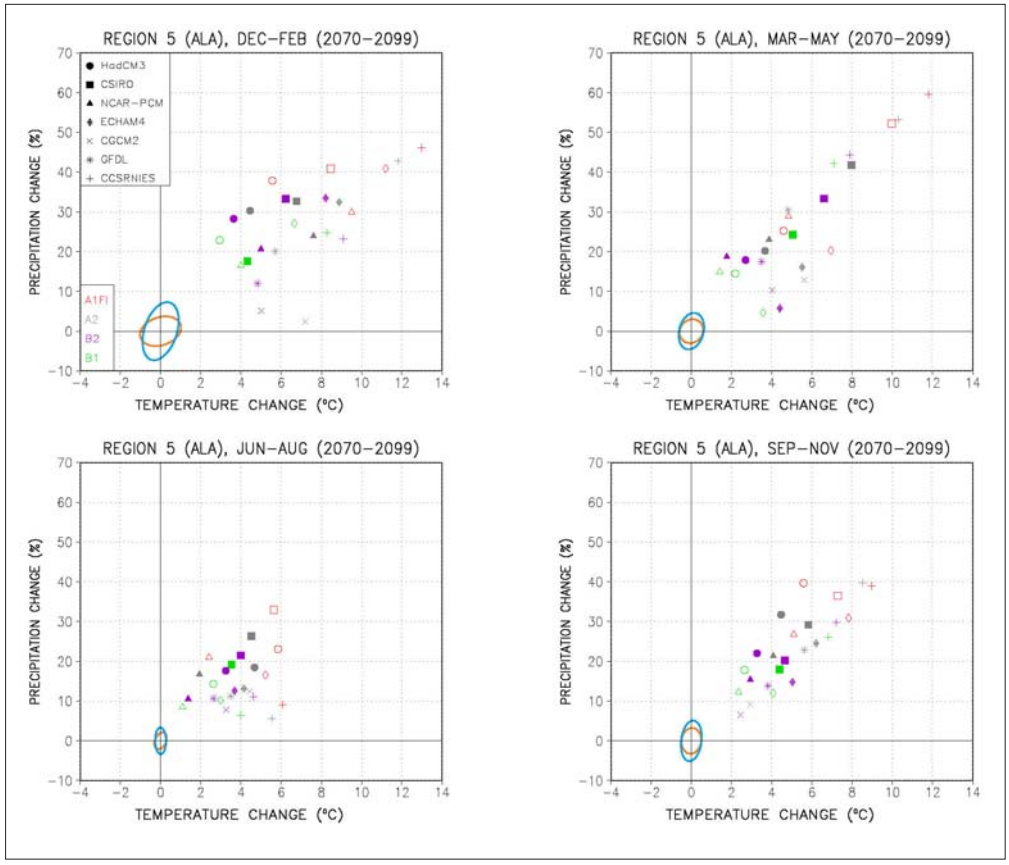

Region 6: E Canada, Greenland, Iceland (2010–2039)

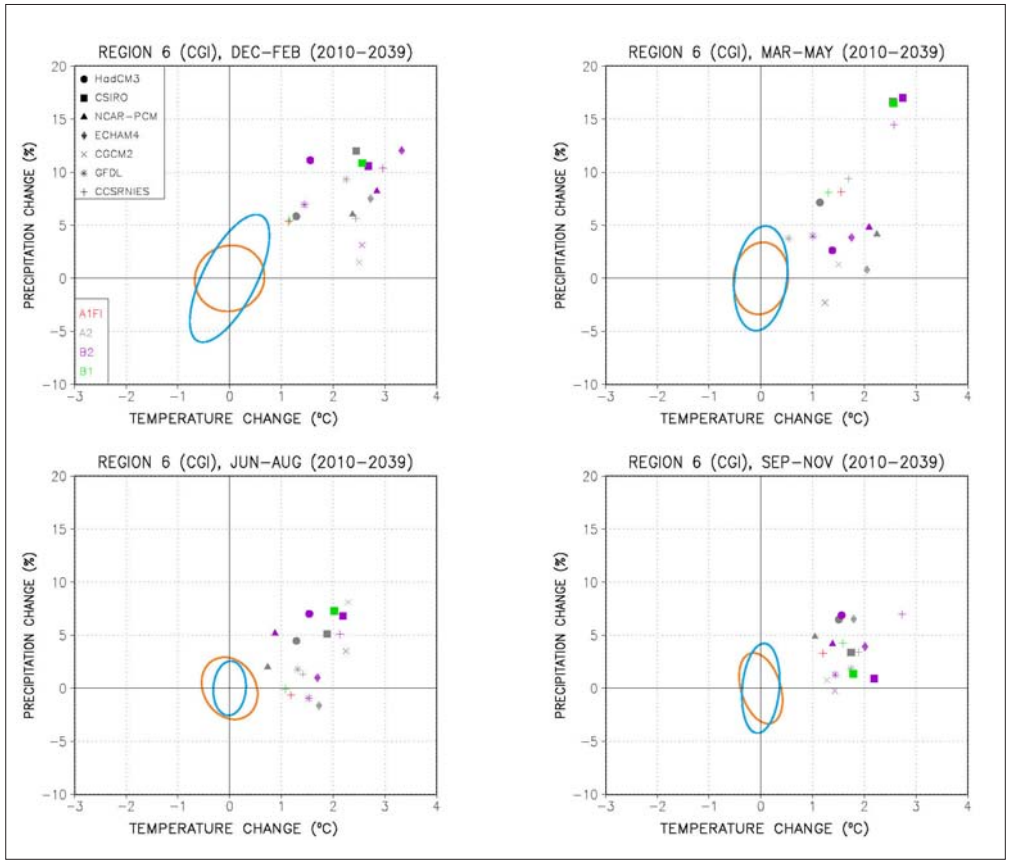

Region 6: E Canada, Greenland, Iceland (2040–2069)

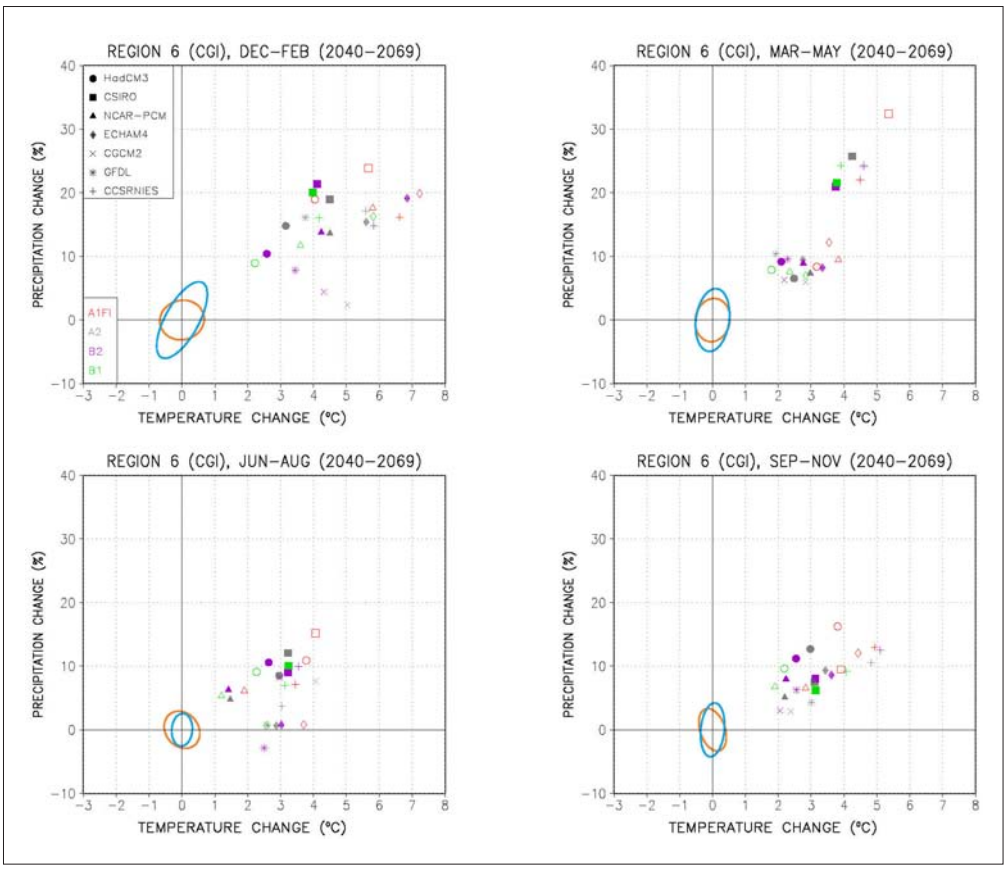

Region 6: E Canada, Greenland, Iceland (2070–2099)

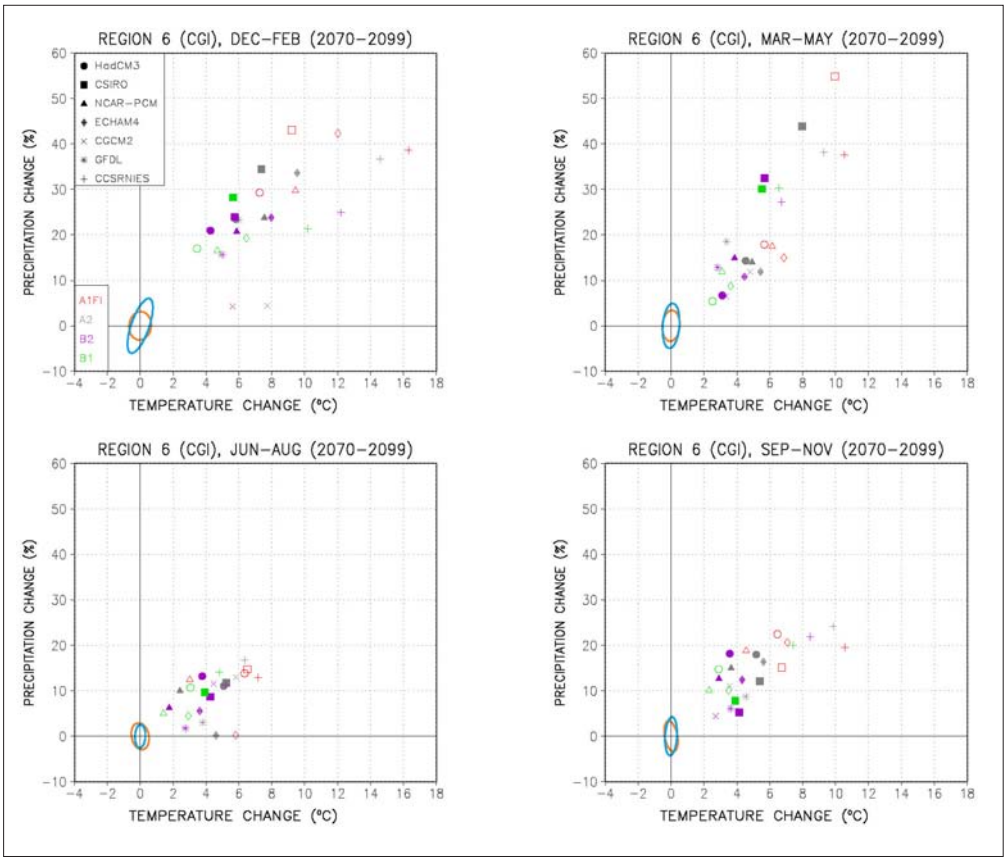

Region 7: Western N America (2010–2039)

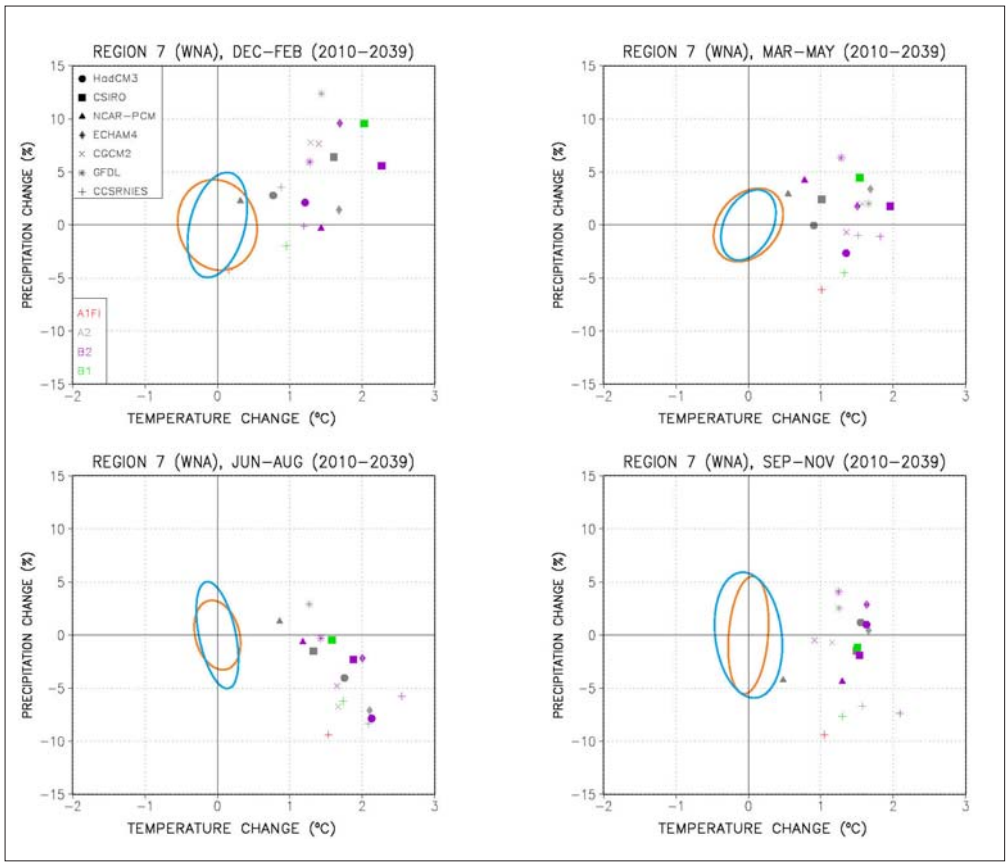

Region 7: Western N America (2040–2069)

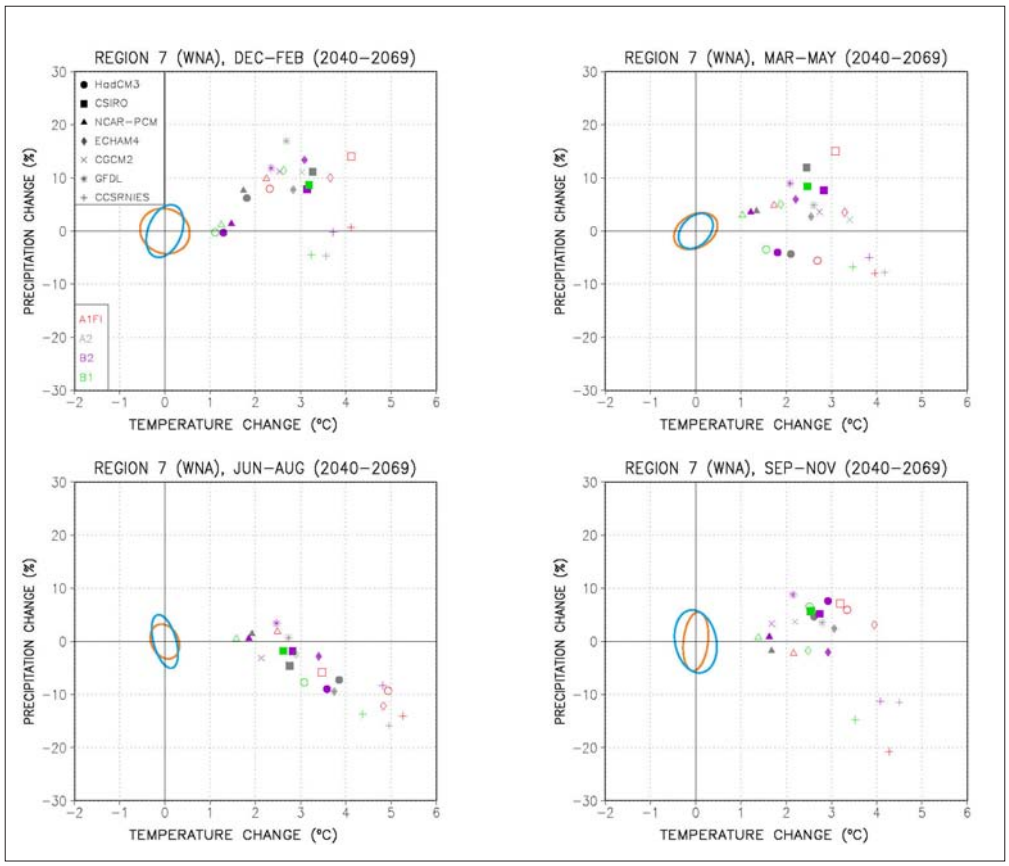

Region 7: Western N America (2070–2099)

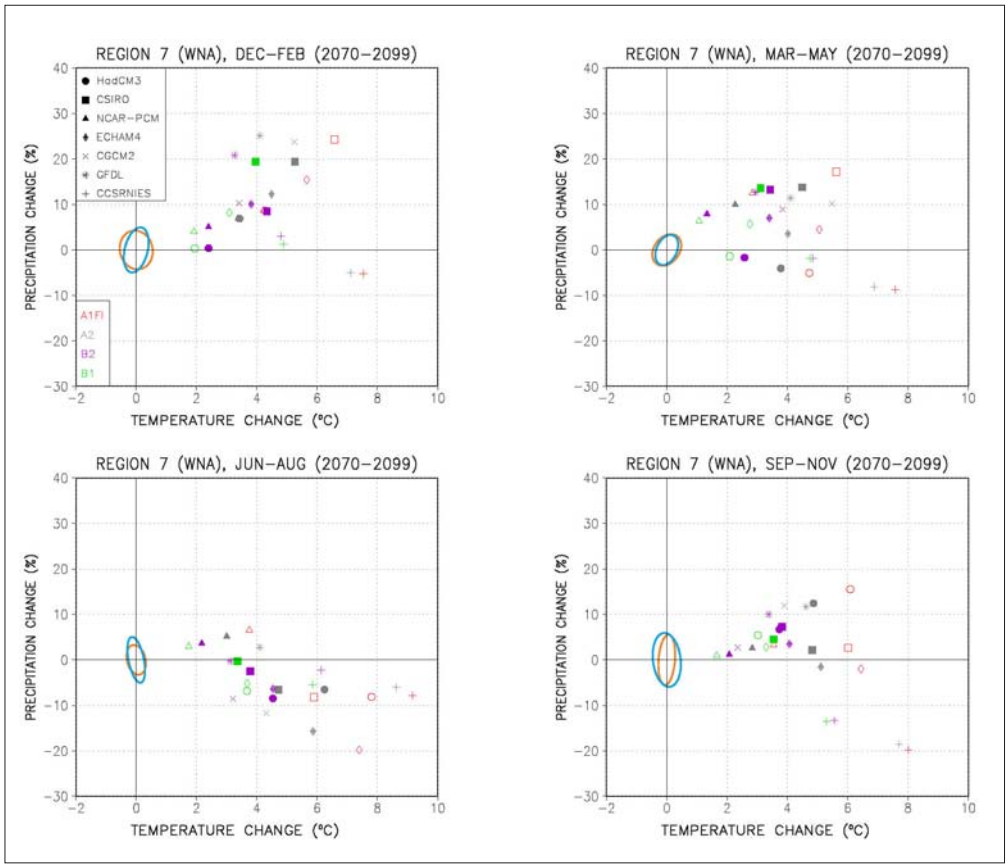

Region 8: Central N America (2010–2039)

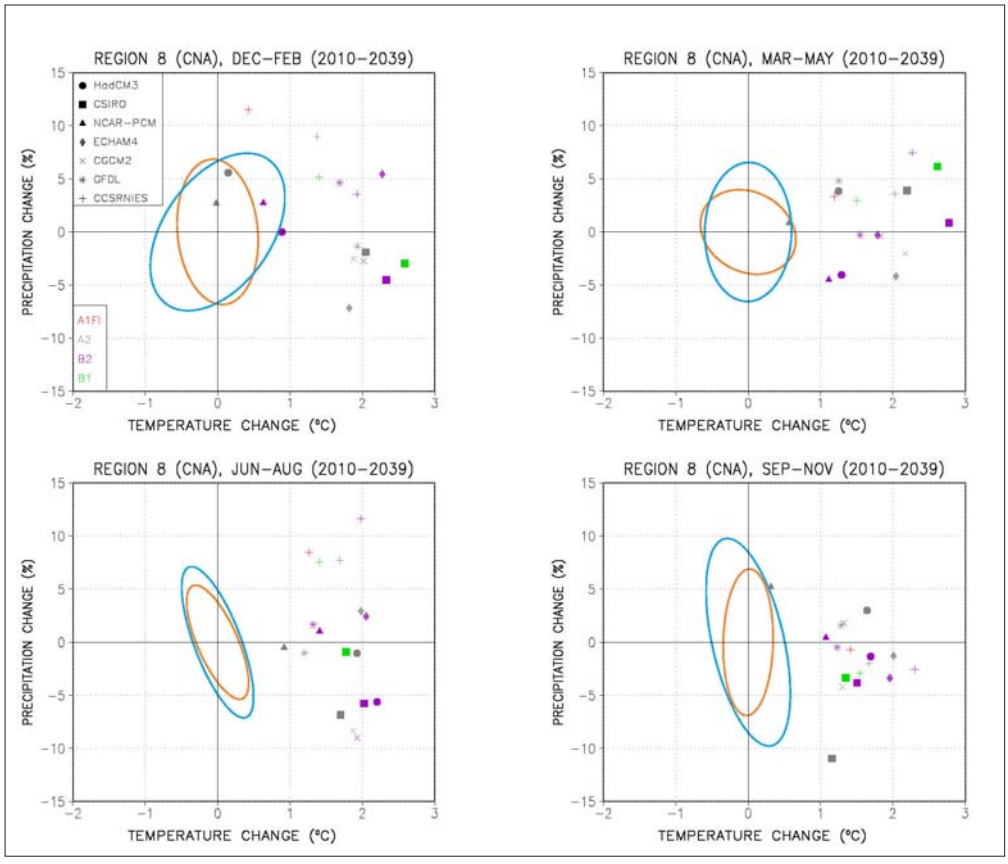

Region 8: Central N America (2040–2069)

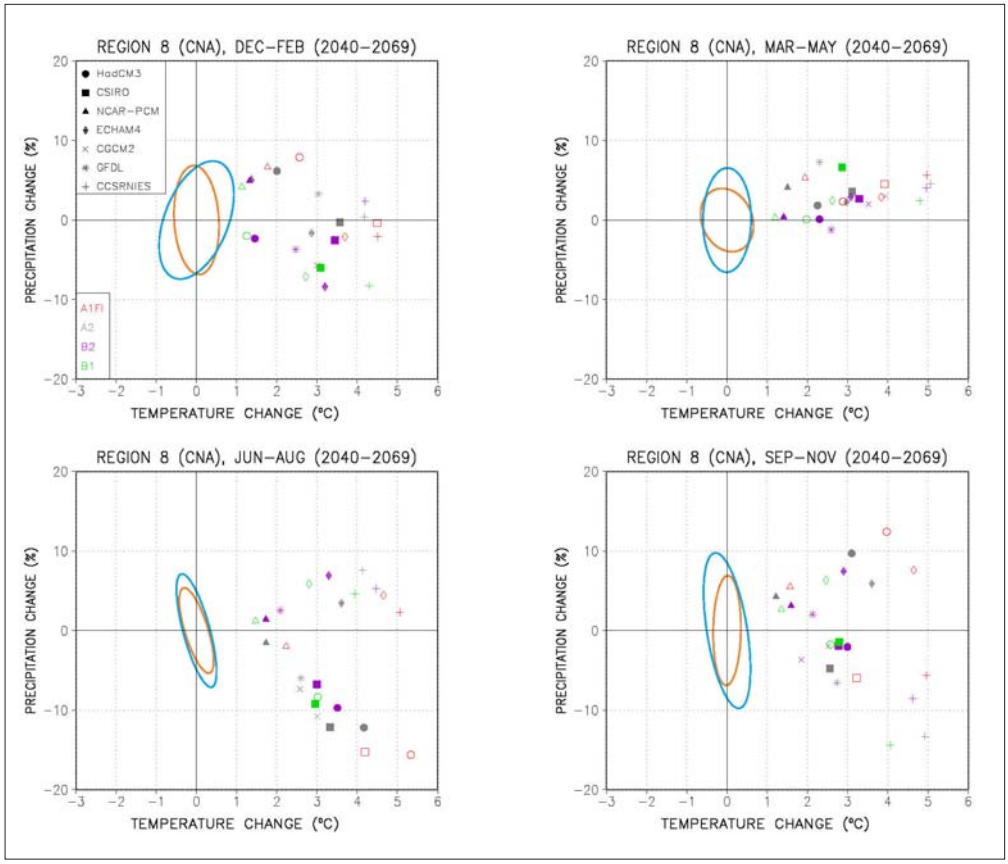

Region 8: Central N America (2070–2099)

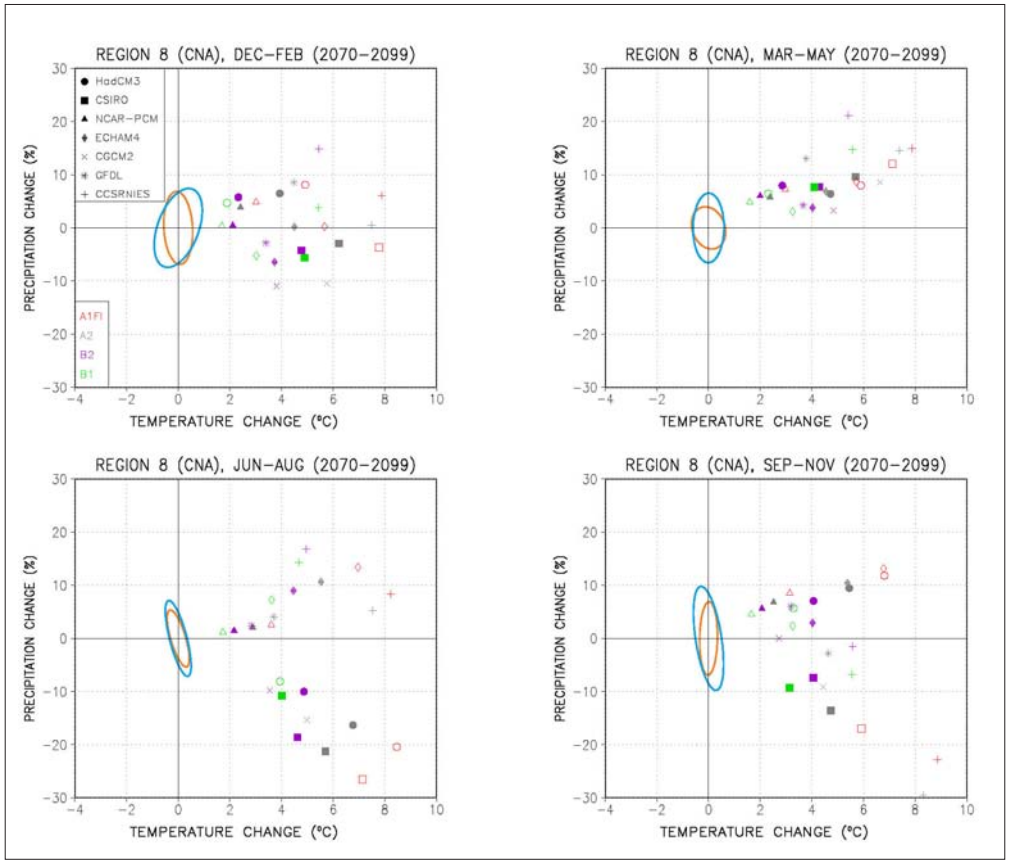

Region 9: Eastern N America (2010–2039)

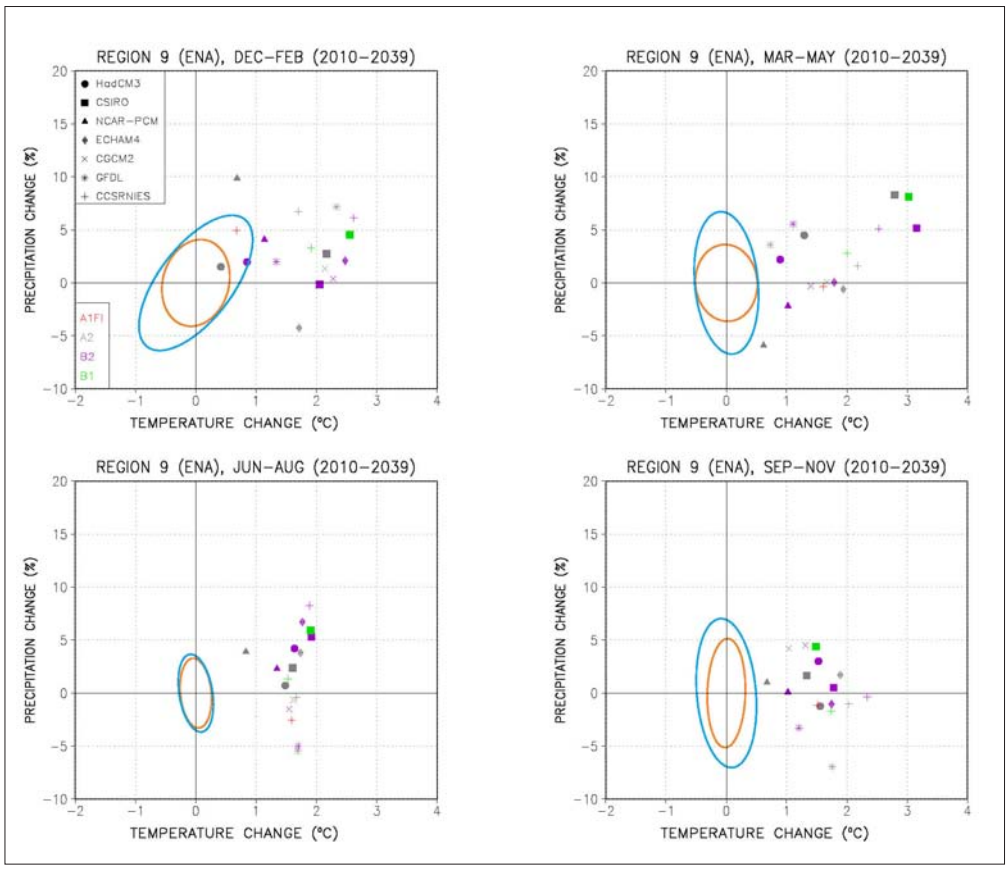

Region 9: Eastern N America (2040–2069)

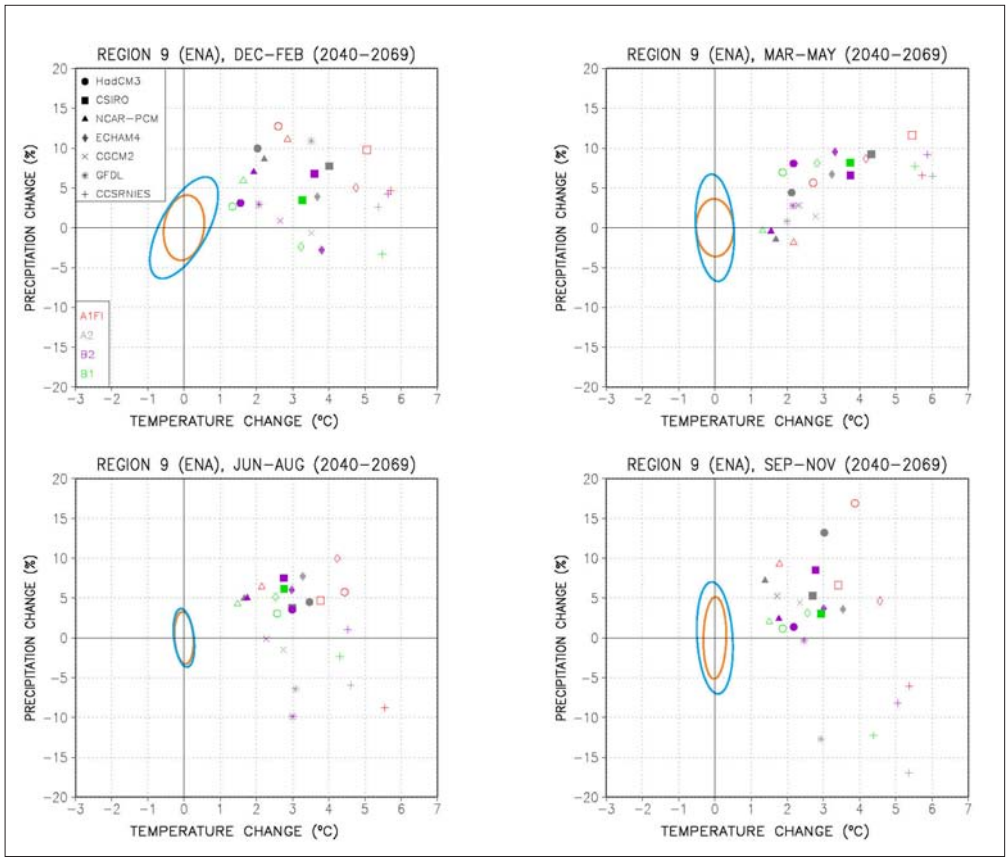

Region 9: Eastern N America (2070–2099)

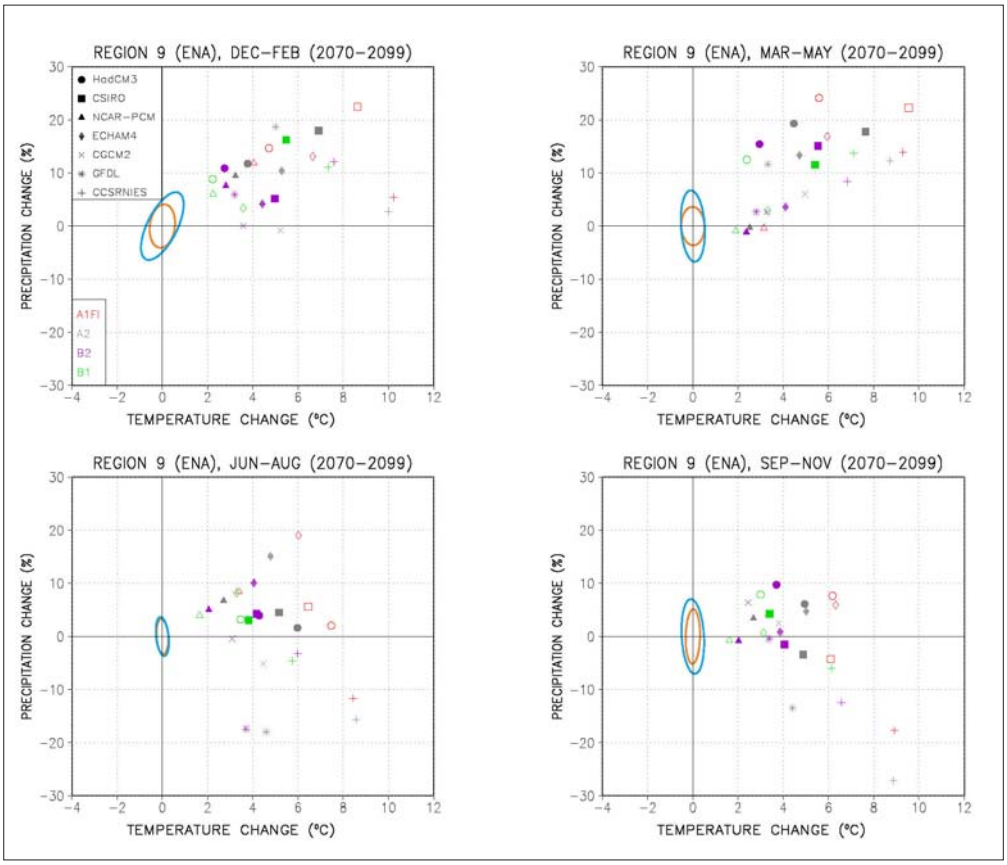

Region 10: Central America (2010–2039)

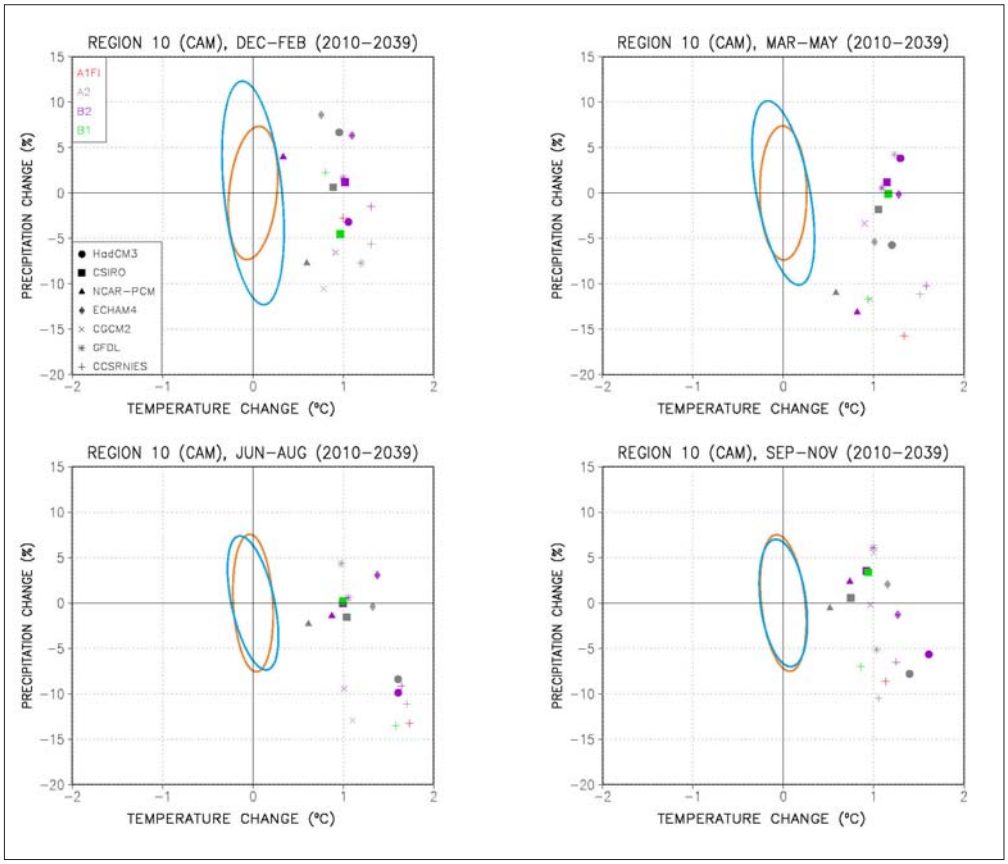

Region 10: Central America (2040–2069)

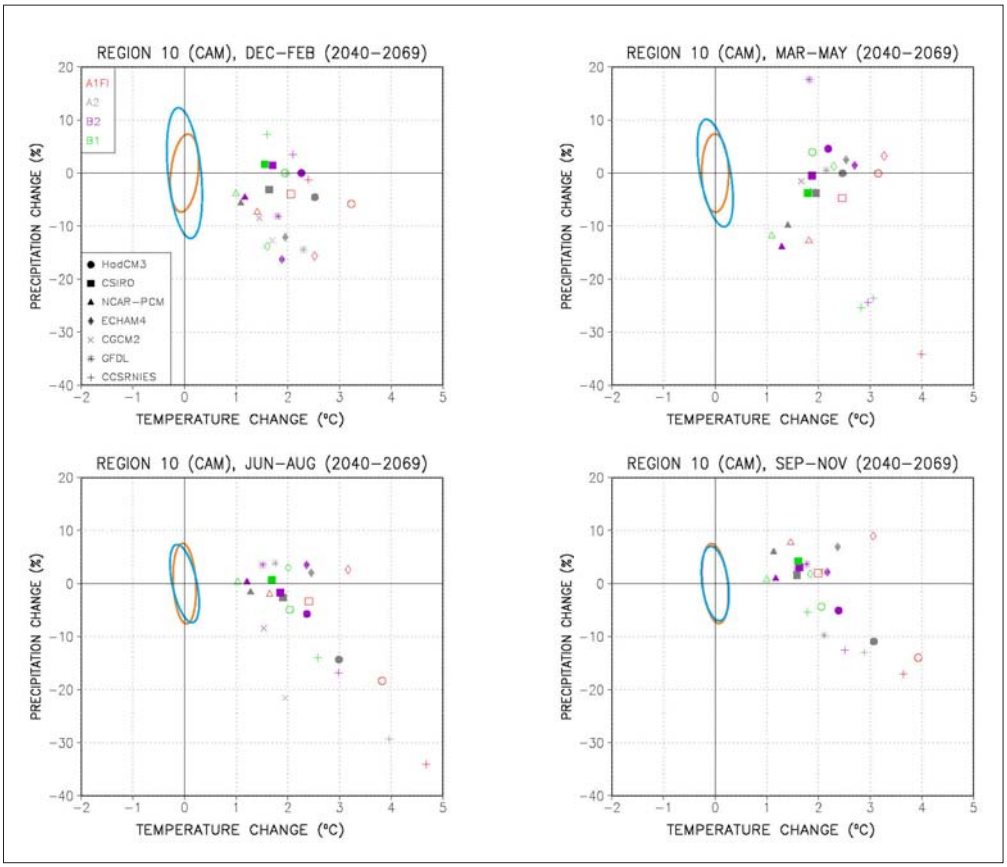

Region 10: Central America (2070–2099)

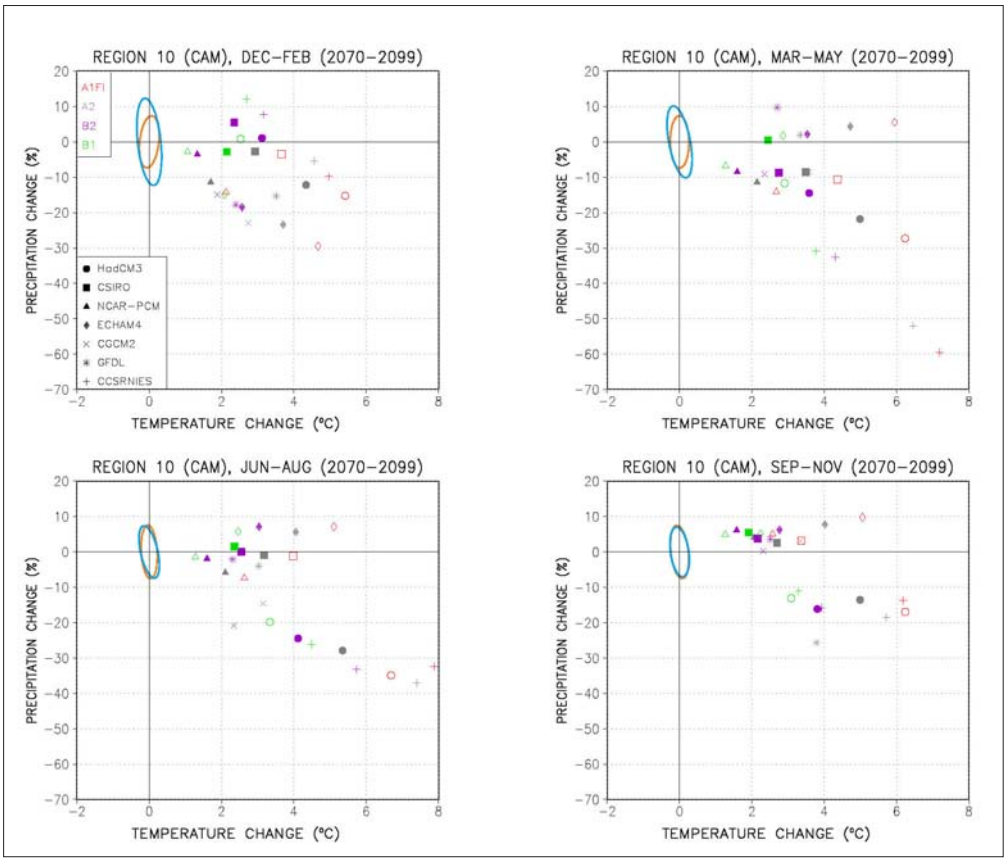

Region 11: Amazonia (2010–2039)

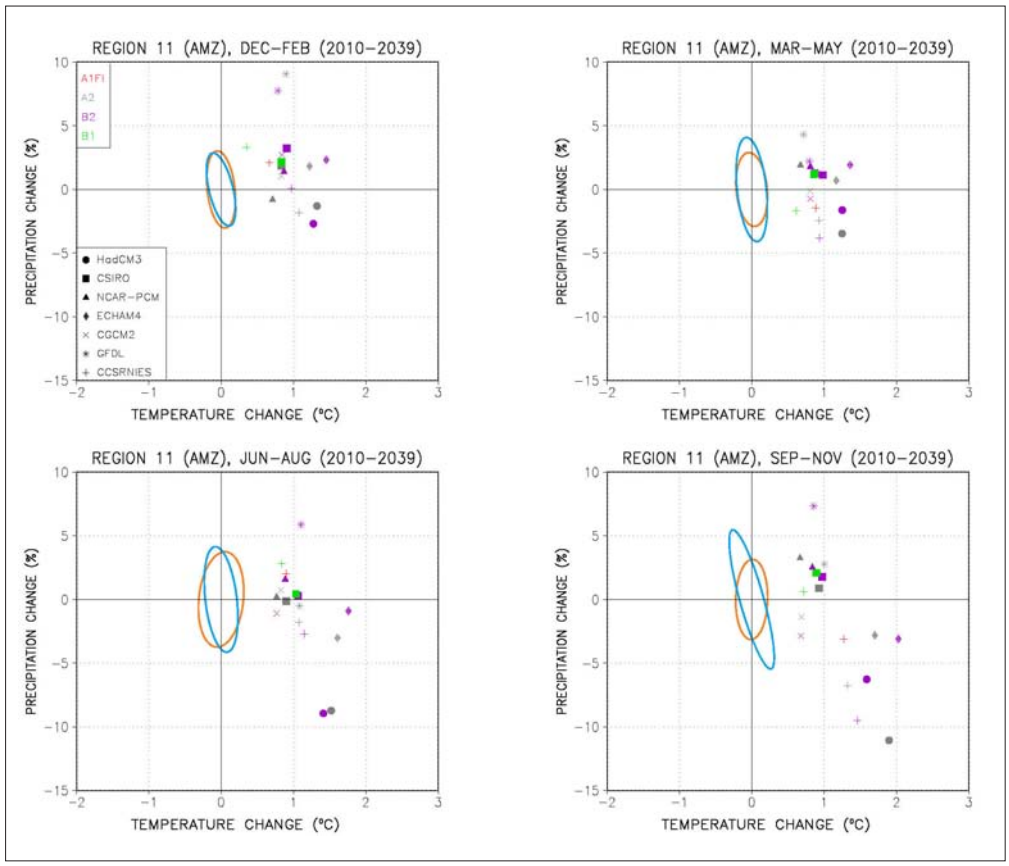

Region 11: Amazonia (2040–2069)

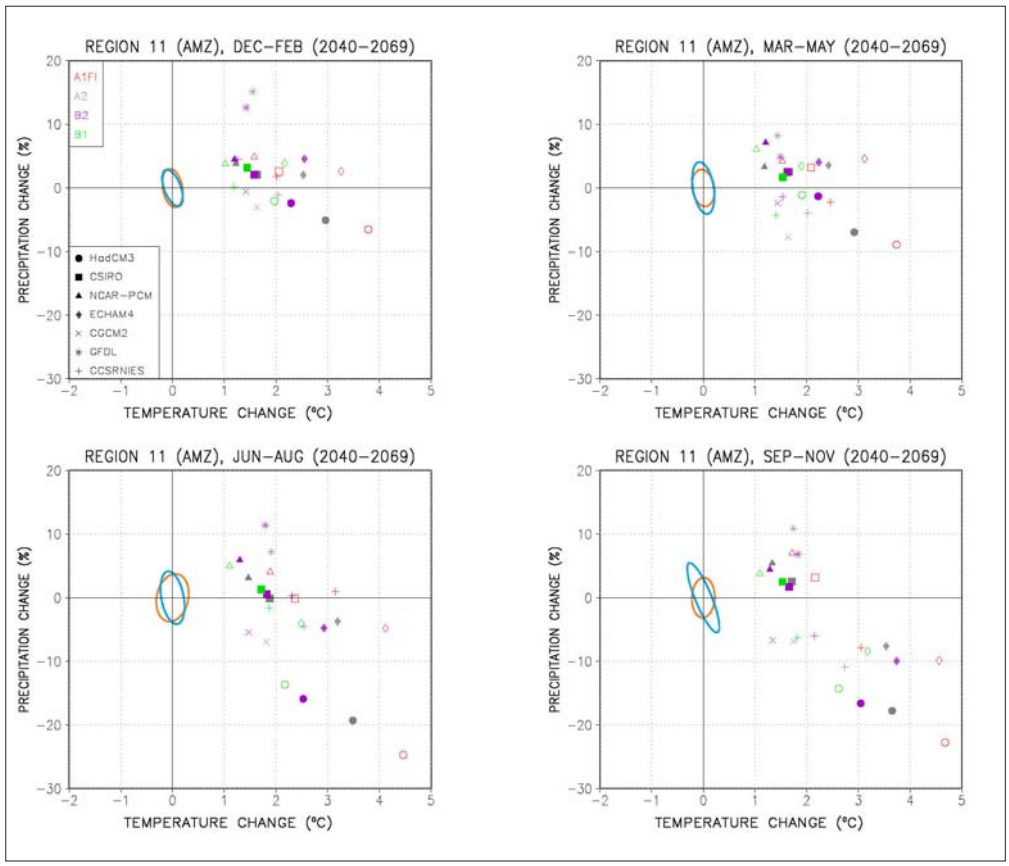

Region 11: Amazonia (2070–2099)

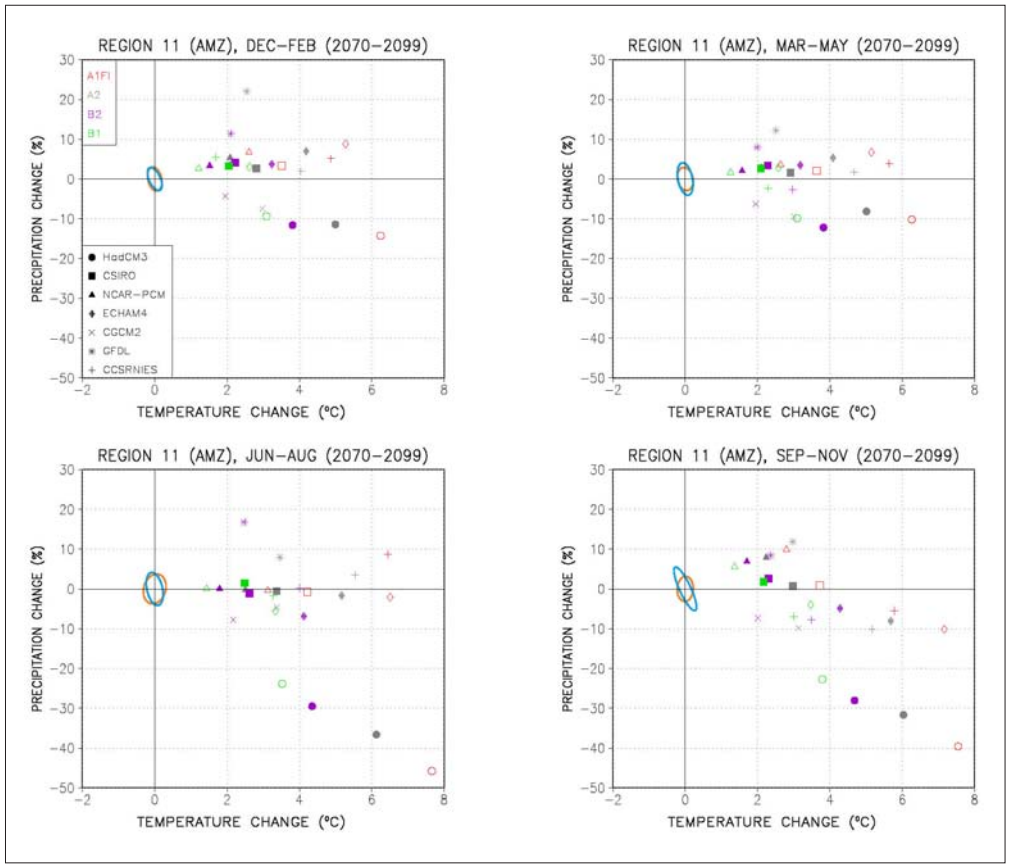

Region 12: Southern S America (2010–2039)

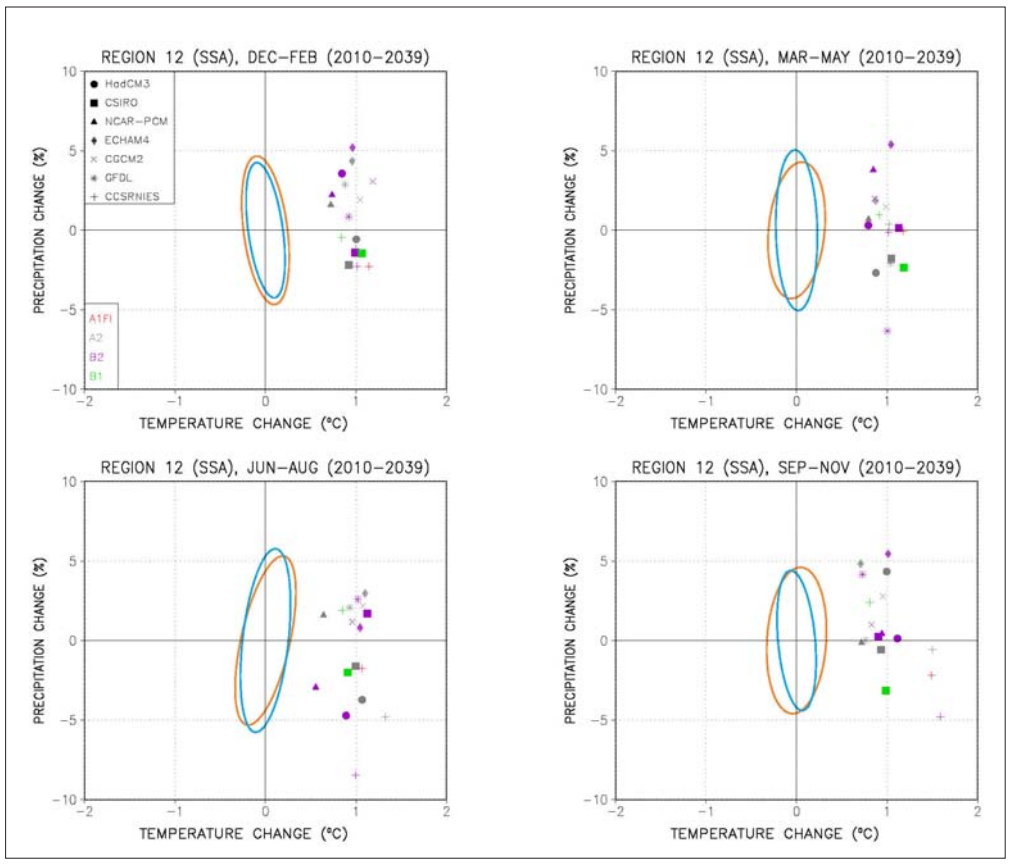

Region 12: Southern S America (2040–2069)

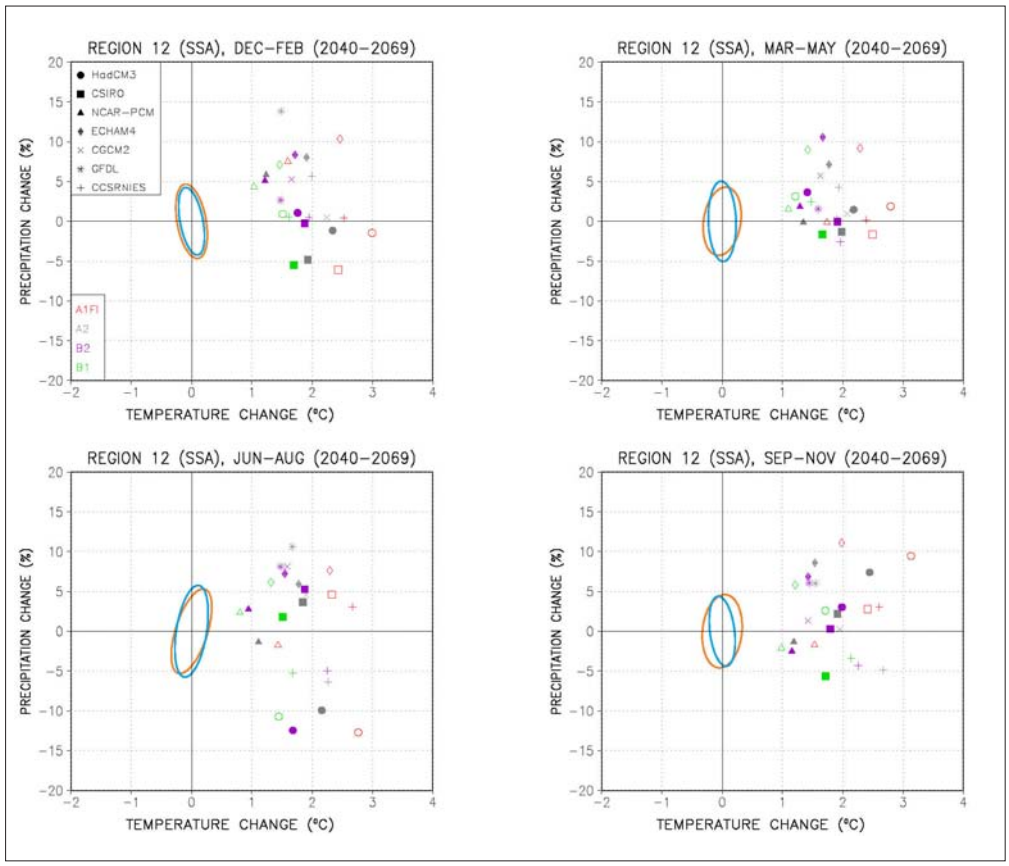

Region 12: Southern S America (2070–2099)

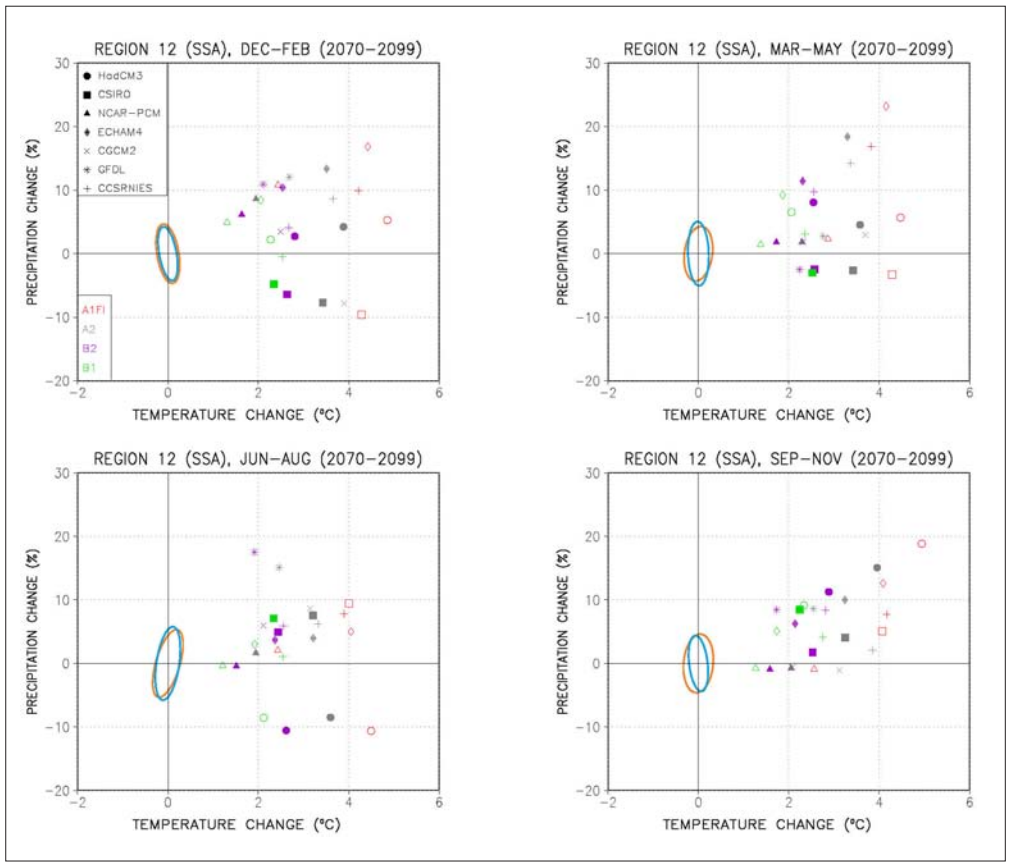

Region 13: Northern Europe (2010–2039)

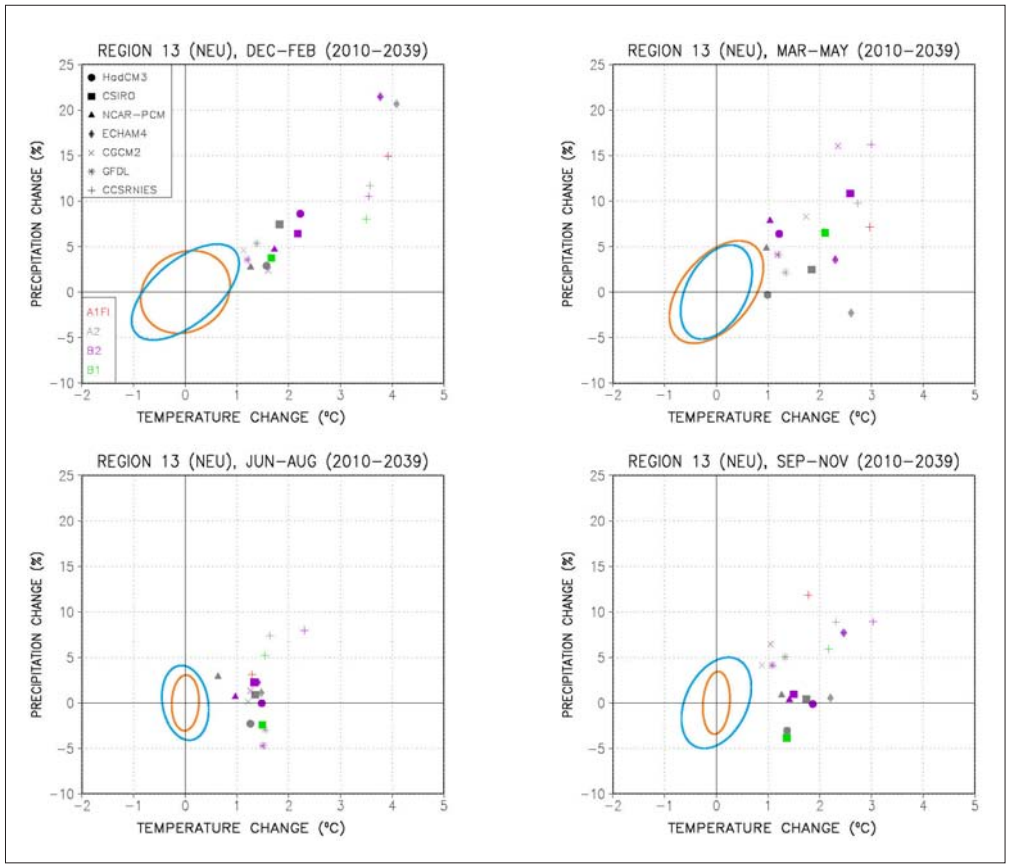

Region 13: Northern Europe (2040–2069)

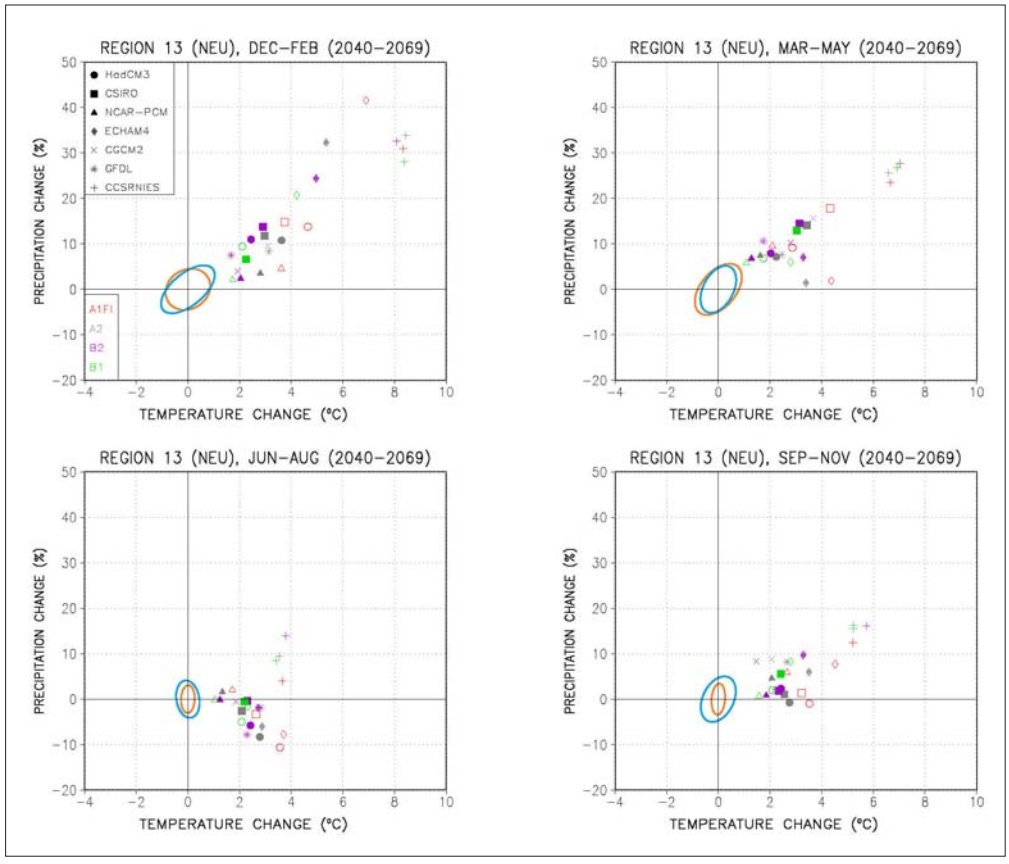

Region 13: Northern Europe (2070–2099)

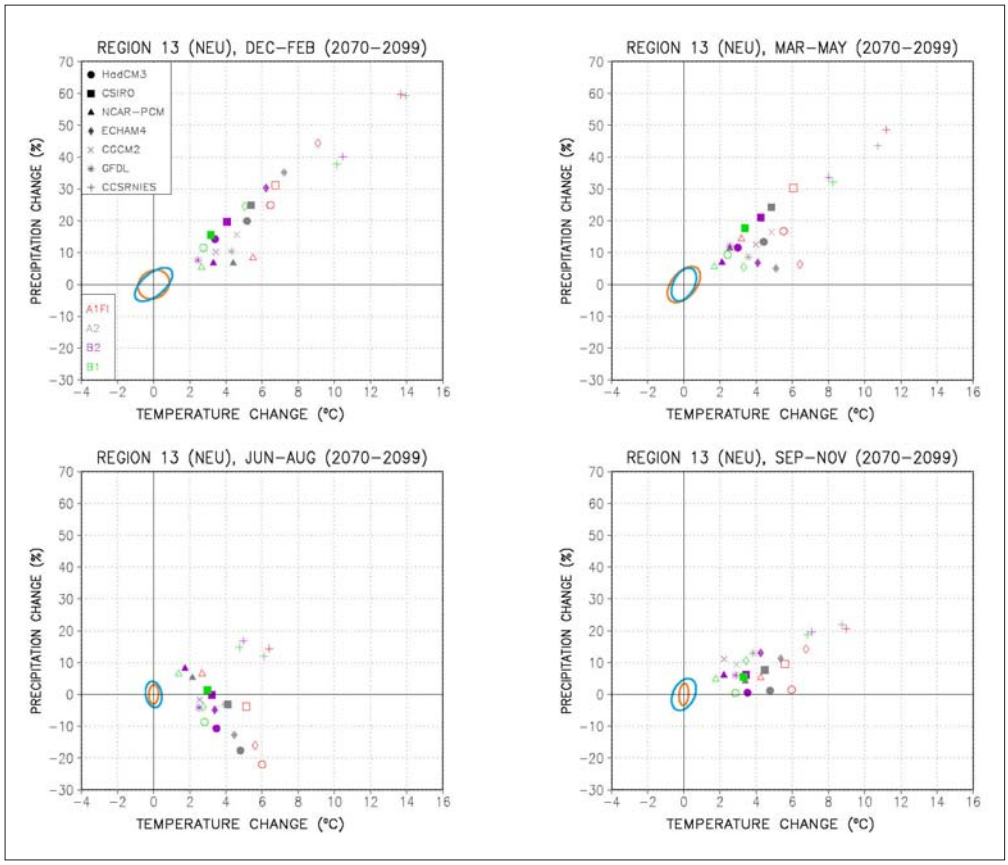

Region 14: S Europe, N Africa (2010–2039)

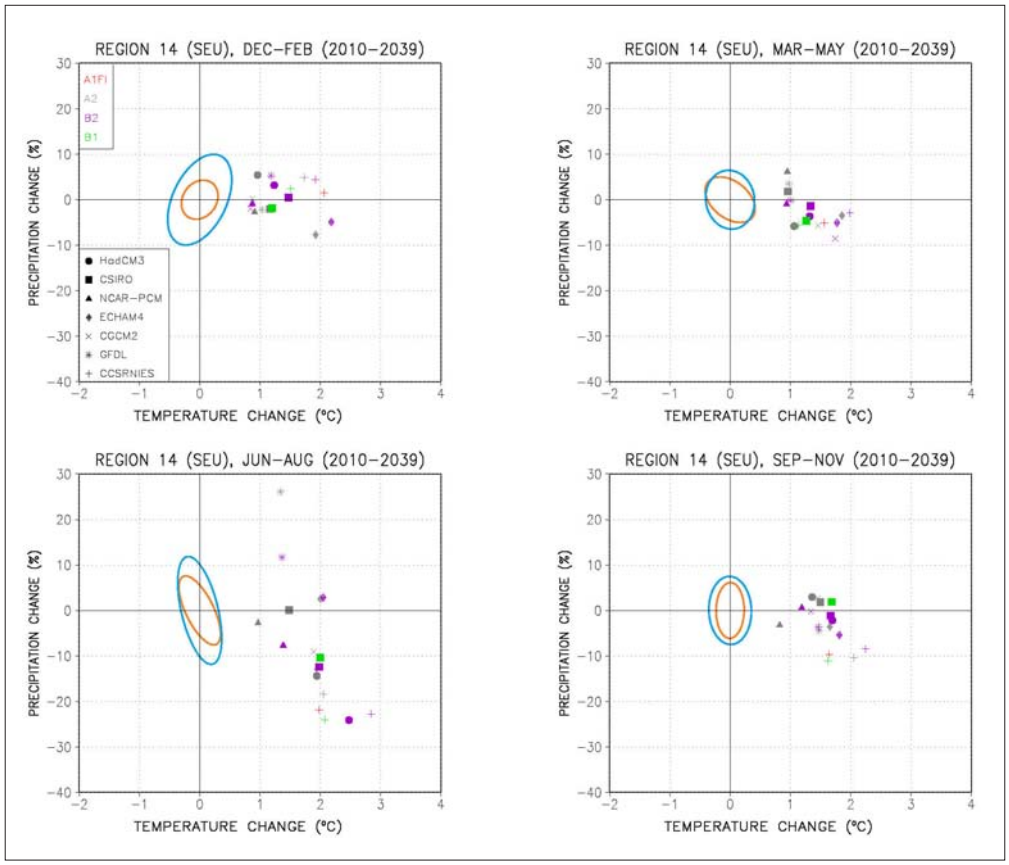

Region 14: S Europe, N Africa (2040–2069)

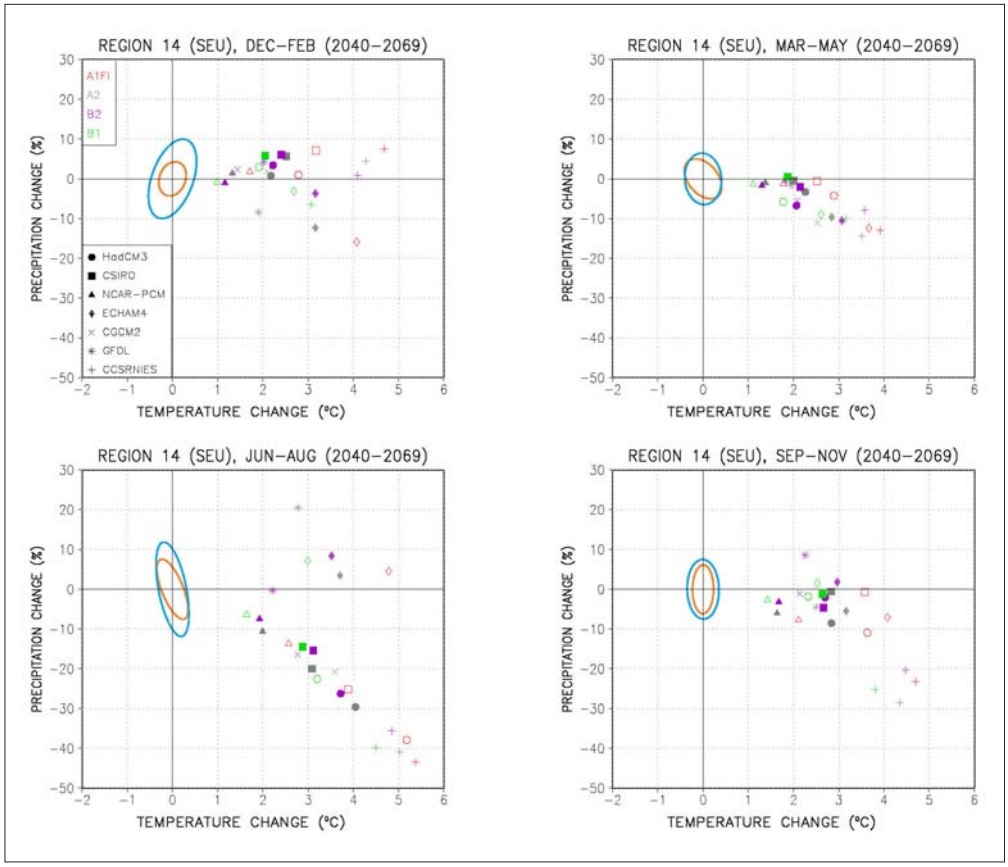

Region 14: S Europe, N Africa (2070–2099)

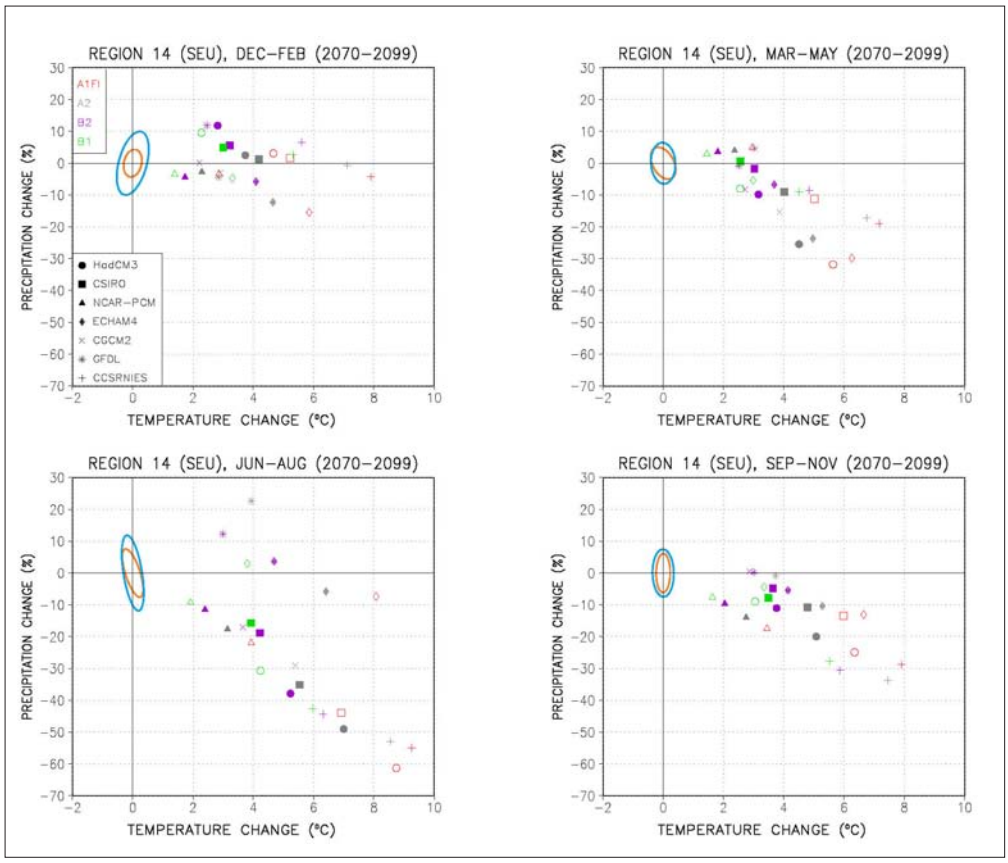

Region 15: Sahara (2010–2039)

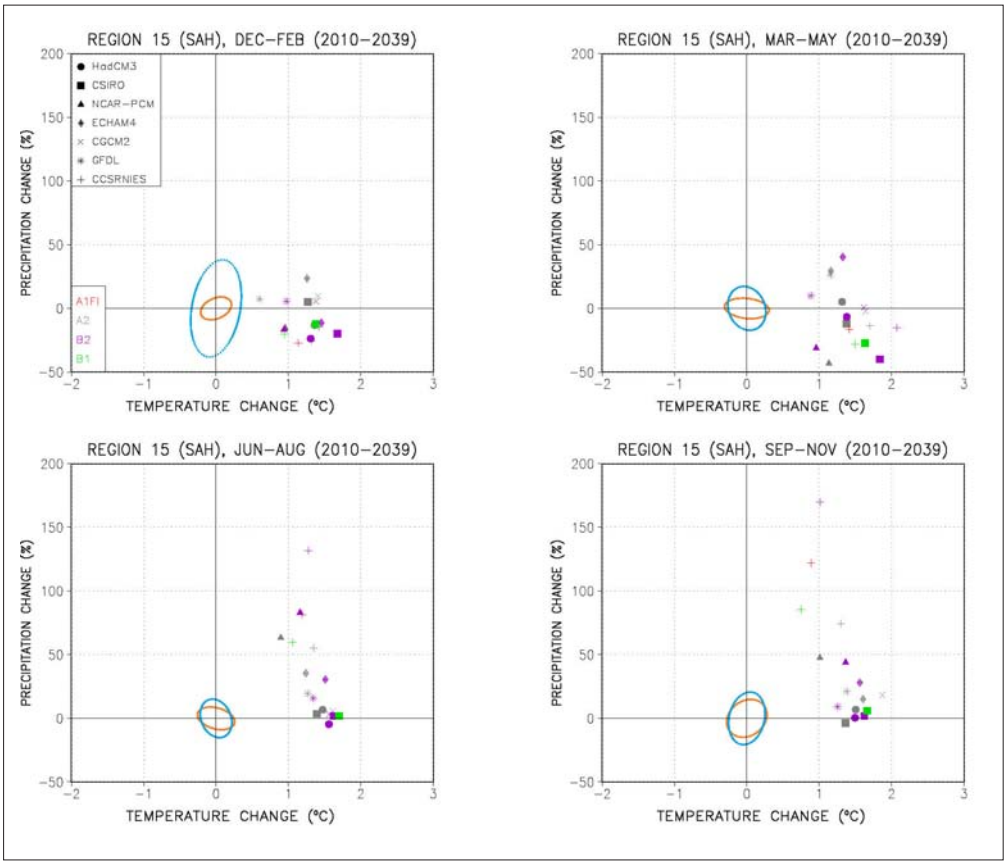

Region 15: Sahara (2040–2069)

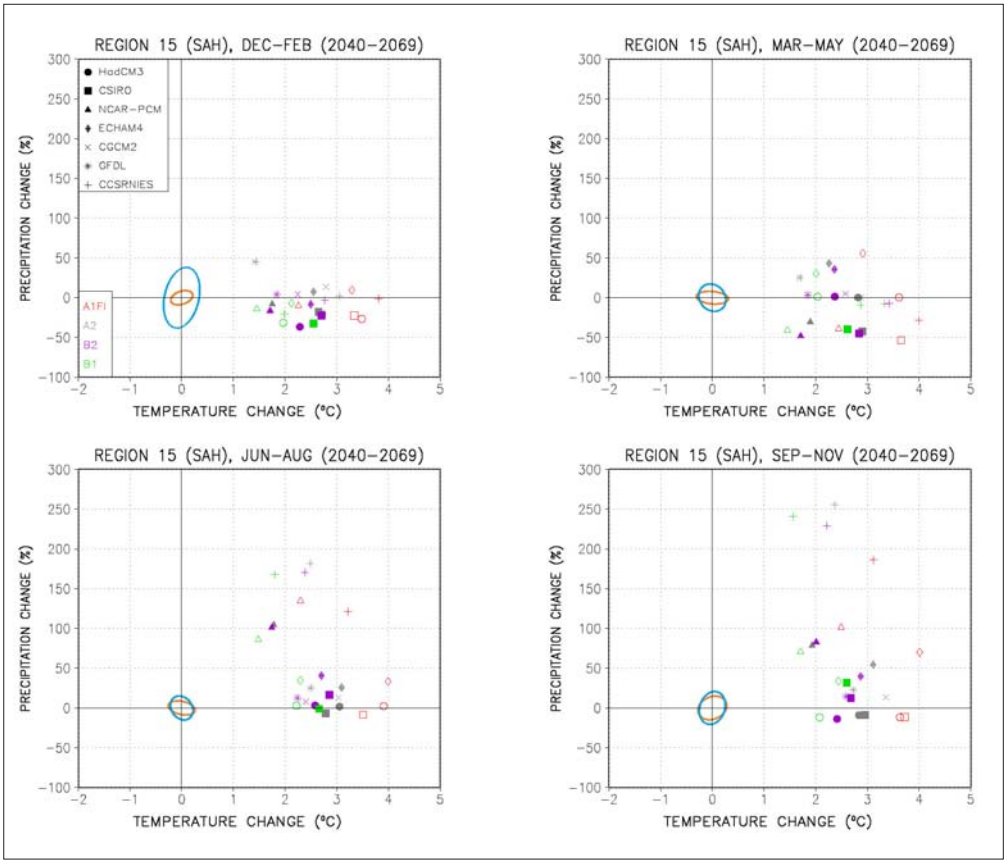

Region 15: Sahara (2070–2099)

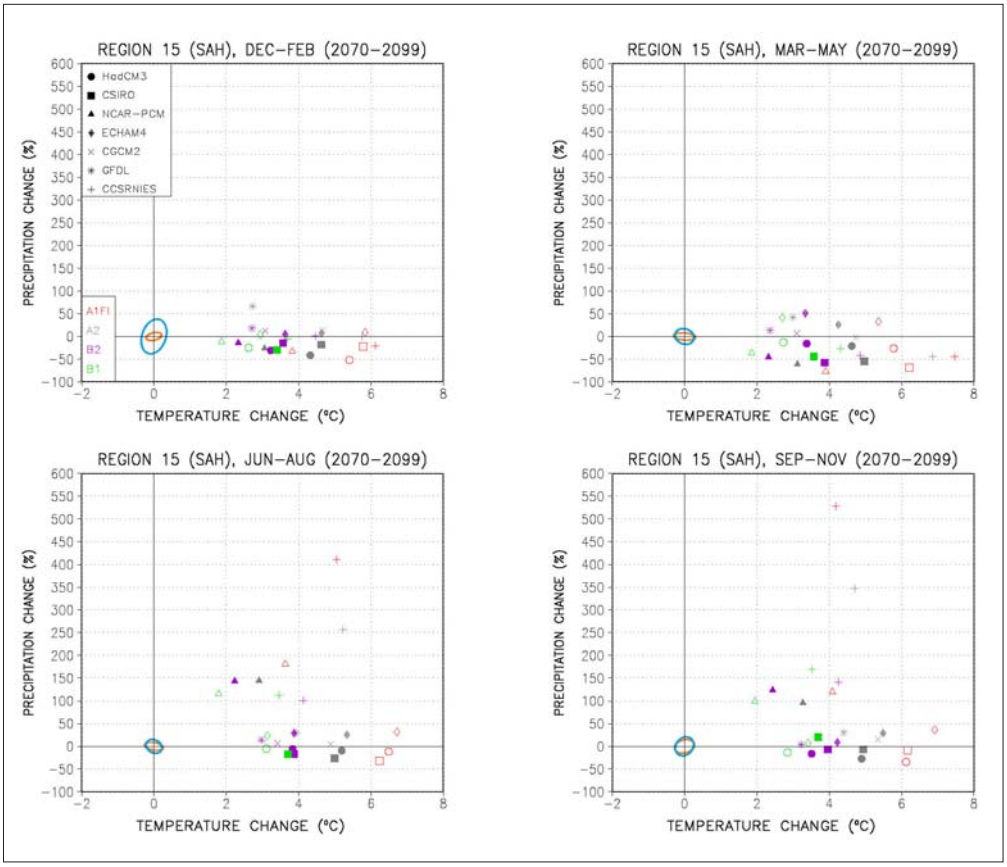

Region 16: Western Africa (2010–2039)

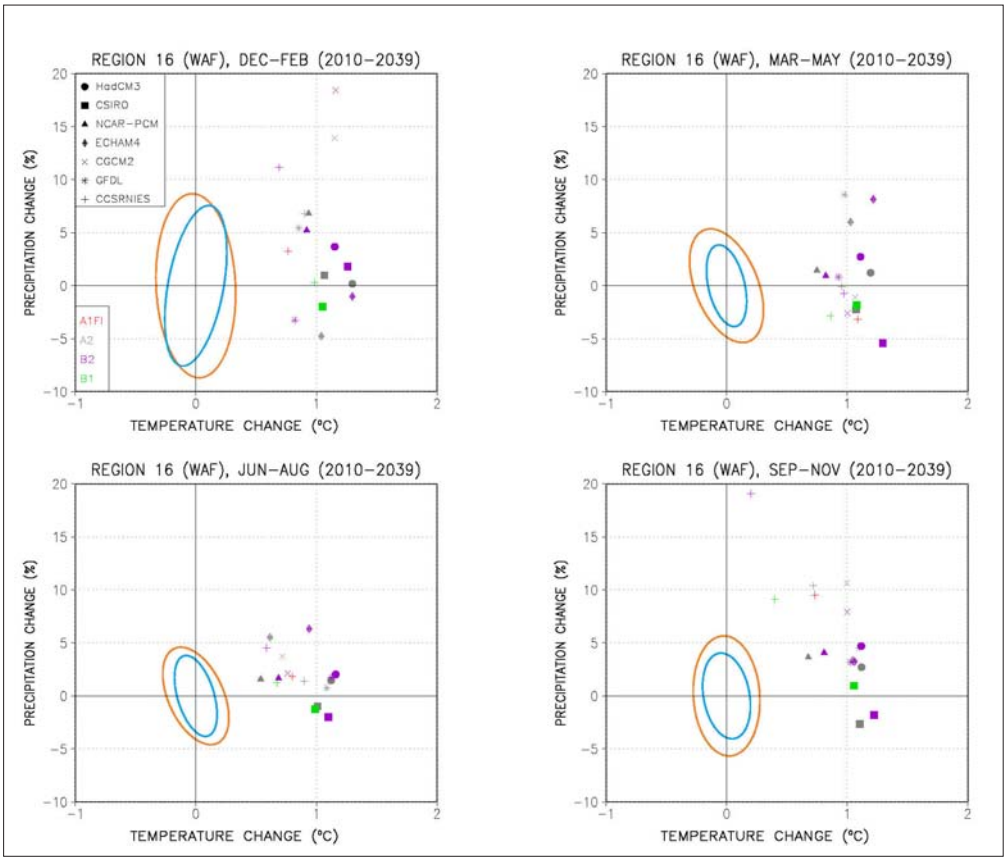

Region 16: Western Africa (2040–2069)

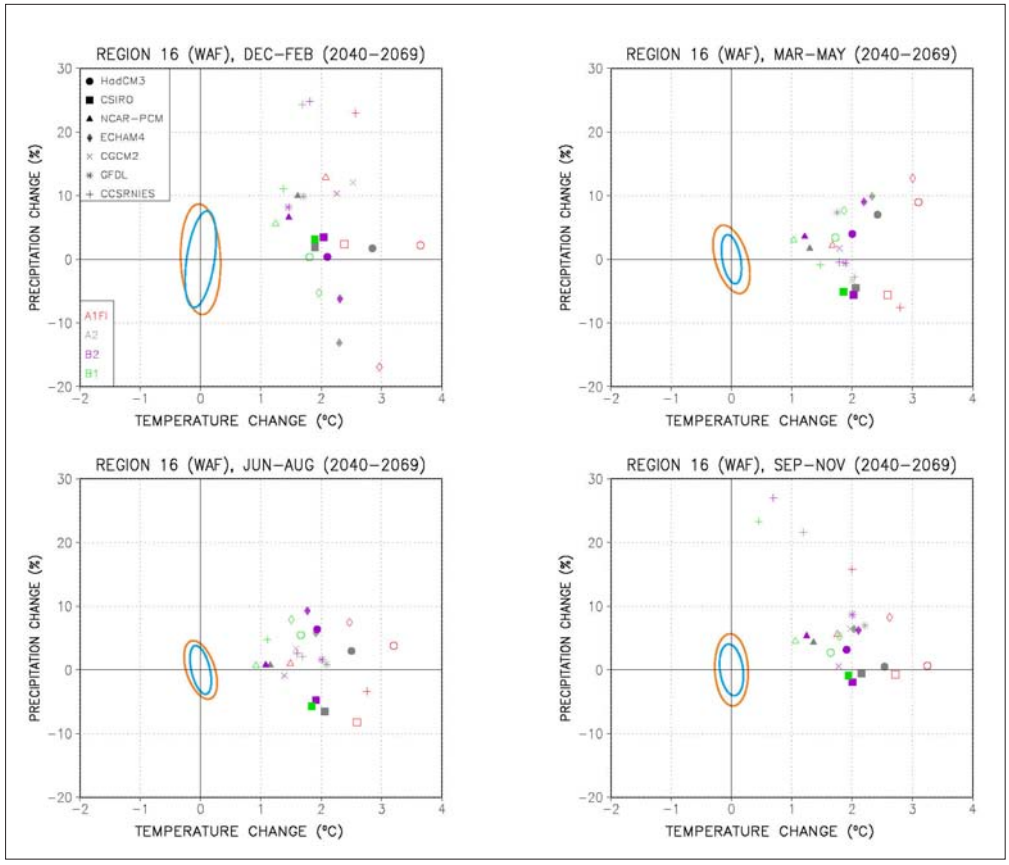

Region 16: Western Africa (2070–2099)

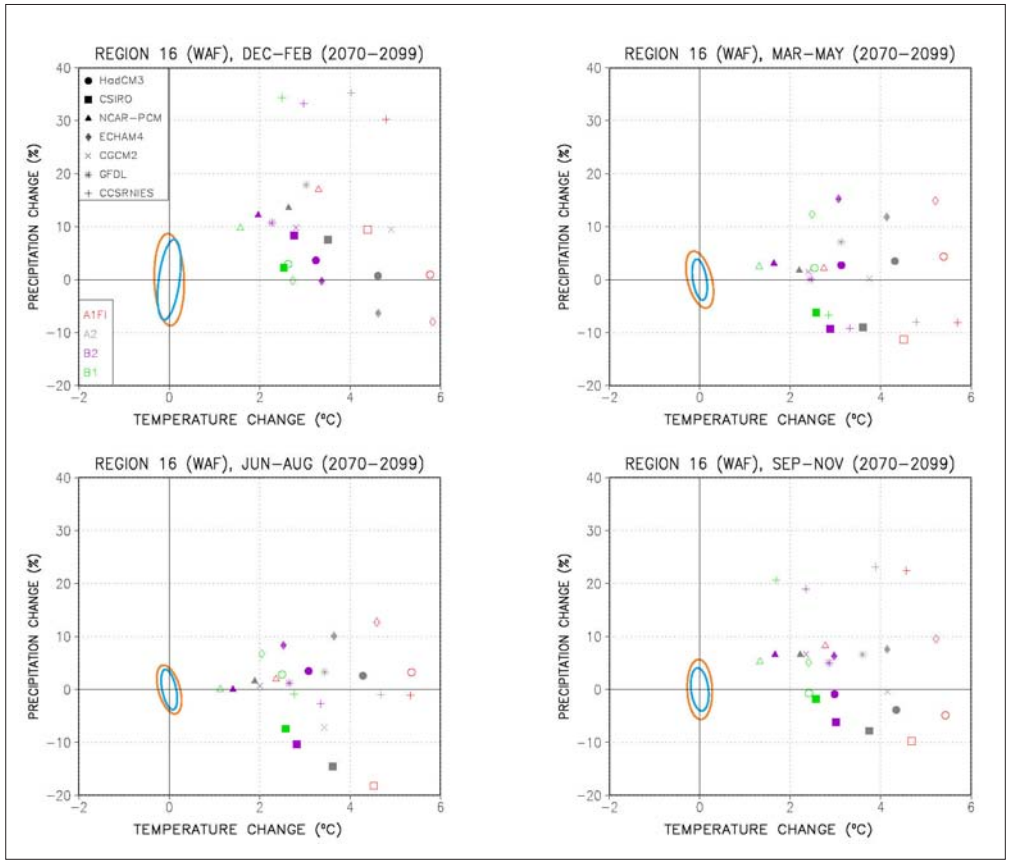

Region 17: Eastern Africa (2010–2039)

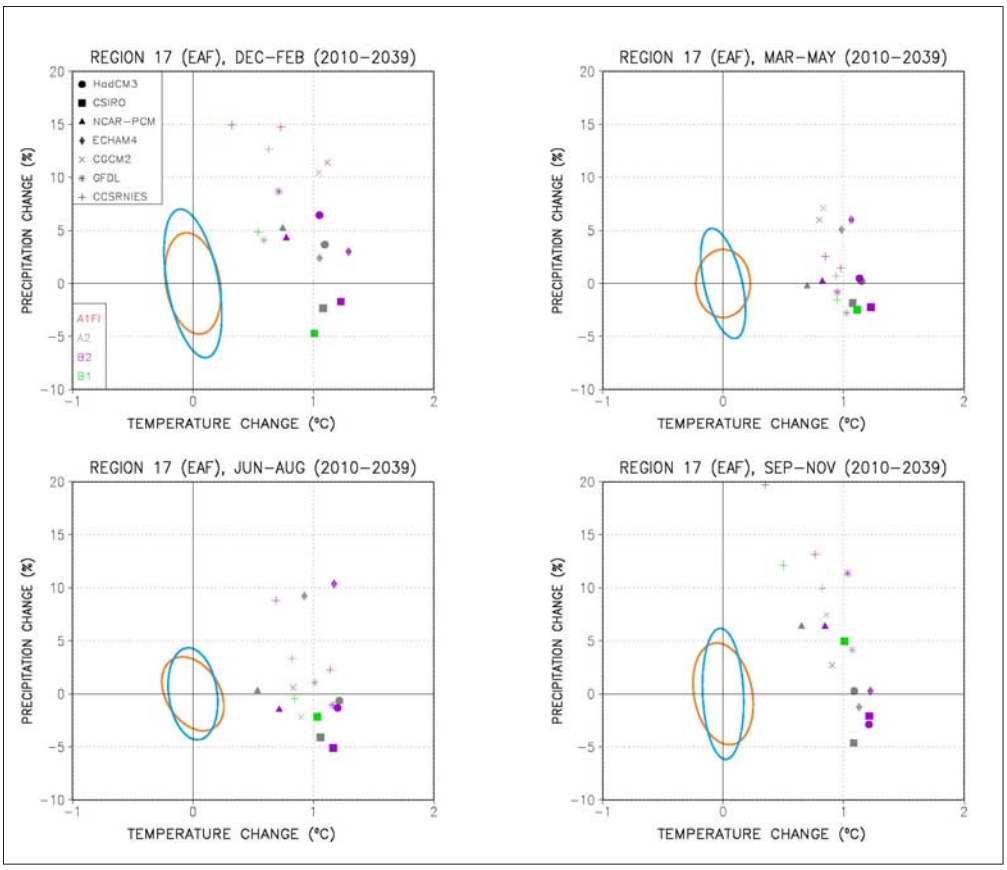

Region 17: Eastern Africa (2040–2069)

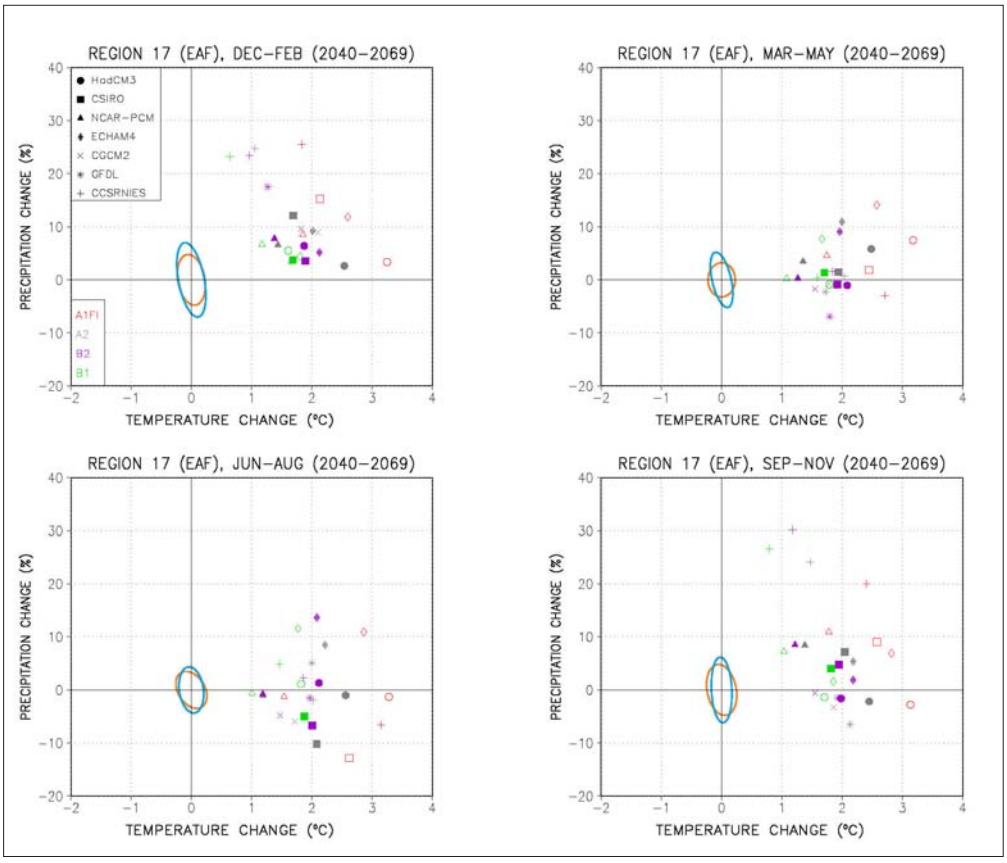

Region 17: Eastern Africa (2070–2099)

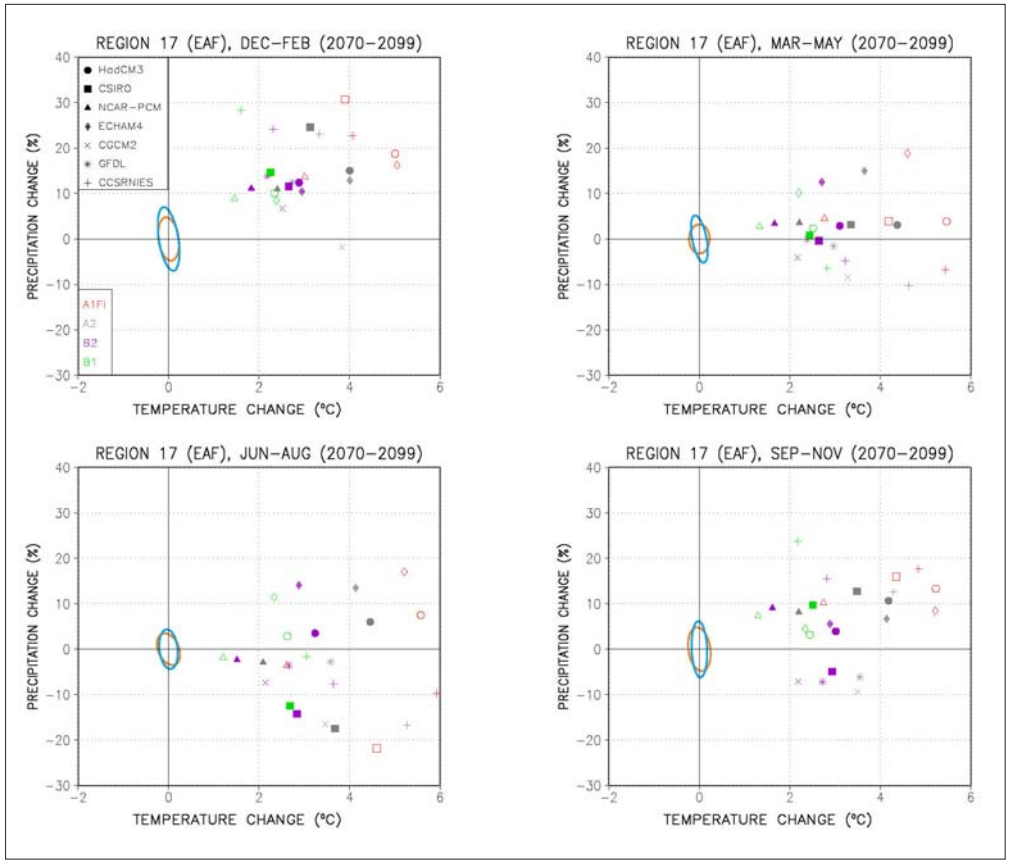

Region 18: Southern Africa (2010–2039)

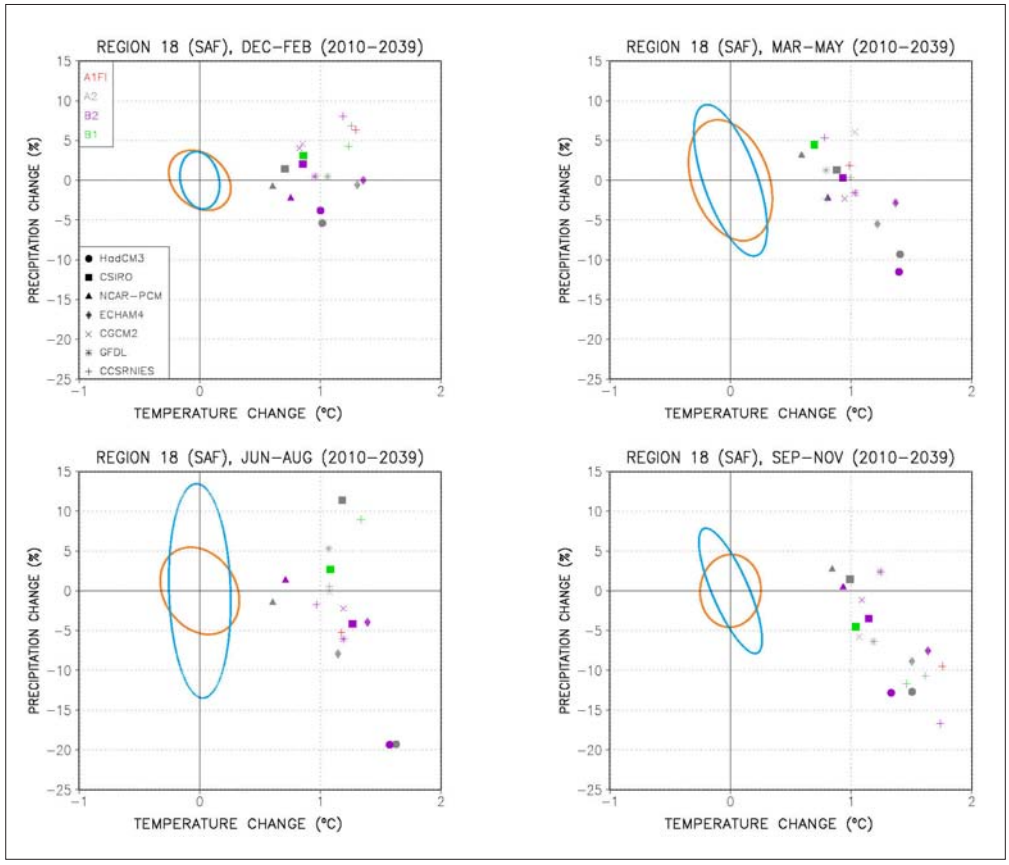

Region 18: Southern Africa (2040–2069)

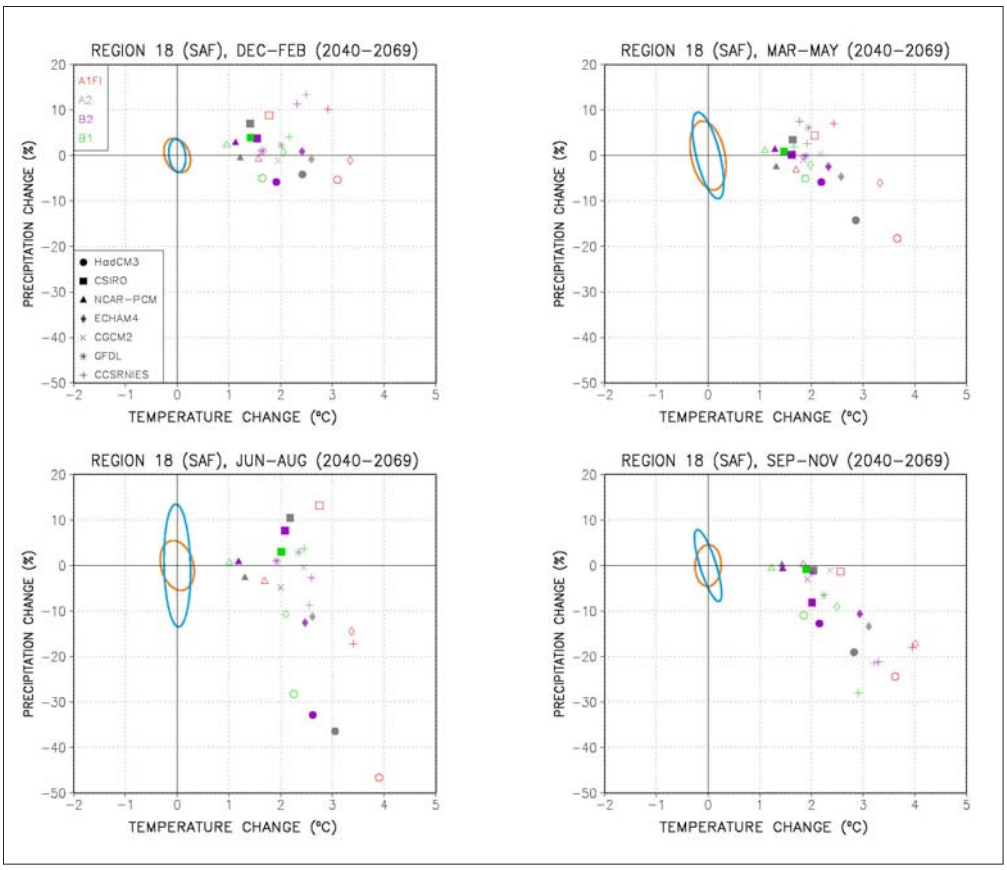

Region 18: Southern Africa (2070–2099)

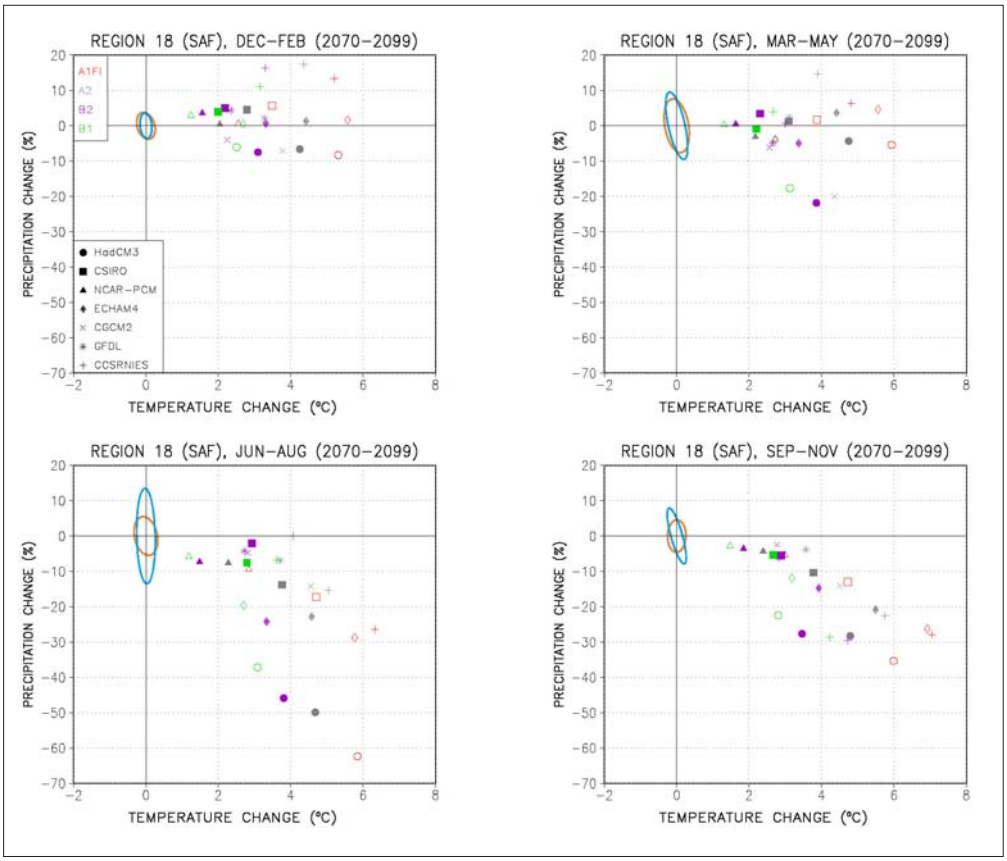

Region 19: Northern Asia (2010–2039)

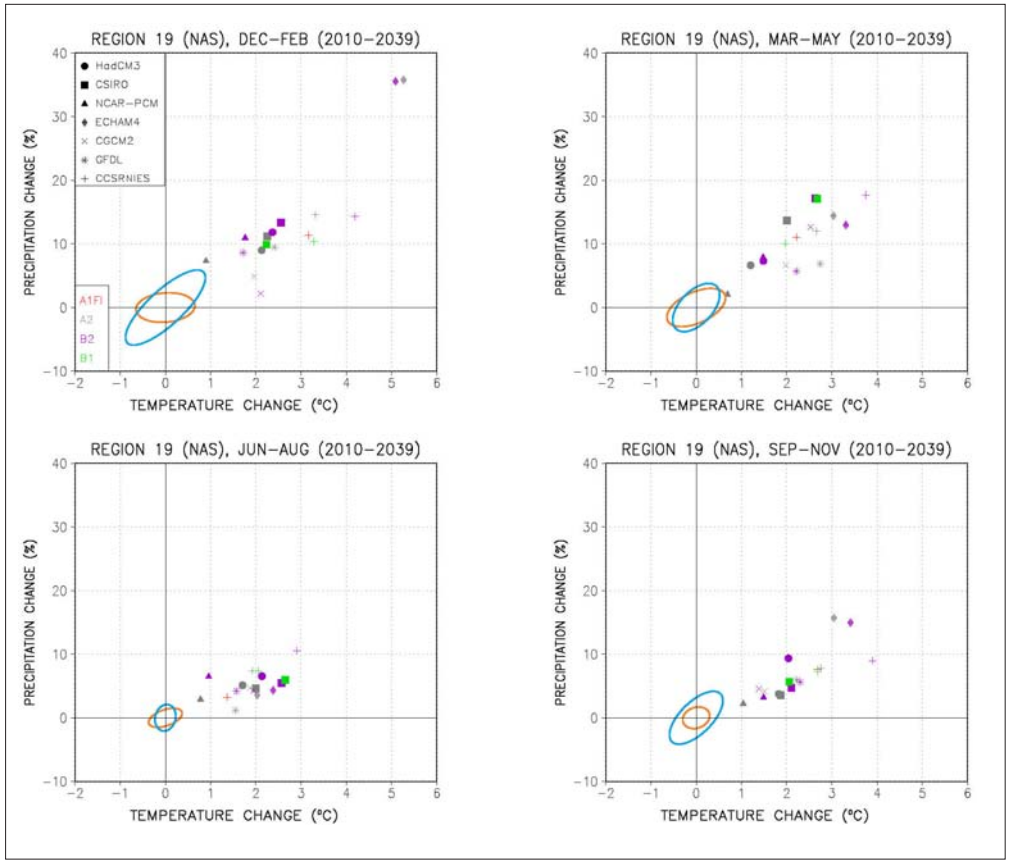

Region 19: Northern Asia (2040–2069)

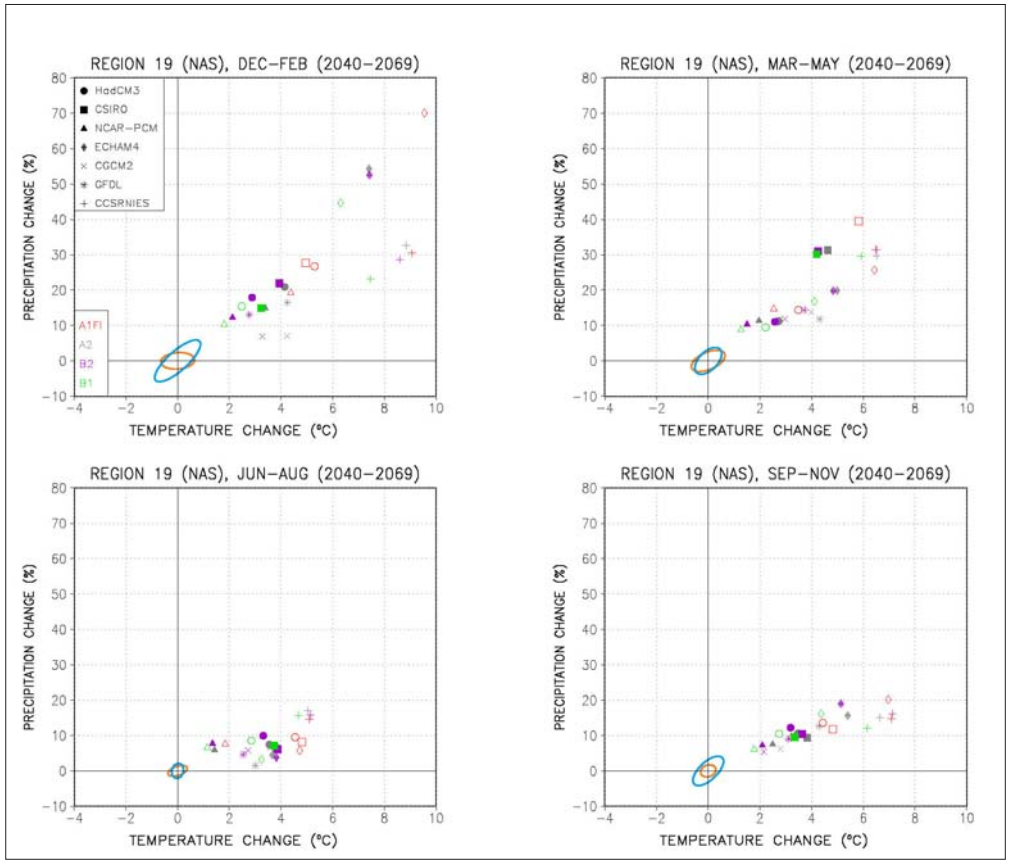

Region 19: Northern Asia (2070–2099)

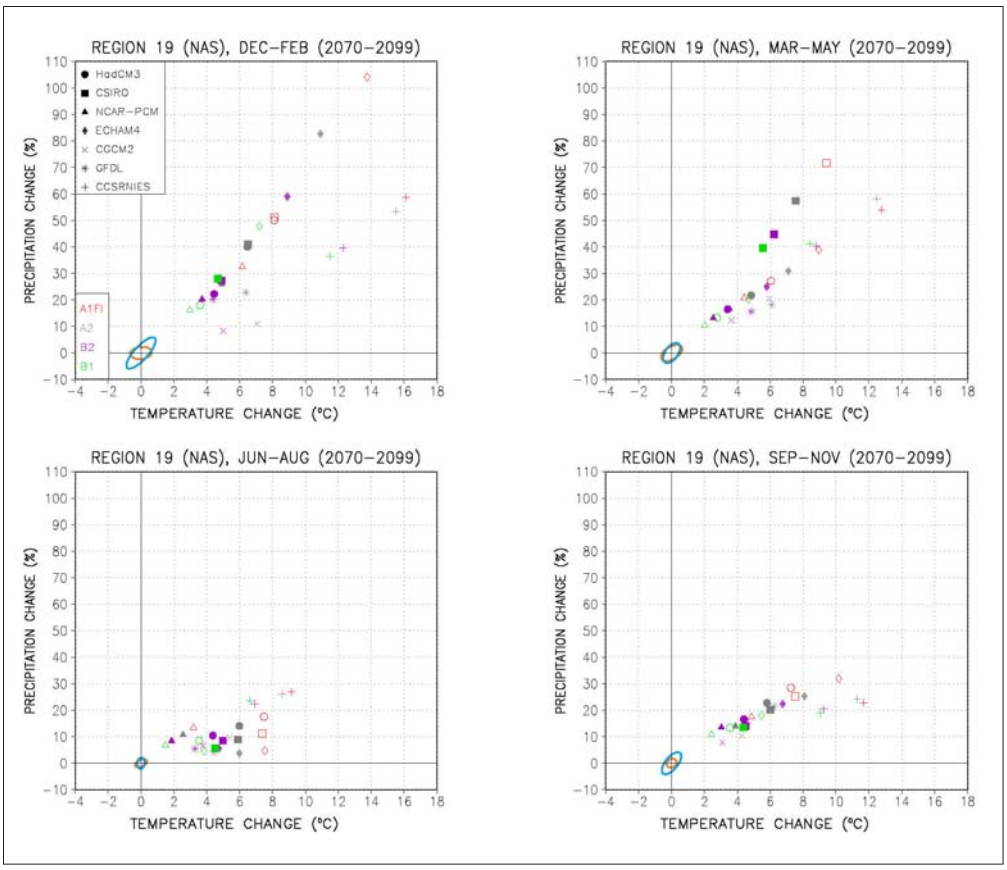

Region 20: Central Asia (2010–2039)

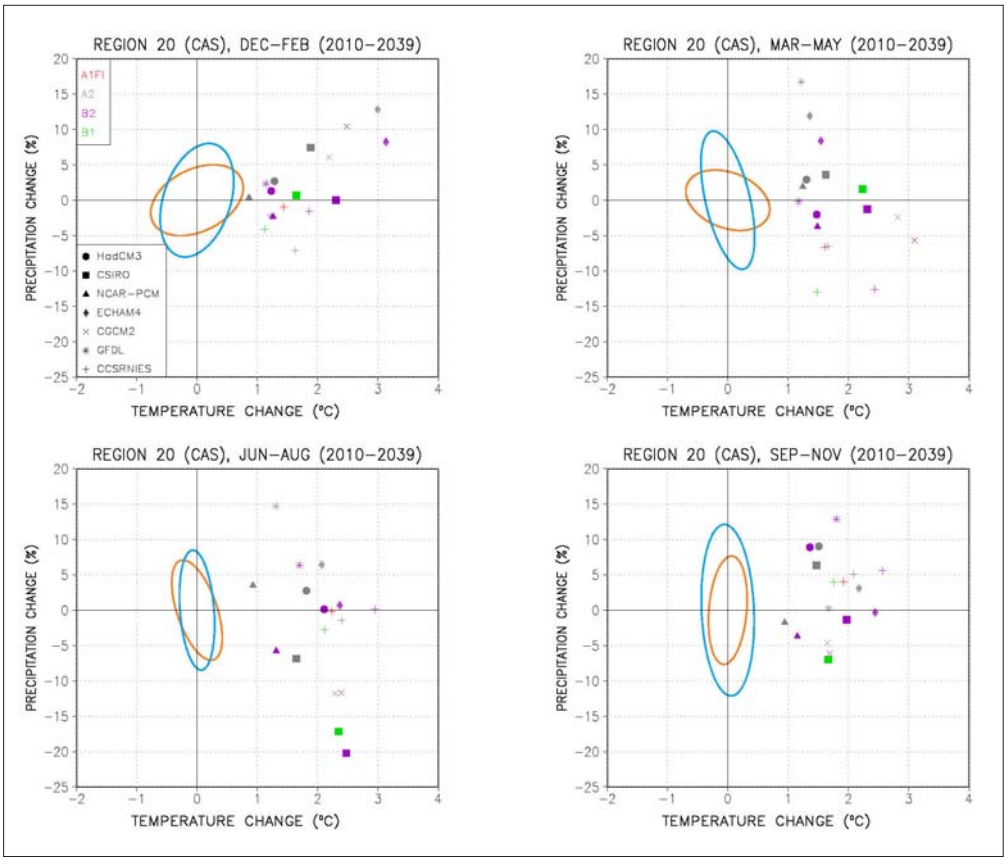

Region 20: Central Asia (2040–2069)

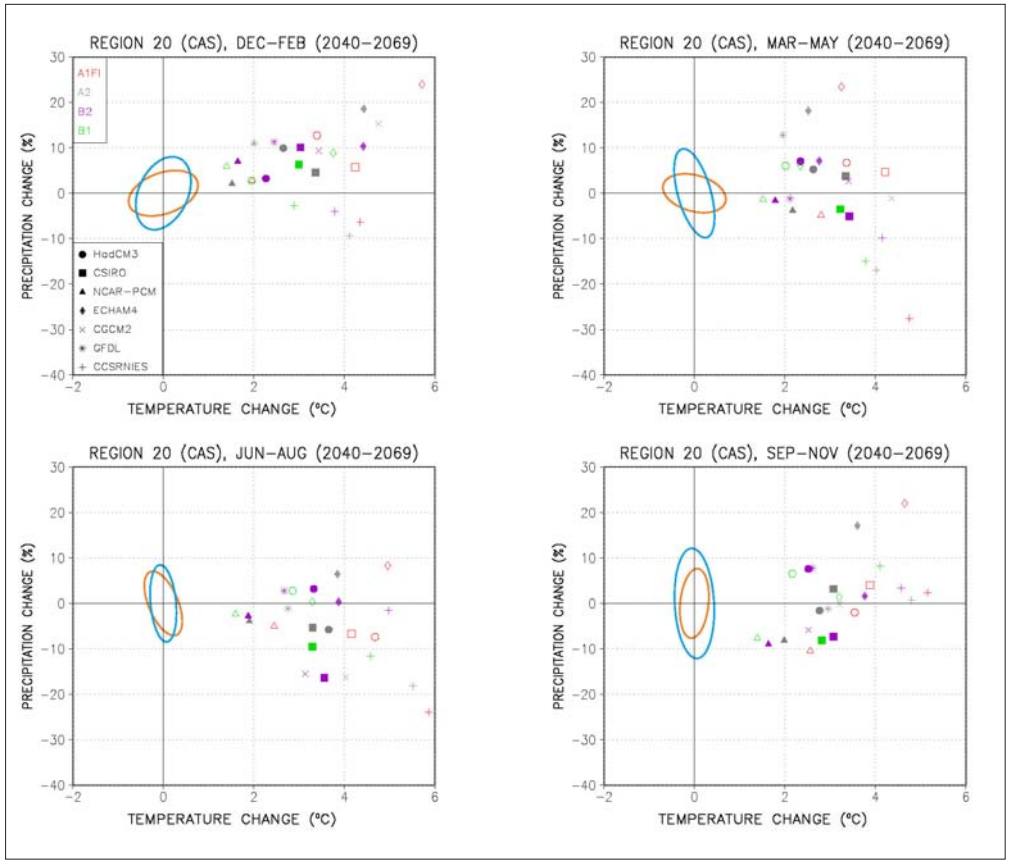

Region 20: Central Asia (2070–2099)

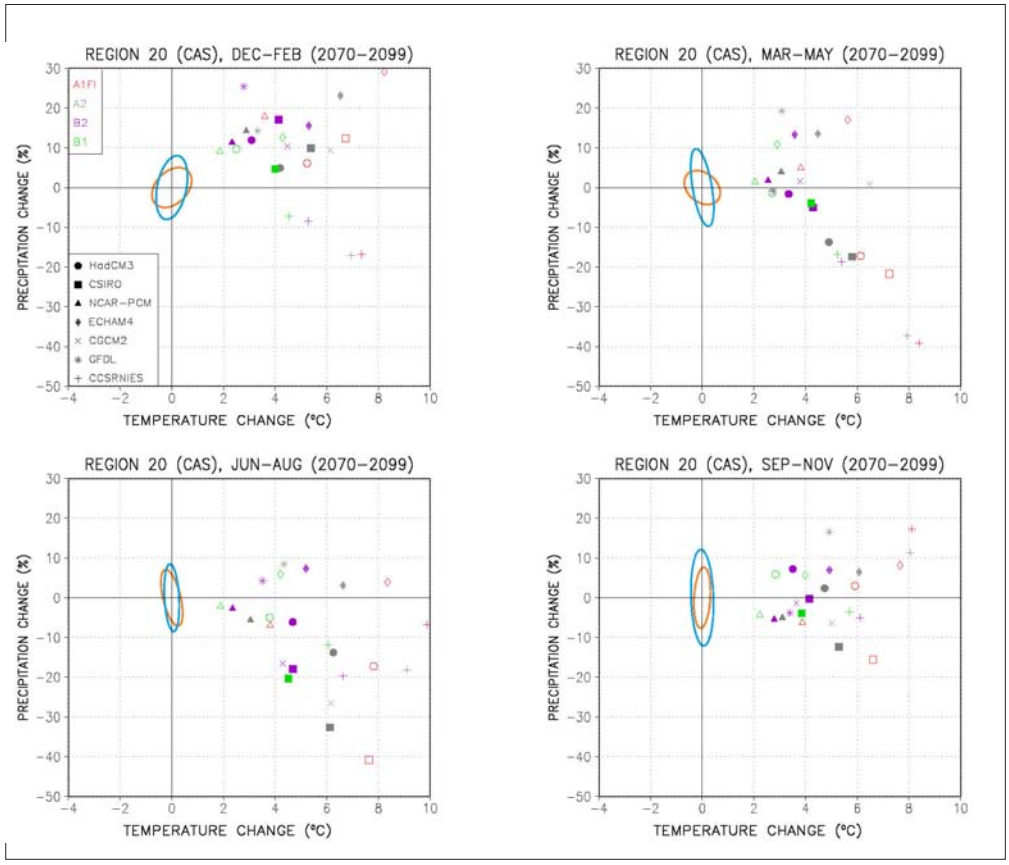

Region 21: Tibetan Plateau (2010–2039)

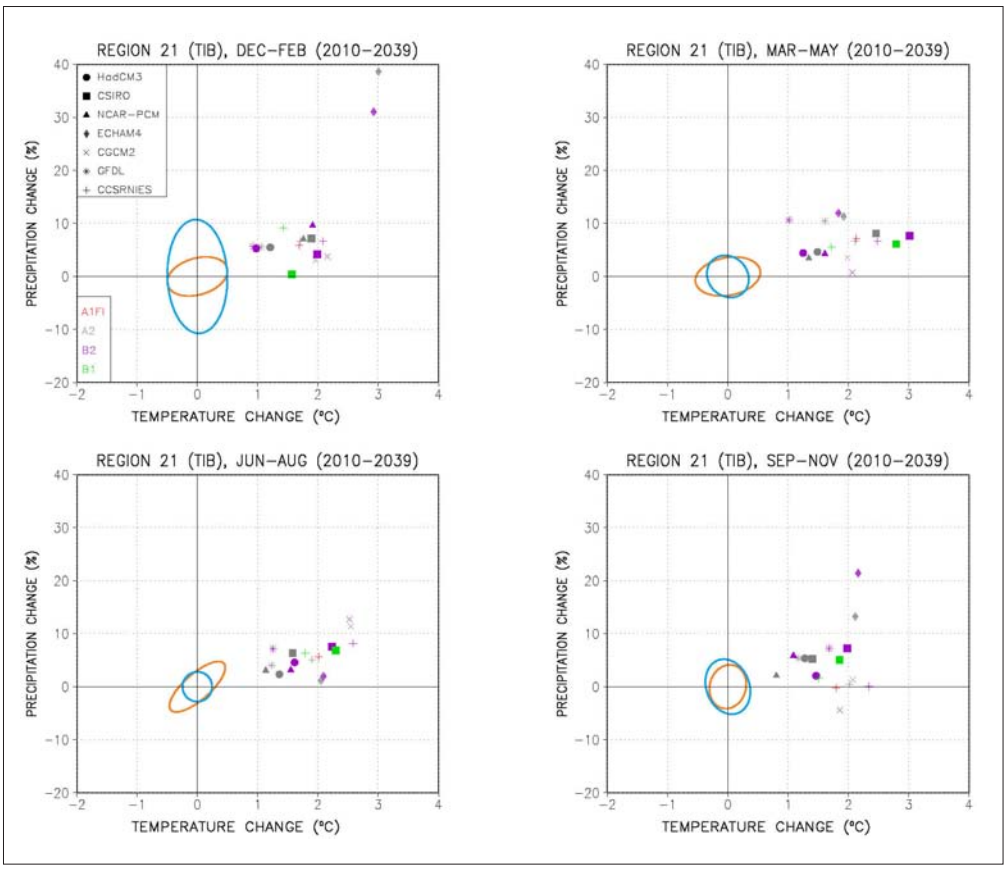

Region 21: Tibetan Plateau (2040–2069)

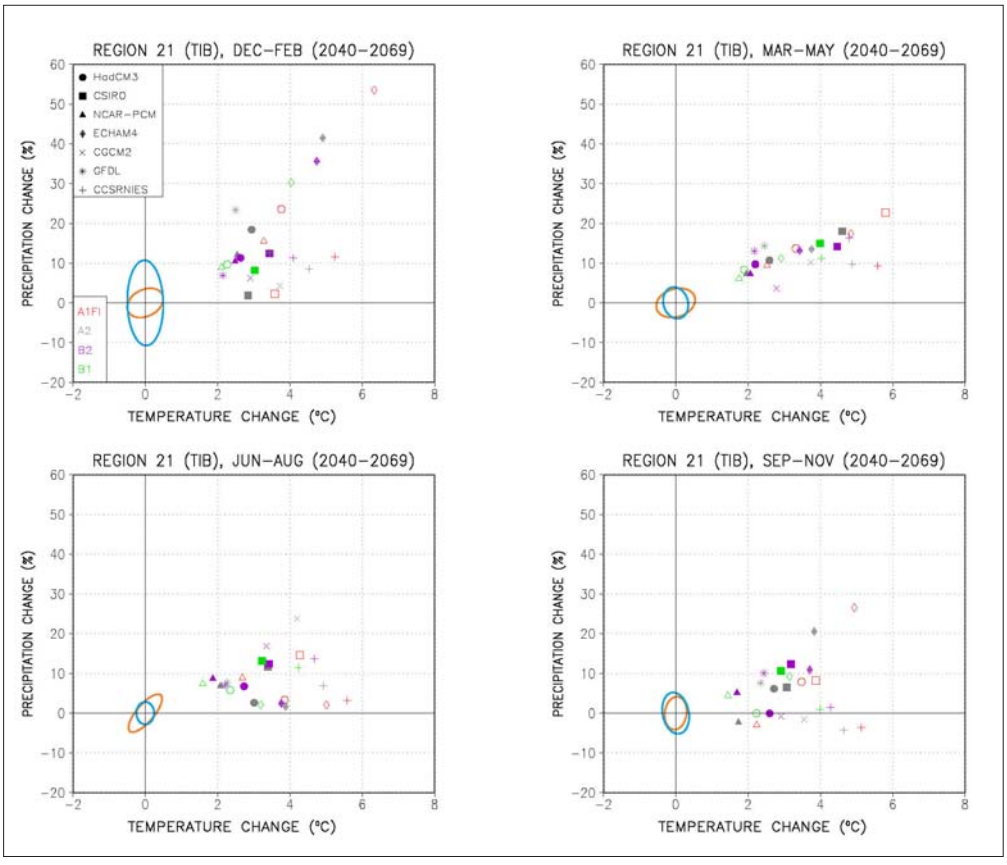

Region 21: Tibetan Plateau (2070–2099)

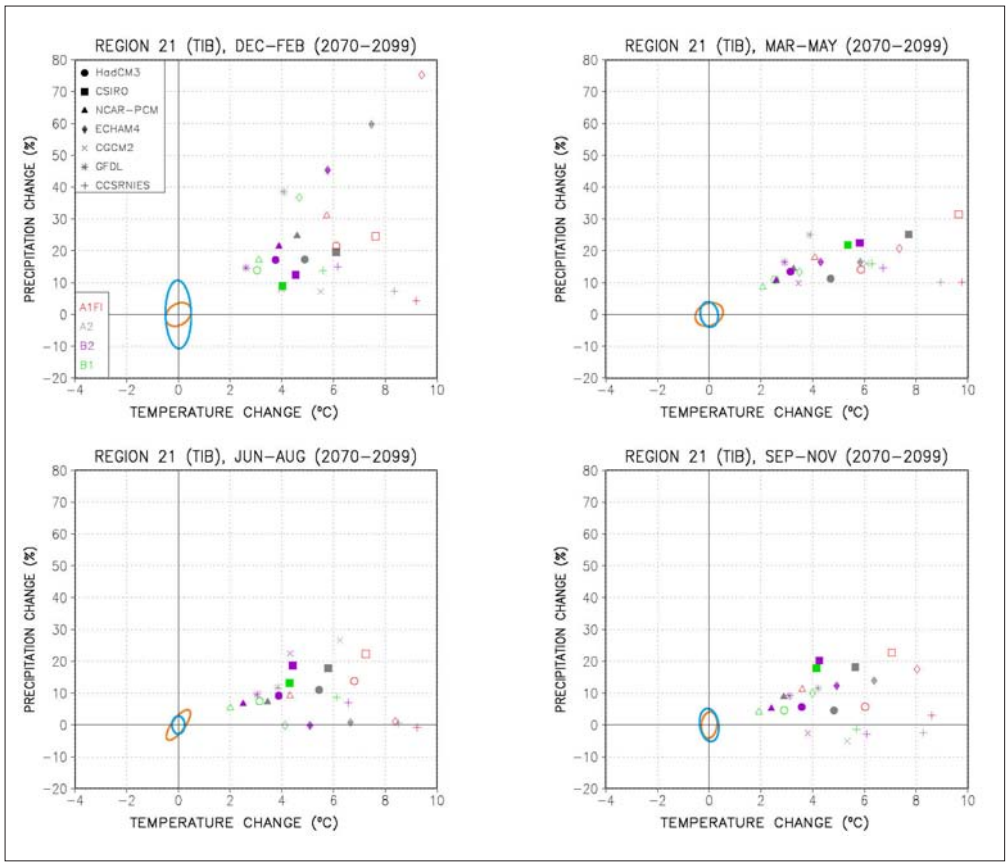

Region 22: Eastern Asia (2010–2039)

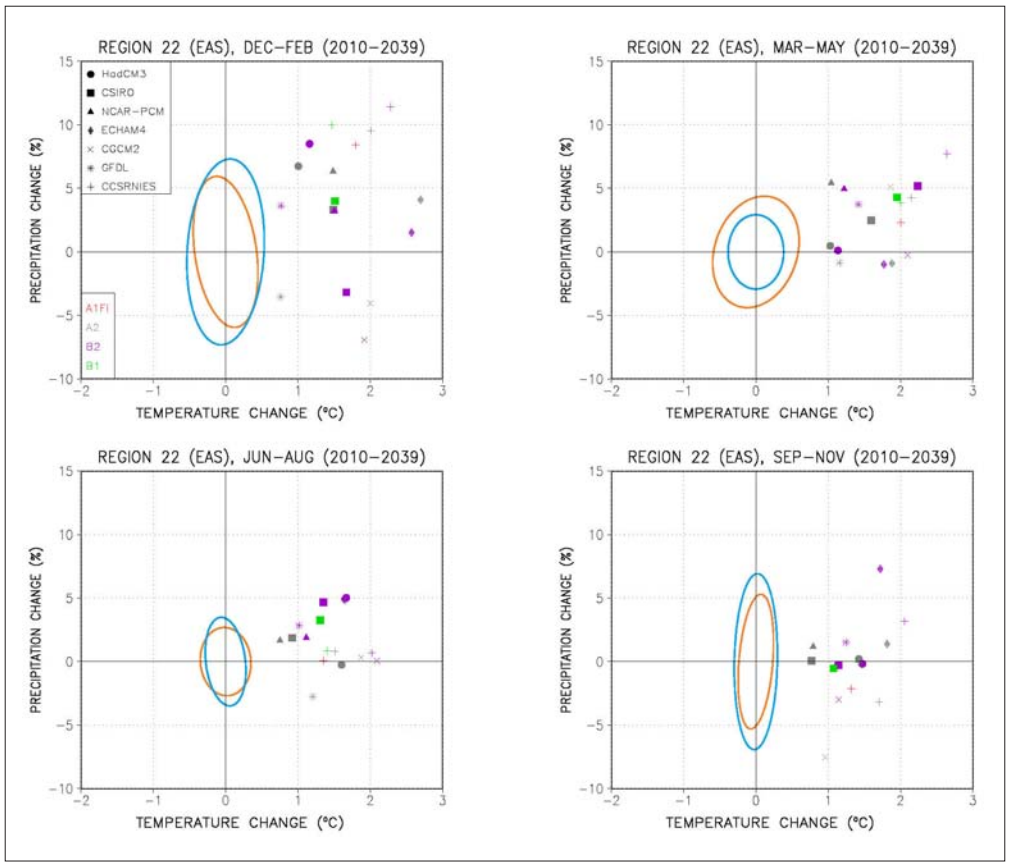

Region 22: Eastern Asia (2040–2069)

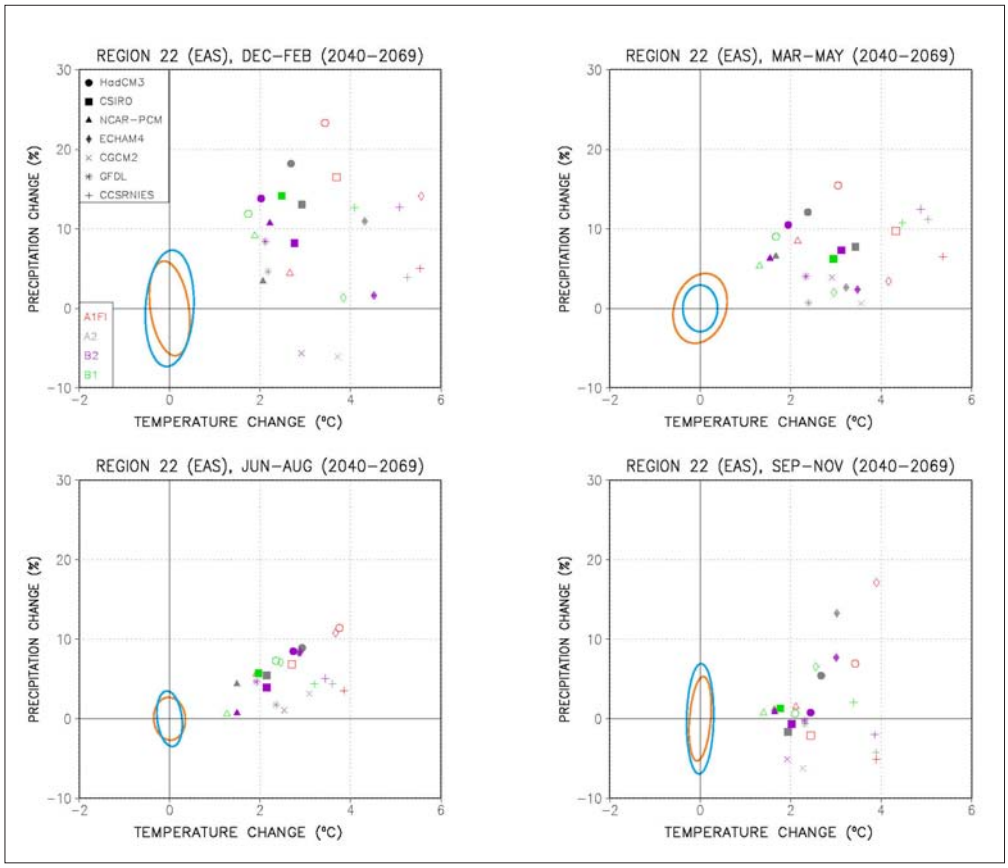

Region 22: Eastern Asia (2070–2099)

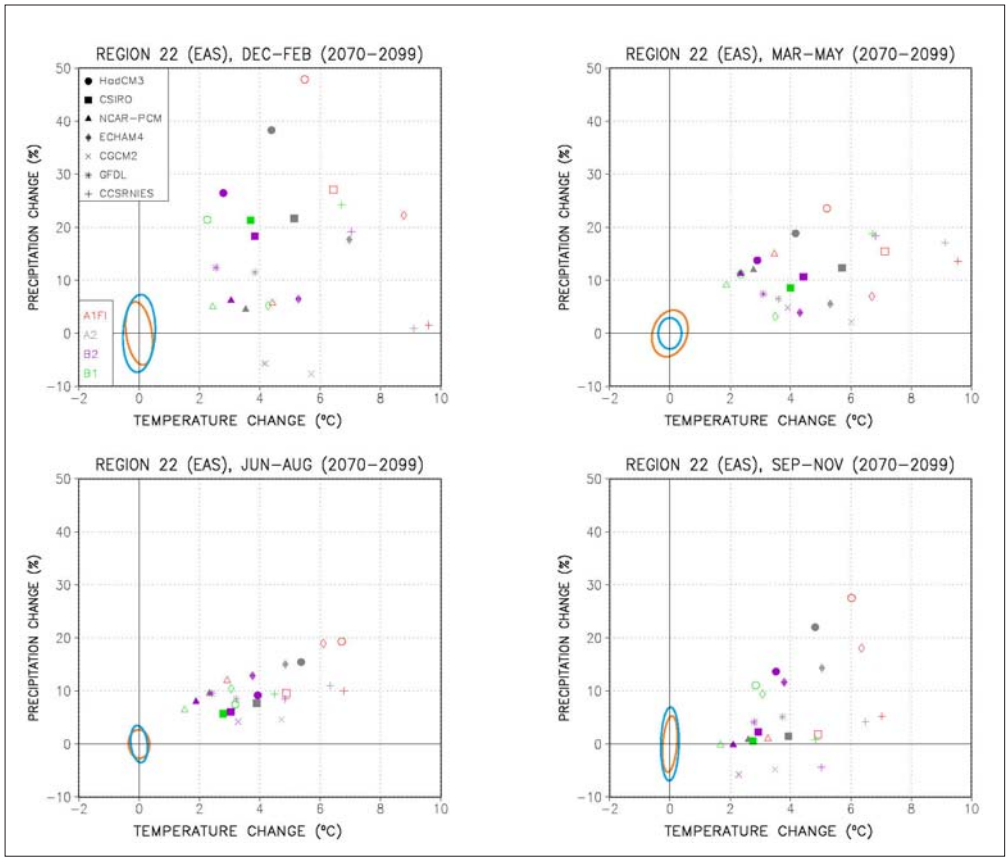

Region 23: Southern Asia (2010–2039)

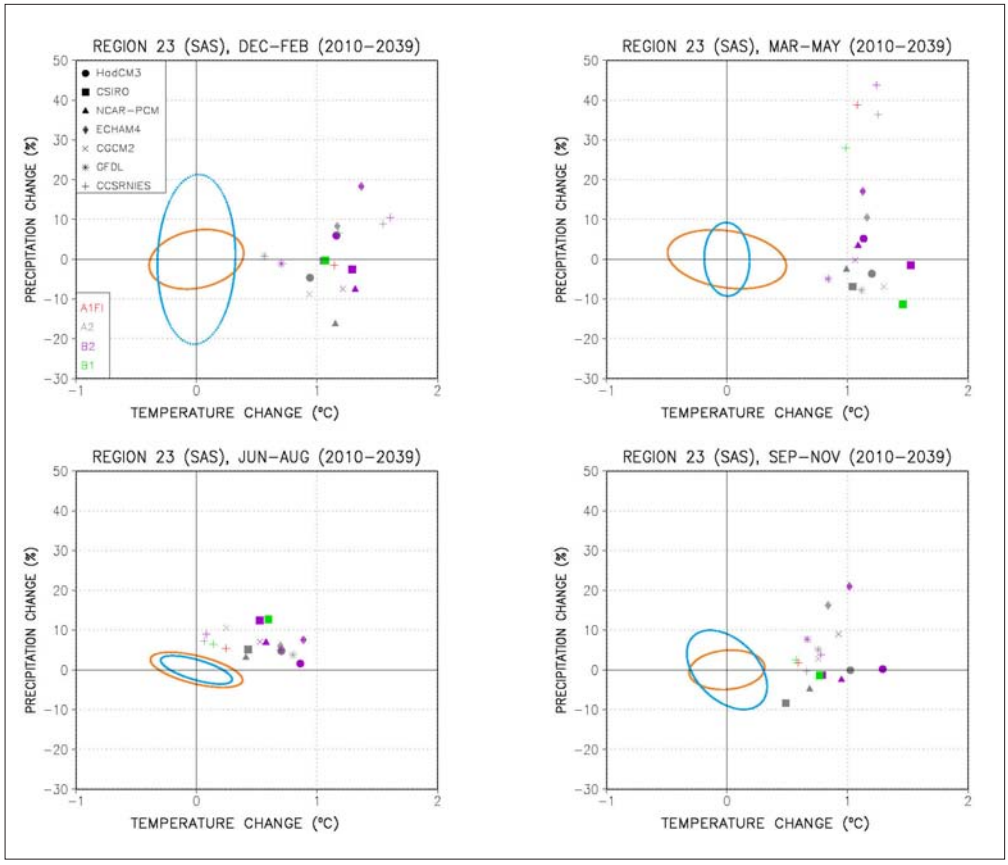

Region 23: Southern Asia (2040–2069)

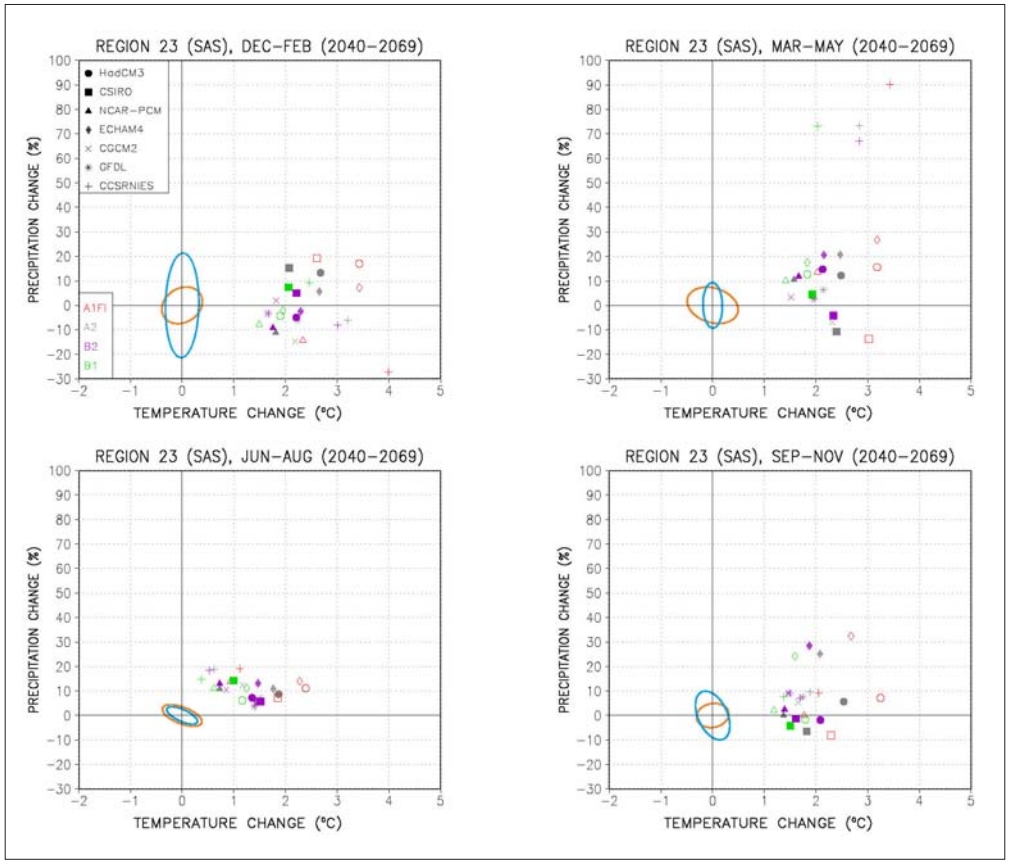

Region 23: Southern Asia (2070–2099)

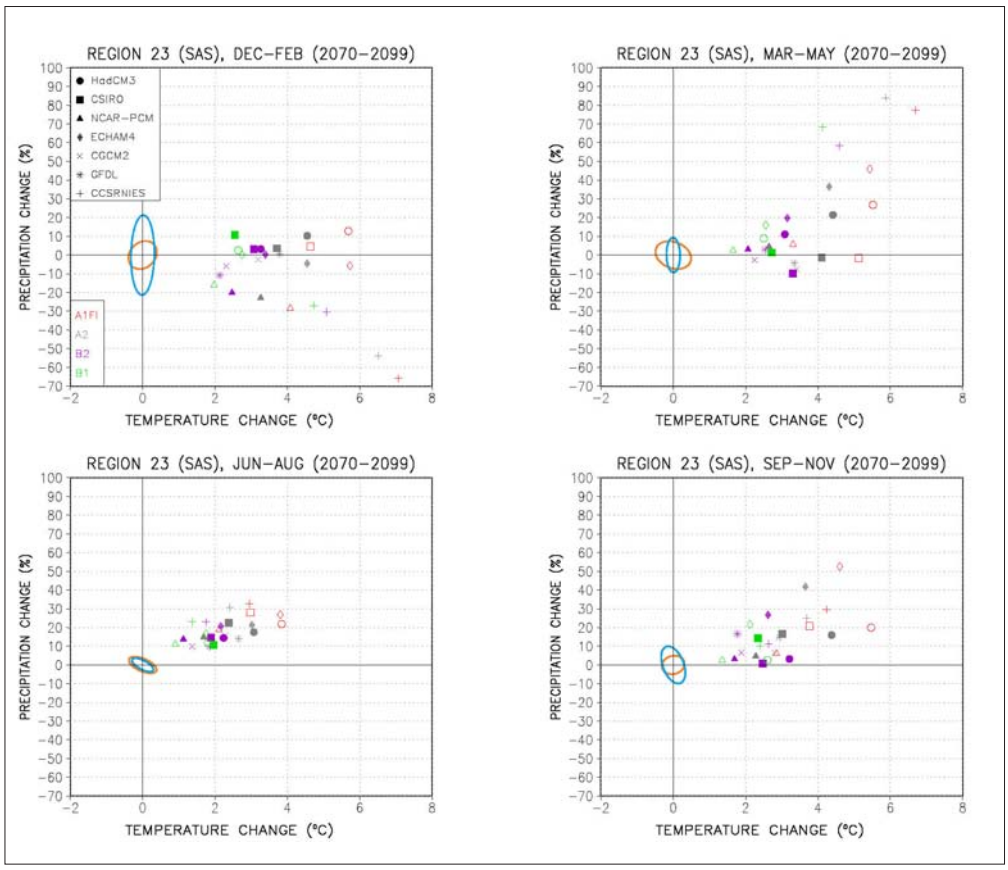

Region 24: Southeast Asia (2010–2039)

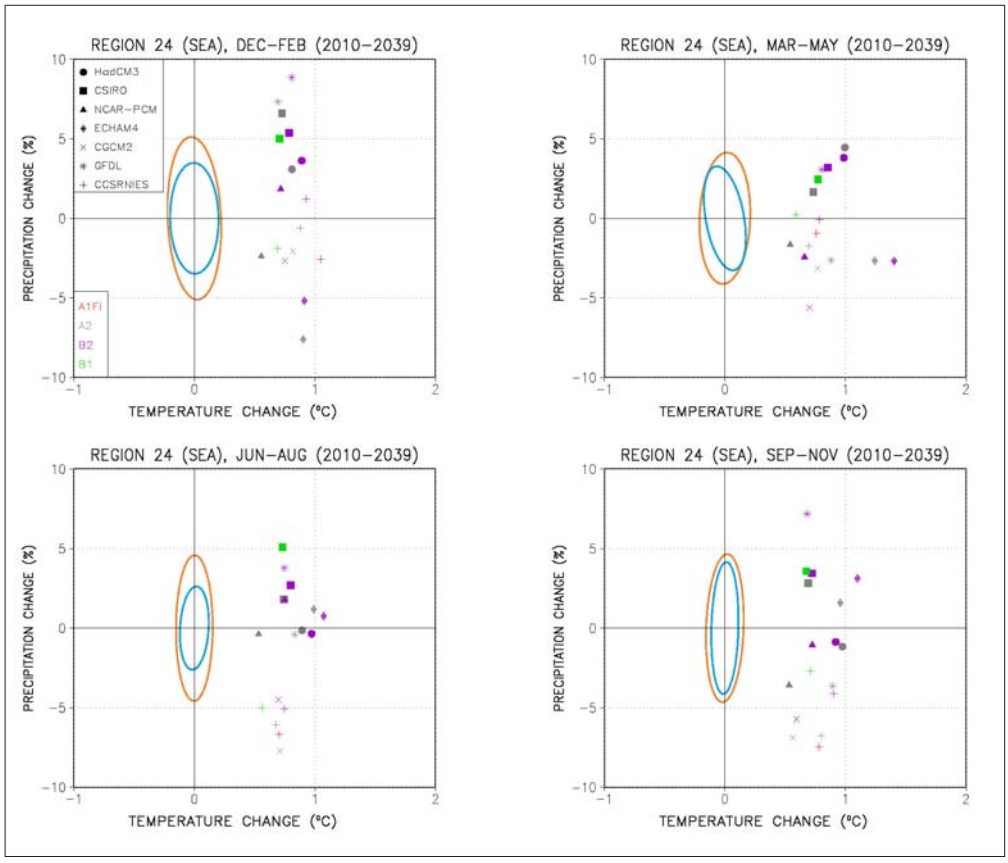

Region 24: Southeast Asia (2040–2069)

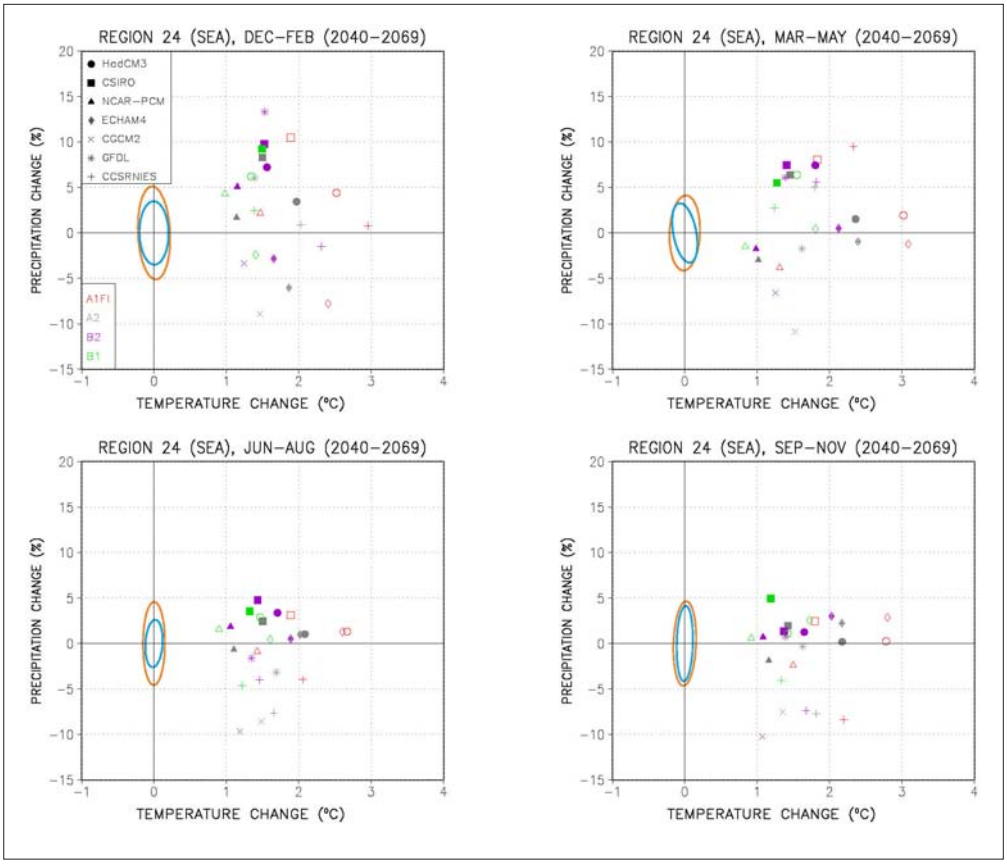

Region 24: Southeast Asia (2070–2099)

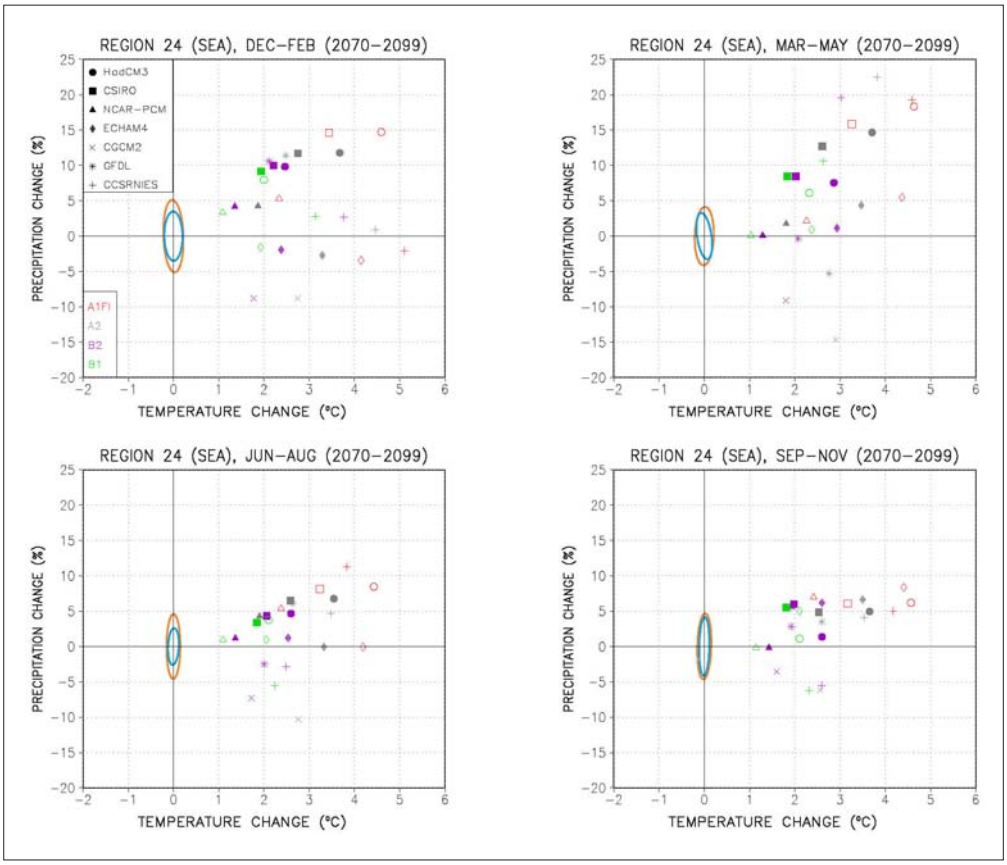

Region 27: Mediterranean (2010–2039)

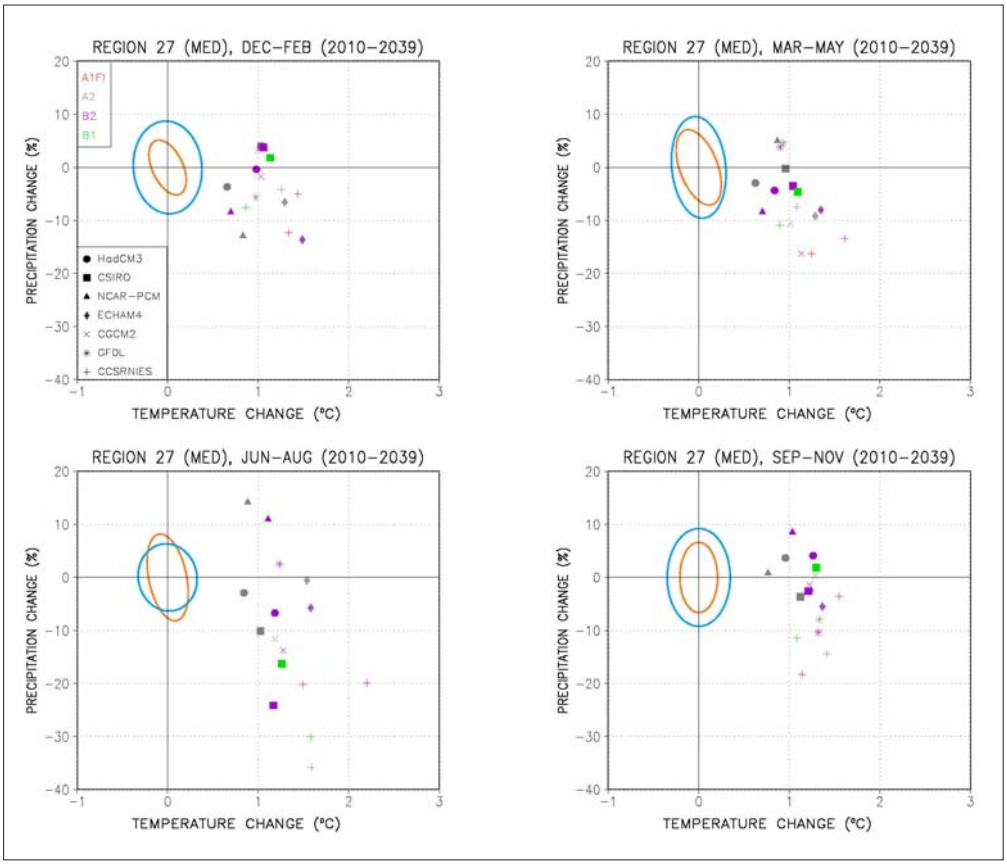

Region 27: Mediterranean (2040–2069)

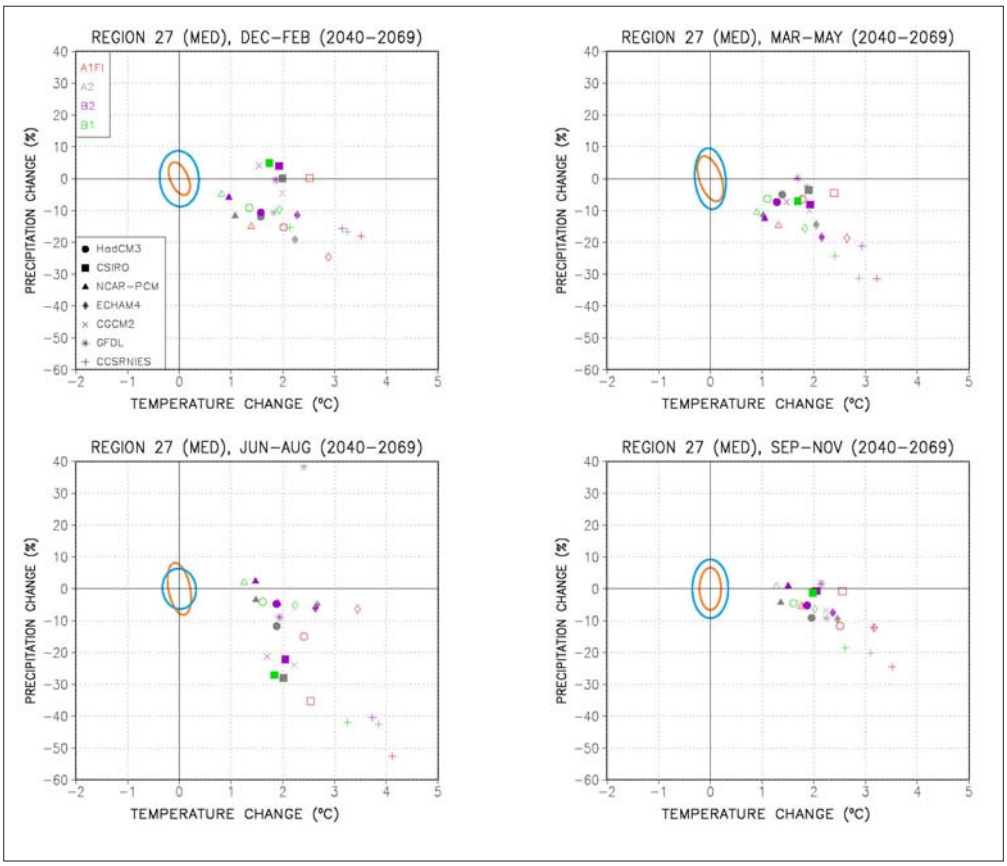

Region 27: Mediterranean (2070–2099)

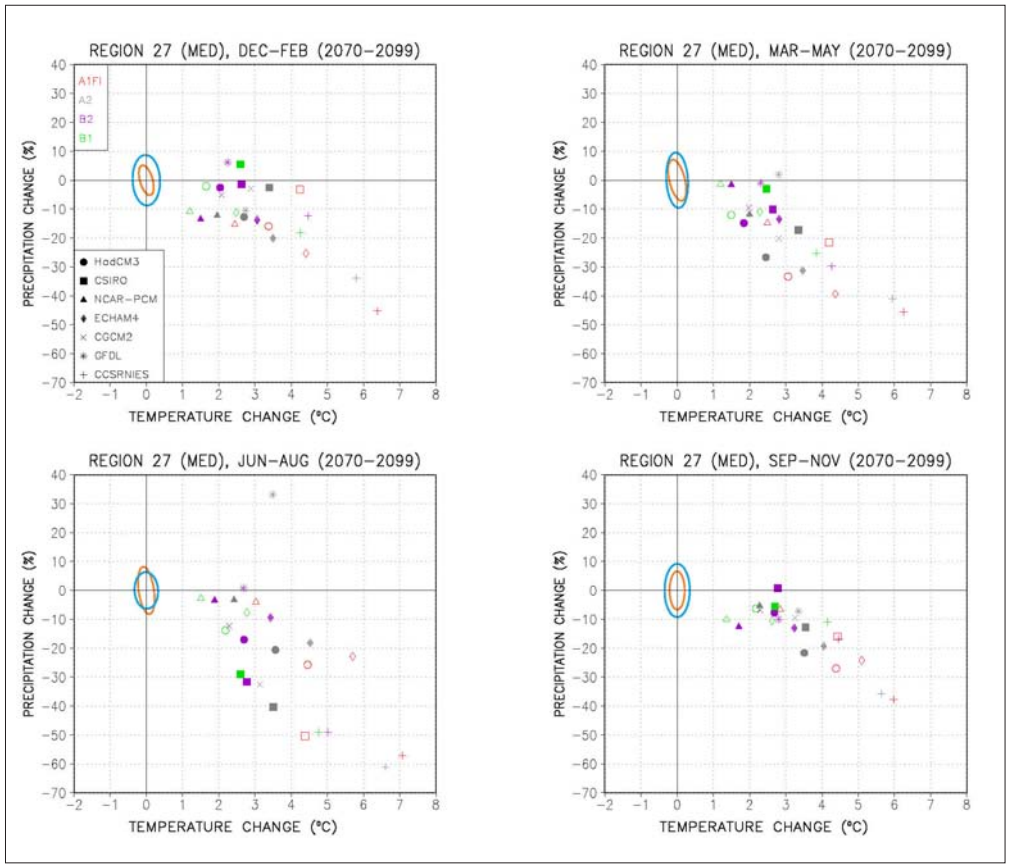

Region 28: Caribbean (2010–2039)

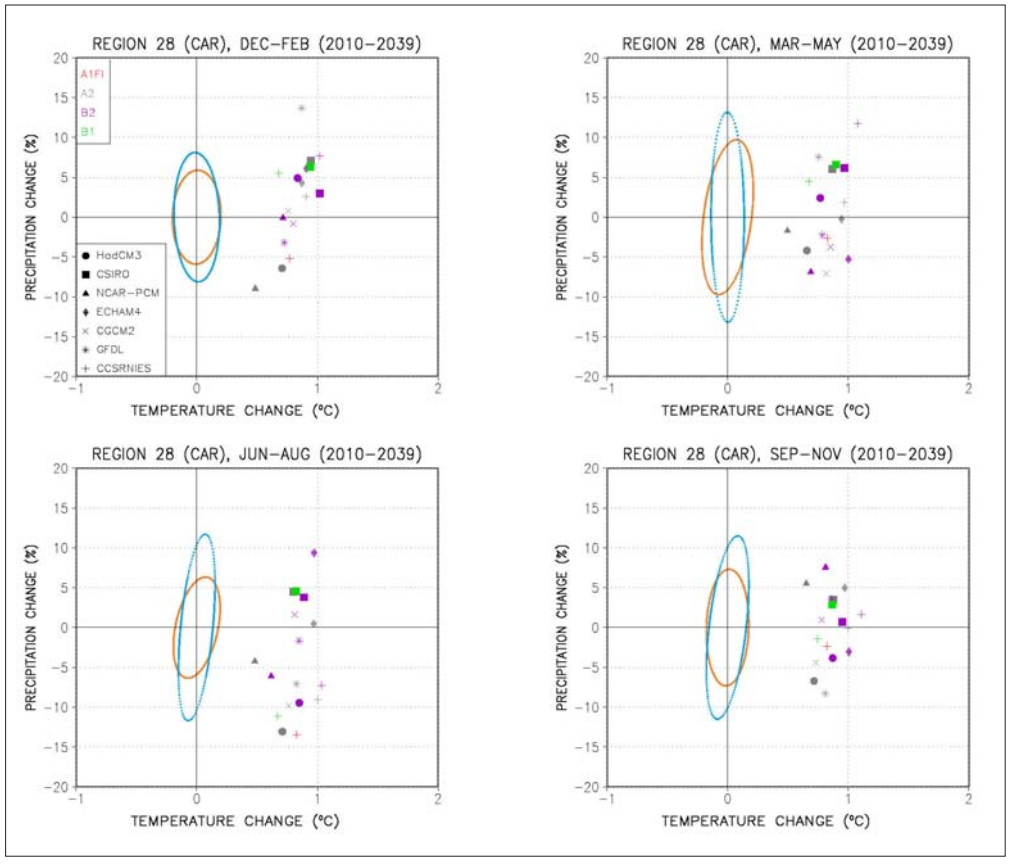

Region 28: Caribbean (2040–2069)

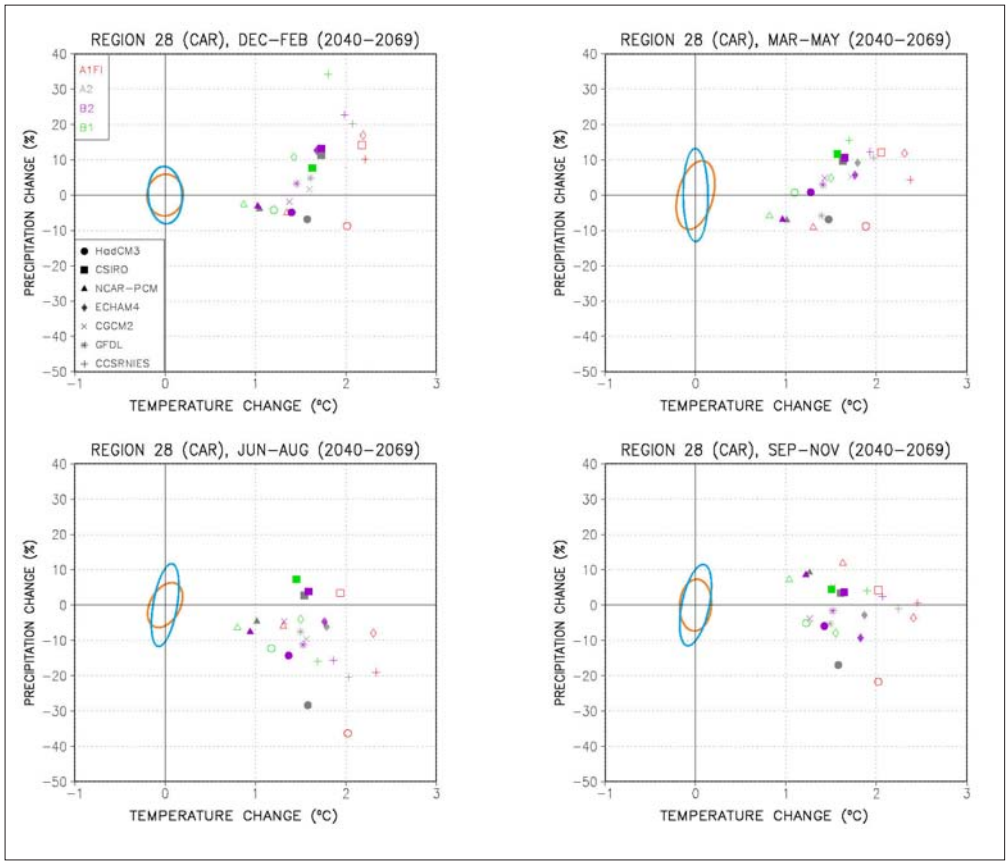

Region 28: Caribbean (2070–2099)

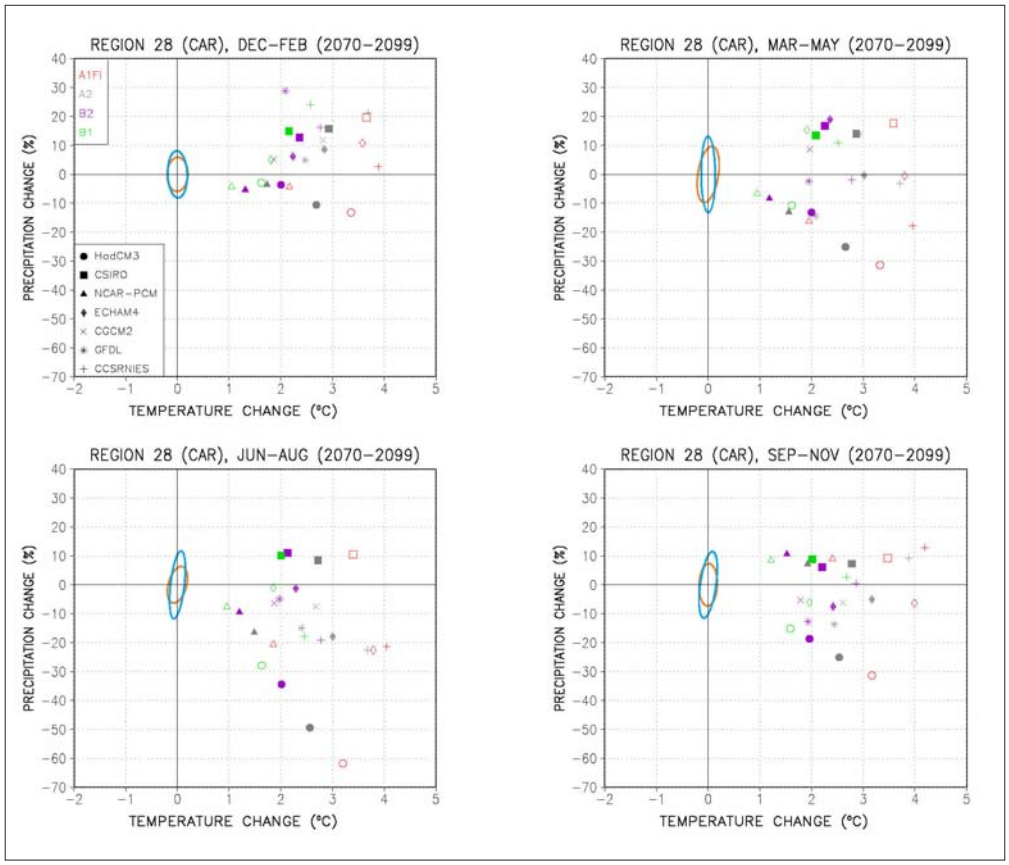

Region 29: Tropical NE Atlantic (2010–2039)

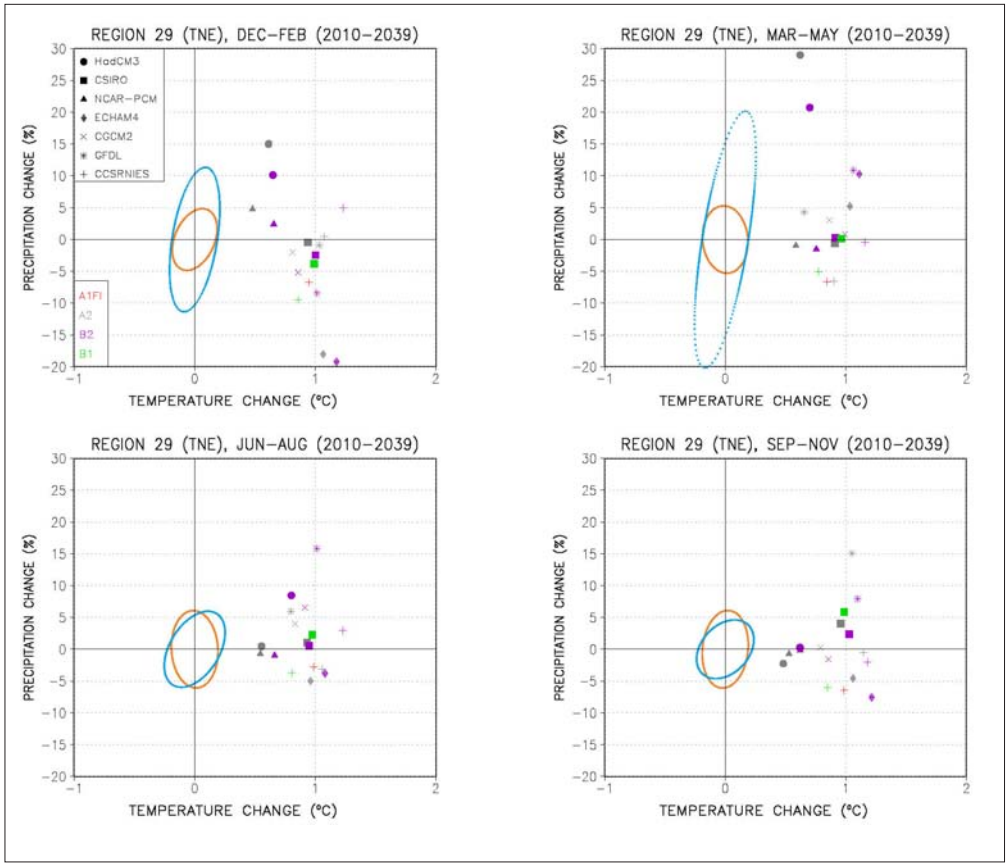

Region 29: Tropical NE Atlantic (2040–2069)

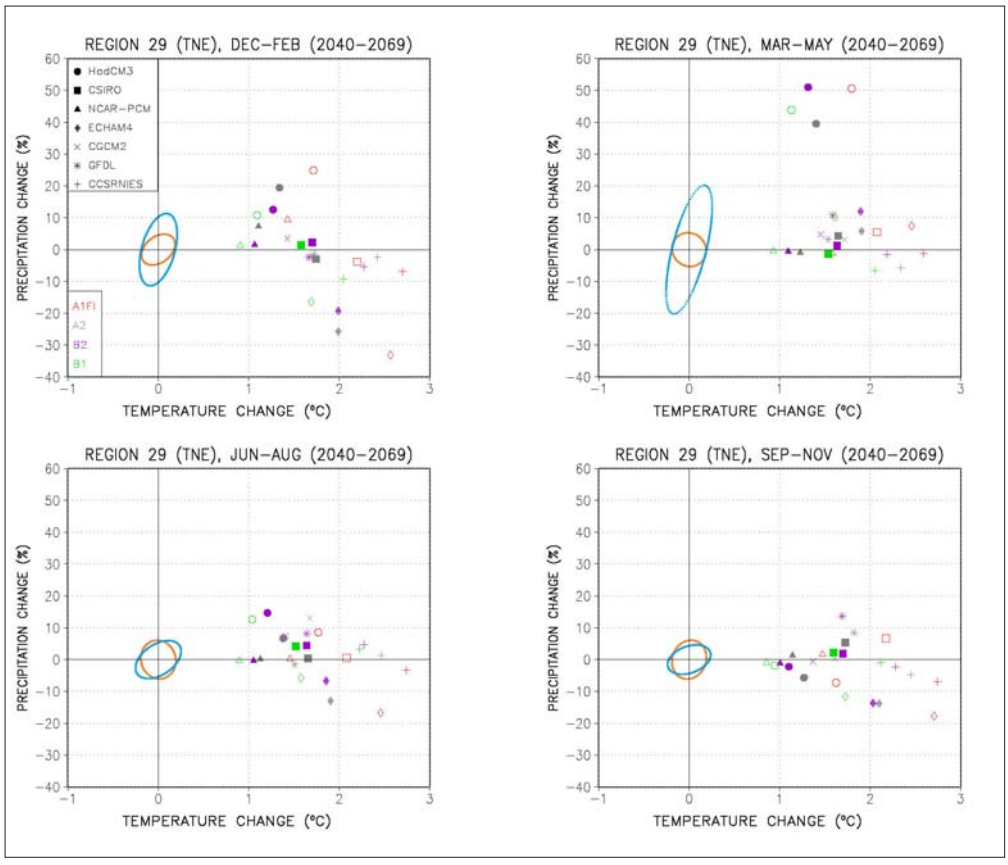

Region 29: Tropical NE Atlantic (2070–2099)

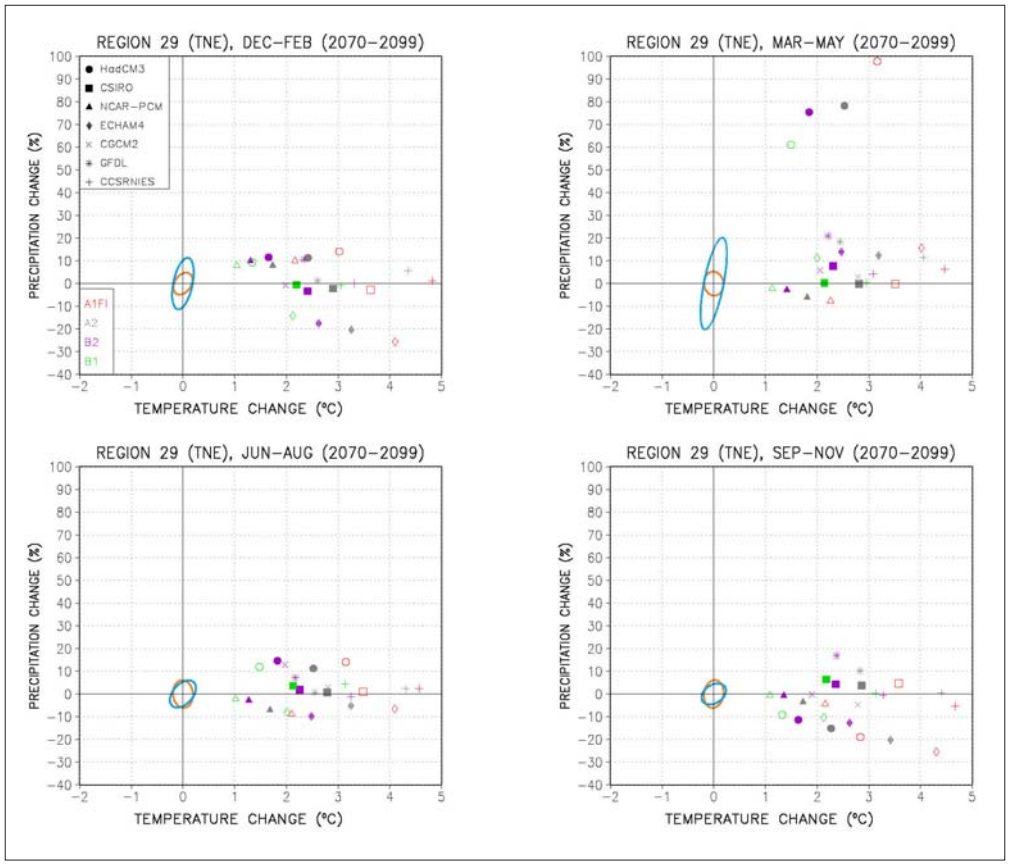

Region 30: Northern Pacific (2010–2039)

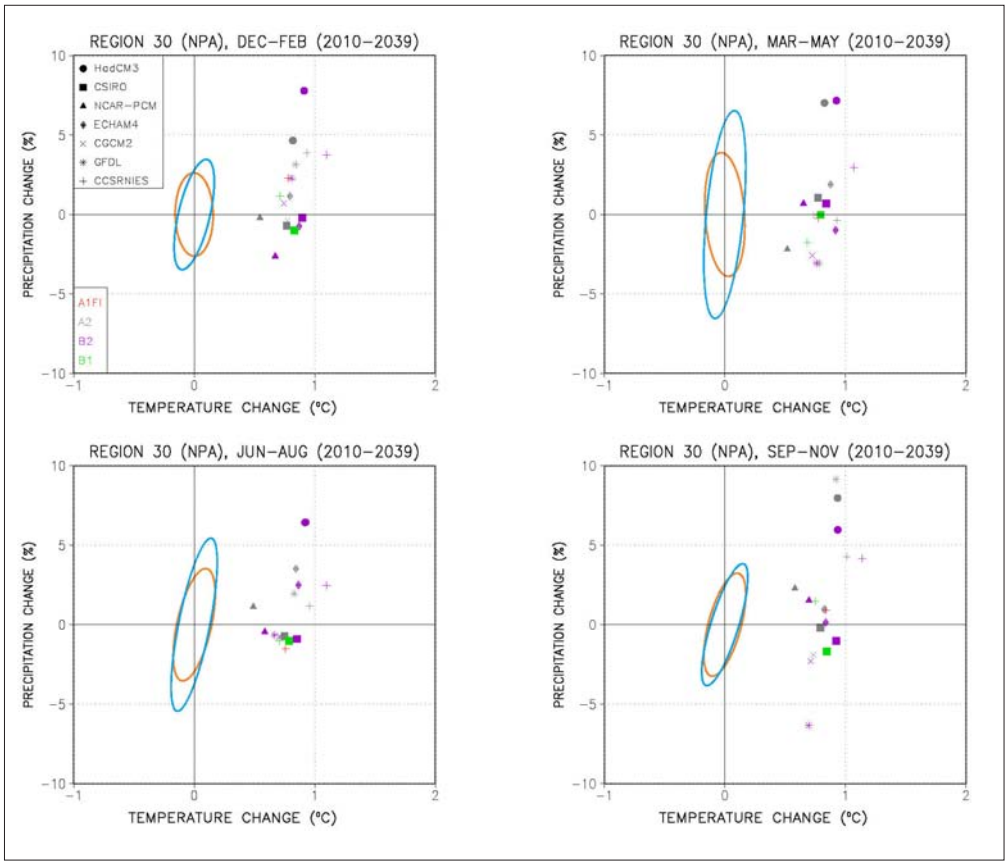

Region 30: Northern Pacific (2040–2069)

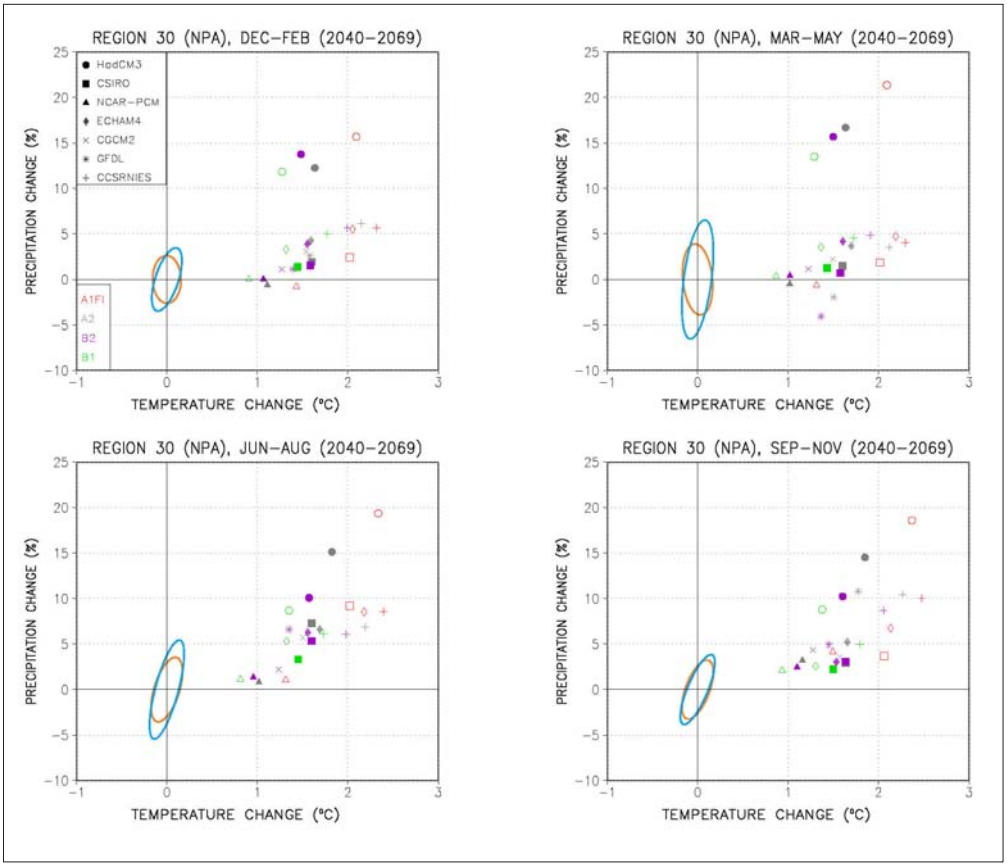

Region 30: Northern Pacific (2070–2099)

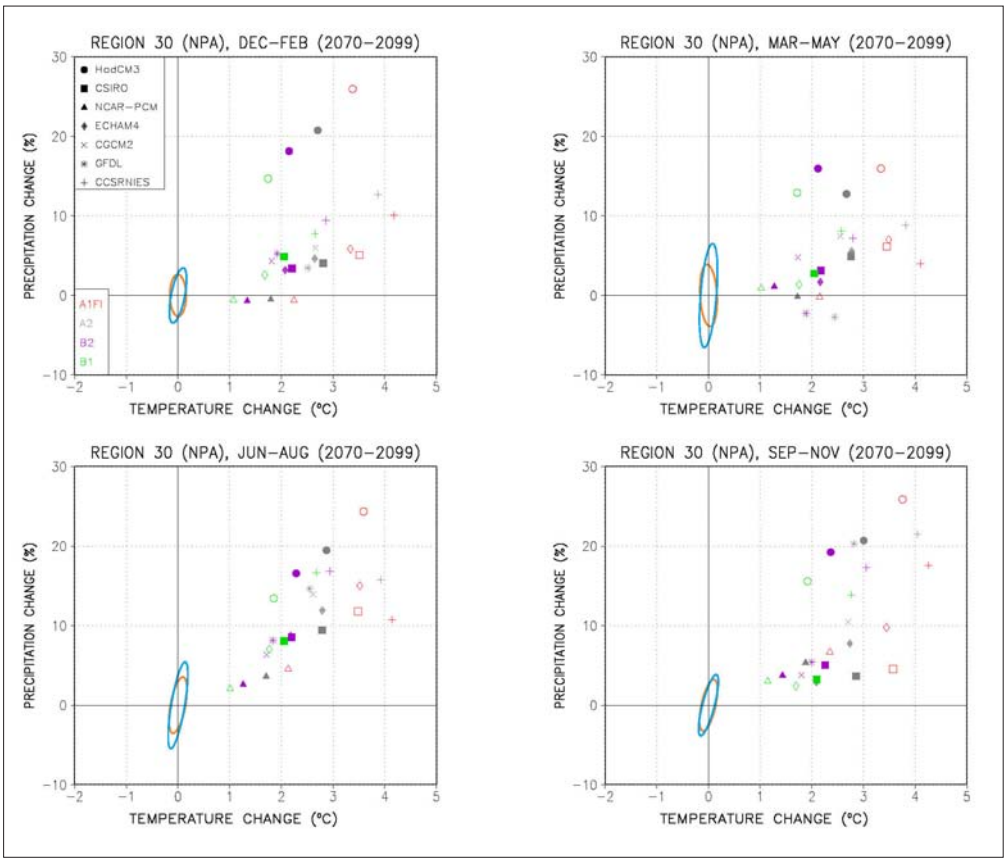

Region 31: Indian Ocean (2010–2039)

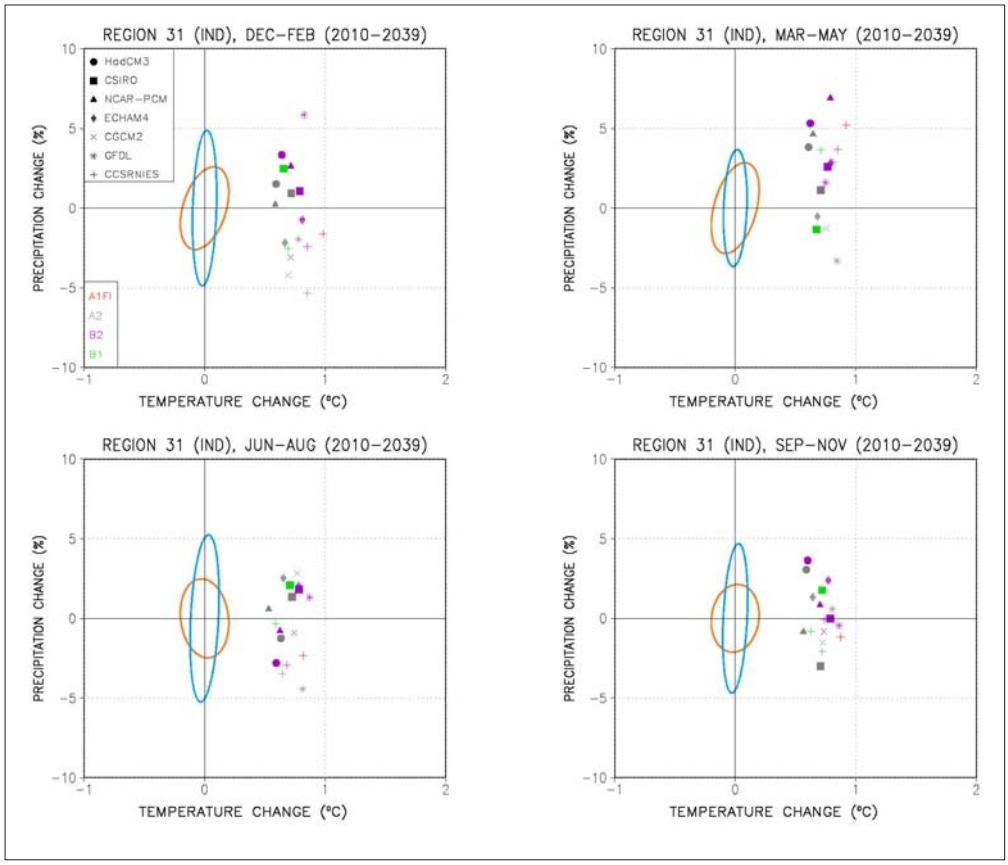

Region 31: Indian Ocean (2040–2069)

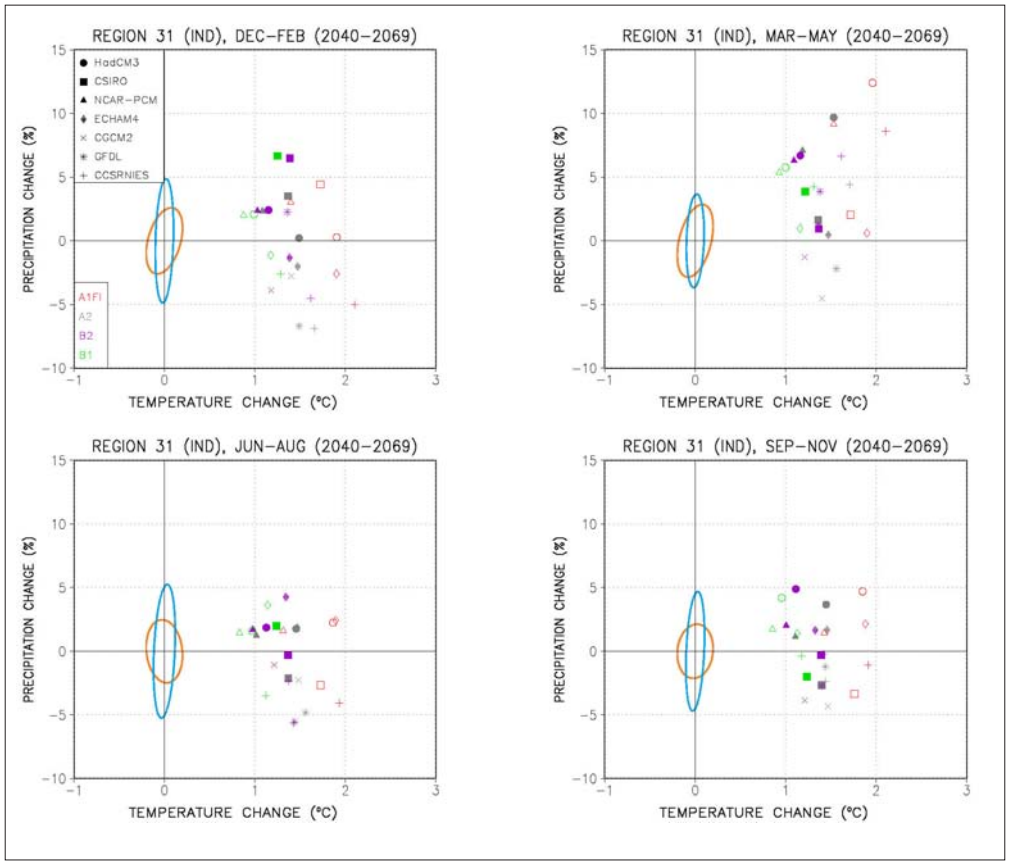

Region 31: Indian Ocean (2070–2099)

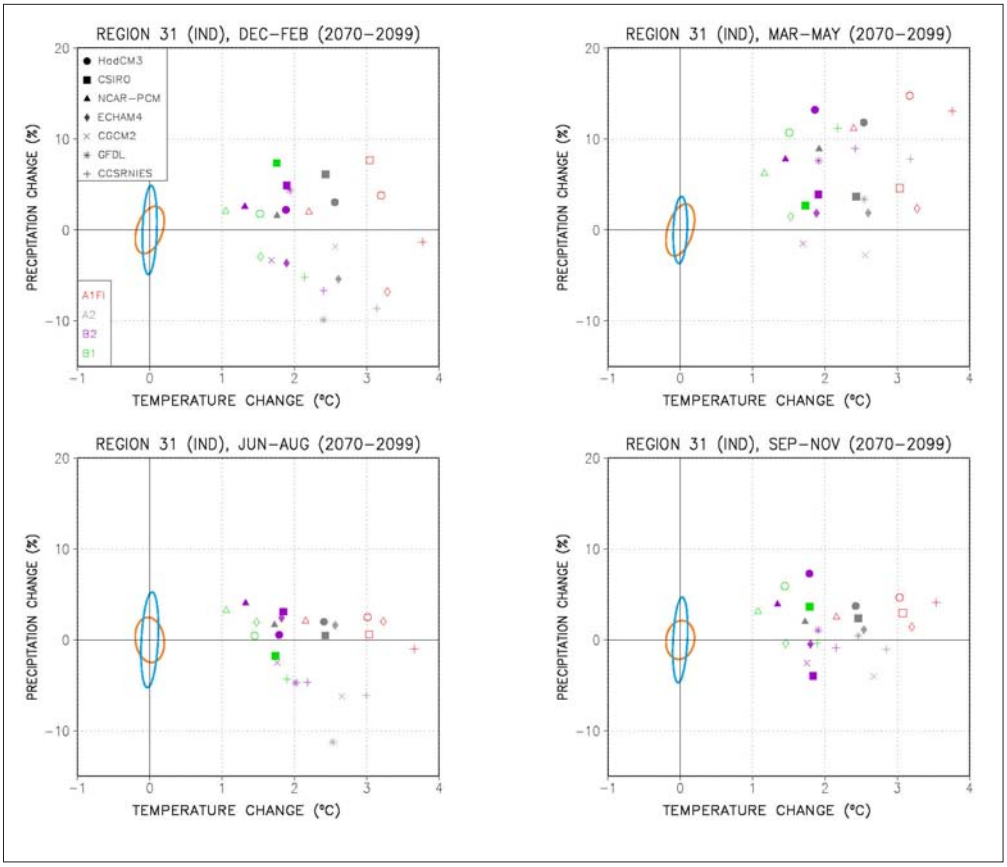

Region 32: Southern Pacific (2010–2039)

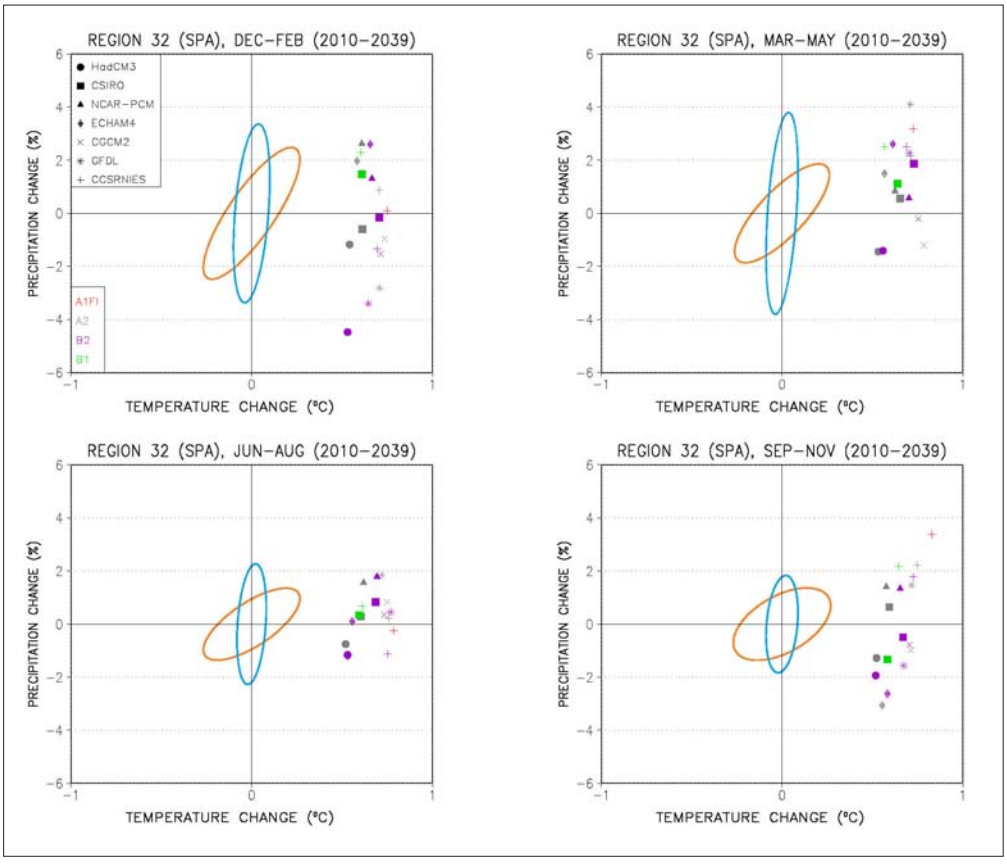

Region 32: Southern Pacific (2040–2069)

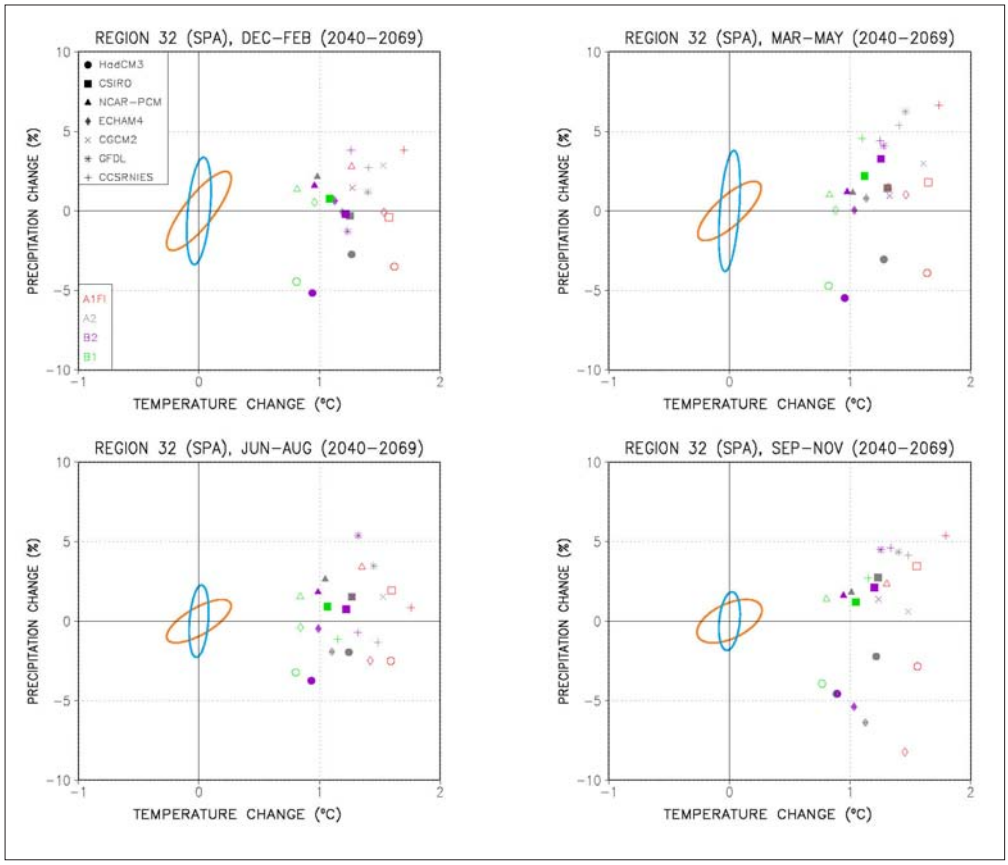

Region 32: Southern Pacific (2070–2099)

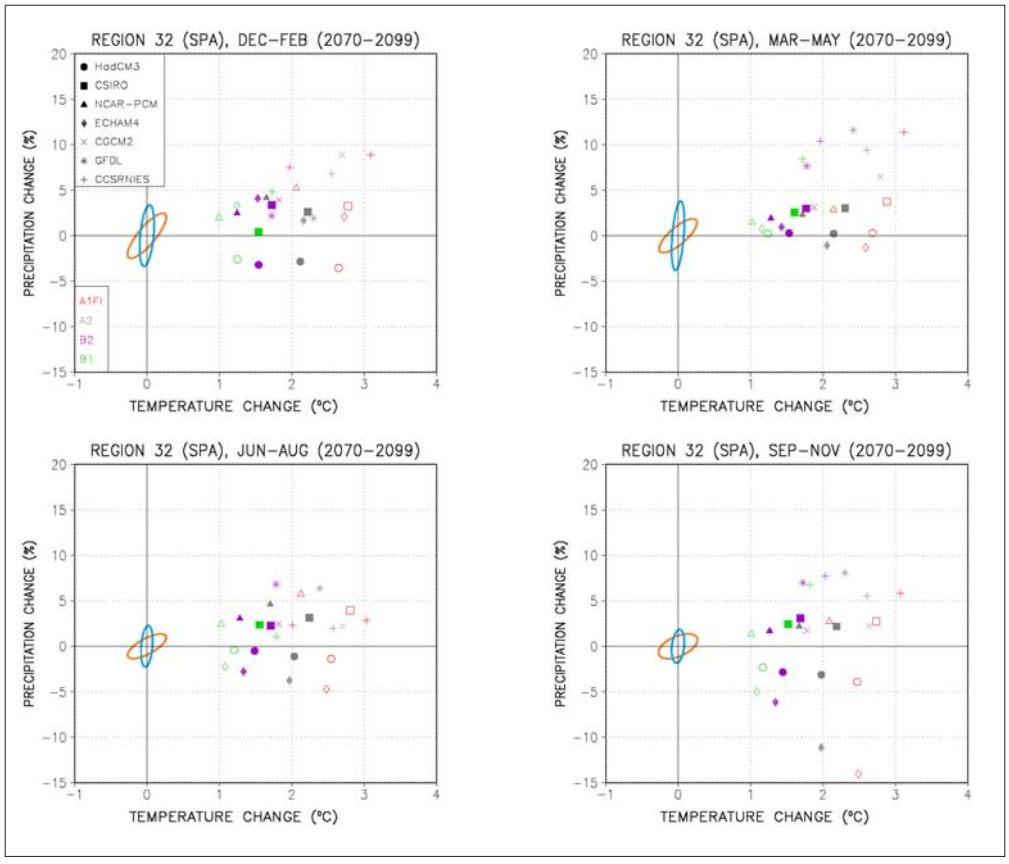

Documentation page

Publisher	Finnish Environment Institute Date: July 2003
Author(s)	Kimmo Ruosteenoja, Timothy R. Carter, Kirsti Jylhä and Heikki Tuomenvirta
Title of publication	Future climate in world regions: an intercomparison of model-based projections for the new IPCC emissions scenarios
Abstract	Projections of changes in seasonal surface air temperature and precipitation for three 30-year periods during the 21st century in 32 sub-continental scale regions are presented. This information may offer useful guidance on the selection of climate scenarios for regional impact studies. The climate changes have been simulated by seven coupled atmosphere-ocean general circulation models (AOGCMs), the greenhouse gas and aerosol forcing being inferred from the SRES emission scenarios A1FI, A2, B1 and B2. For a majority of the AOGCMs, simulations have only been conducted for scenarios A2 and B2. Projections for other scenarios were then extrapolated from the available runs applying a pattern-scaling technique. In tests, this method proved to be fairly accurate, the correlation between the AOGCM-simulated and the corresponding pattern-scaled response to the A2 scenario for the end of the 21th century being generally ~ 0.97 – 0.99 for temperature and ~ 0.9 or higher for precipitation. Projected changes of temperature and precipitation are presented in the form of 384 scatter diagrams. The model-simulated temperature changes were almost invariably statistically significant, i.e., they fell clearly outside the natural multi-decadal variability derived from 1000-year unforced coupled AOGCM simulations. For precipitation, fewer modelled changes were statistically significant, especially in the earliest projection period 2010–2039. Differences in the projections given by various models were substantial, of the same order of magnitude by the end of the century as differences among the responses to separate forcing scenarios. Nevertheless, the surface air temperature increased in all regions and seasons. For precipitation, changes with both sign occurred, but an increase of regional precipitation was more common than a decrease. All models simulate higher precipitation at high latitudes and enhanced summer monsoon precipitation for Southern and Eastern Asia. There was agreement between models that precipitation declines in Australia, Southern Africa and the Mediterranean region in certain seasons. The results presented on the scatter diagrams are also available in numerical form from the IPCC Data Distribution Centre.
Keywords	climate change, regional scenarios, impacts, SRES emissions scenarios, climate models, uncertainty, greenhouse gases, aerosols, pattern-scaling technique
Publication series and number	The Finnish Environment 644
Theme of publication	International Cooperation
Project name and number, if any	Climate scenario development, No. ZA01017
Financier/ commissioner	Ministry for Foreign Affairs of Finland, Government of Canada, Intergovernmental Panel on Climate Change Trust Fund
Project organization	Finnish Environment Institute, Finnish Meteorological Institute

ISSN	ISBN
1238-7312	952-11-1463-0 (nid.) 952-11-1464-9 (PDF)
No. of pages: 83	Language: English
Restrictions: public	Price: 25 euro

For sale at/ distributor	Edita Ltd, tel. +358 9 566 0266, Oy Edita Ab, Asiakaspalvelu, Pl 800, 00043 Edita e-mail: asiakaspalvelu@edita.fi www-server: http://www.edita.fi/netmarket
Financier of publication	Finnish Environment Institute, Ministry for Foreign Affairs of Finland, Government of Canada, Intergovernmental Panel on Climate Change Trust Fund
Printing place and year	Tummavuoren Kirjapaino, Vantaa 2003

Kuvailulehti

Julkaisija	Suomen ympäristökeskus	Julkaisuaika Heinäkuu 2003
Tekijä(t)	Kimmo Ruosteenoja, Timothy R. Carter, Kirsti Jylhä and Heikki Tuomenvirta	
Julkaisun nimi	Future climate in world regions: an intercomparison of model-based projections for the new IPCC emissions scenarios Ilmastomallien antamien alueellisten muutosennusteiden vertailua käytettäessä IPCC:n uusia päästöskenaarioita	
Tiivistelmä	Raportissa esitetään arvioita voimistuvan kasvihuoneilmiön vaikutuksista lämpötiloihin ja sademääriin eri vuodenaikoina maapallon 32 alueella. Arviot annetaan kolmelle peräkkäiselle 30-vuotiselle jaksolle alkaneella vuosisadalla, ja niitä voidaan hyödyntää tutkittaessa ilmastonmuutoksien alueellisia vaikutuksia. Esitetyt skenaariot pohjautuvat seitsemällä kytketyllä valtameri-ilmakehämallilla tehtyihin ilmastonmuutoskokeisiin, joissa kasvihuonekaasujen ja leijuvien hiukkasten tulevat pitoisuudet perustuvat SRES-päästöskenaarioihin A1F1, A2, B1 ja B2. Useimmista malleista käytettävissä olivat kuitenkin vain A2- ja B2-skenaarioita vastaavat ajot. Muitten skenaarioitten mukaiset muutokset laskettiin tällöin käyttämällä ns. vakiokaaviomenetelmää, jossa tietyn mallin antama ilmastonmuutoksen alueellisen jakauman muoto oletetaan samaksi päästöskenaariosta riippumatta. Menetelmä osoittautui varsin tarkaksi; simuloitaessa vuosisadan viimeisten vuosikymmenien ilmastoa suoraan mallista saadun ja vakiokaaviotekniikalla lasketun lämpötilan alueellisen muutoksen välinen korrelaatio oli suuruusluokkaa 0.99. Myös sademäärän muutoksille vastaava korrelaatio oli vähintään noin 0.9. Mallien antamat ilmastonmuutosarviot esitetään yhteensä 384 pistediagrammikuvan avulla. Mallien ennustama lämpötilan nousu oli lähes poikkeuksetta tilastollisesti merkitsevää, eli se ylitti selvästi pitkän malliajon kuvaaman ilmaston luonnollisen vaihtelun. Sademäärän muutokset sen sijaan eivät useinkaan olleet merkitseviä, eivät etenkään tutkittaessa jaksoa 2010-39. Eri mallien ennustamat lämpötilan ja sademäärän muutokset poikkesivat toisistaan huomattavasti. Lämpötila nousi kaikilla tutkituilla alueilla, mutta sademäärissä esiintyi sekä nousua että laskua, joskin nousua enemmän. Korkeilla leveysasteilla sademäärät lisääntyvät kaikissa mallikokeissa, ja myös Aasian kesämonsuuniin liittyvät sateet voimistuvat. Toisaalta mallit olivat yksimielisiä siitä, että sateet vähenevät ainakin joinakin vuodenaikoina Australiassa, Afrikan eteläosissa ja Välimeren ympäristössä. Pistediagrammikuvissa esitetyt tiedot ovat saatavissa myös numeromuodossa IPCC:n tietopankista (IPCC Data Distribution Centre).	
Asiasanat	ilmastonmuutos, alueelliset skenaariot, vaikutukset, SRES päästöskenaariot, ilmastomallit, epävarmuus, kasvihuonekaasut, aerosolit, vakiokaaviomenetelmä	
Julkaisusarjan nimi ja numero	Suomen ympäristö 644	
Julkaisun teema	Kansainvälinen yhteistyö	
Projektihankkeen nimi ja projektinumero	Climate scenario development, No. ZA01017	
Rahoittaja/ toimeksiantaja	Ulkoministeriö, Kanadan valtio, Hallitusten välisen ilmastopaneelin (IPCC) säätiö	
Projektiryhmään kuuluvat organisaatiot	Suomen ympäristökeskus, Ilmatieteen laitos	
	ISSN 1238-7312	ISBN 952-11-1463-0 (nid.) 952-11-1464-9 (PDF)
	Sivuja 83	Kieli englanti
	Luottamuksellisuus julkinen	Hinta 25 euroa
Julkaisun myynti/ jakaja	Oy Edita Ab, Asiakaspalvelu, Pl 800, 00043 Edita puh. (09) 566 0266, telefax (09) 566 0380, sähköpostiosoite: asiakaspalvelu@edita.fi www-palvelin: http://www.edita.fi/netmarket	
Julkaisun kustantaja	Suomen ympäristökeskus, Ulkoministeriö, Kanadan valtio, Hallitusten välisen ilmastopaneelin (IPCC) säätiö	
Painopaikka ja -aika	Tummavuoren Kirjapaino, Vantaa 2003	

Presentationsblad

Utgivare	Finlands miljöcentral Datum: Juli 2003
Författare	Kimmo Ruosteenoja, Timothy R. Carter, Kirsti Jylhä och Heikki Tuomenvirta
Publikationens titel	Future climate in world regions: an intercomparison of model-based projections for the new IPCC emissions scenarios Jämförelse av regionala klimatprojektioner beräknade med nya IPCC-scenarier
Sammandrag	Projektioner av förändringar i temperatur och nederbörd under olika årstider presenteras i tre perioder om 30 år för 32 områden på olika kontinenter. Denhär informationen kan vara till nytta när man väljer klimatscenarier för regionala effektstudier. Klimatförändringarna har simulerats med sju flödeskopplade atmosfär-ocean-modeller (AOGCM-modeller). Antaganden om växthusgaser och aerosoler i atmosfären har härletts ur SRES-emissionsscenarierna A1F1, A2, B1 och B2. Simuleringarna gjordes enbart med A2- och B2-scenarierna för de flesta AOGCM-modellerna. Projektioner för de andra skenarierna extrapolerades sedan utgående från de resultat som fanns till hands. Här användes en mönsteravbildningsteknik (pattern-scaling), som innebär att man antar att mönstret i klimatförändringens regionala fördelning är den samma oberoende av utsläppsscenariet. Det visade sig att avbildningstekniken är mycket noggrann. I simuleringar med A2 scenariet för de sista decennierna under innevarande sekel var korrelationen mellan AOGCM-resultaten och den motsvarande avbildningen i allmänhet 0,97 – 0,99 för temperaturen och 0,9 eller högre för nederbörden. Rapporten innehåller projektioner för temperatur- och nederbördsförändringar i form av 384 punktdiagram. Den simulerade temperaturstegringen var definitivt utan undantag statistiskt signifikant, dvs den var större än variabiliteten i AOGCM-resultaten för en tusenårsperiod utan externa störningar. Förändringarna i nederbörden var däremot mera sällan signifikanta, speciellt inte i den första perioden 2010-2039. De olika modellerna gav sinsemellan avsevärt olika temperatur- och nederbördsprojektioner. Vid slutet av seklet var skillnaderna mellan modellernas resultat av samma storleksordning som skillnaderna mellan responserna på olika skenarier. Temperturen steg i varje fall under alla årstider i alla regioner. Nederbörden ökade i de flesta regioner, även om minskningar i nederbörden förekom i en del regioner. Alla modeller gav en ökning i nederbörden vid höga latituder och kraftigare sommarmonsunregn i Syd- och Östasien. Å andra sidan var modellerna eniga om att nederbörden kommer att minska åtminstone under någon årstid i Australien, södra Afrika och i Medelhavsområdet. Resultaten i punktdiagrammen kan erhållas även i numeriskt format från IPCC-databanken (IPCC Data Distribution Centre).
Nyckelord	klimatförändringar, regionala scenarier, effekter, SRES utsläppsscenarier, klimatmodeller, osäkerhet, växthusgaser, aerosoler, mönsteravbildningsteknik
Publikationsserie och nummer	Miljön i Finland 644
Publikationens tema	Internationellt samarbete
Projektets namn och nummer	Climate scenario development, No. ZA01017
Finansiär/ uppdragsgivare	Utrikesministeriet, Kanadas regering, Medel från IPCC Trust Fund
Organisationer i projektgruppen	Finlands miljöcentral, Meteorologiska institutet
ISSN: 1238-7312 ISBN: 952-11-1463-0 (nid.) 952-11-1464-9 (PDF) Sidantal: 83 Språk: engelska Offentlighet: offentlig Pris: 25 euro	
Beställningar/ distribution	Edita Ab, Kundservice, Pl 800, 00043 Edita puh. (09) 566 0266, telefax (09) 566 0380, e-mail: asiakaspalvelu@edita.fi www-server: http://www.edita.fi/netmarket
Förläggare	Finlands miljöcentral, Utrikesministeriet, Kanadas regering, Medel från IPCC Trust Fund
Tryckeri/ tryckningsort och -år	Tummavuoren Kirjapaino Ab, Vantaa 2003

INTERNATIONAL COOPERATION

Future climate in world regions: an intercomparison of model-based projections for the new IPCC emissions scenarios

In 2000, the Intergovernmental Panel on Climate Change (IPCC) released a new set of scenarios describing projected emissions of greenhouse gases and aerosols during the 21st century. Preliminary estimates of the implications of these scenarios for climate in 32 world regions were presented in a previous report in this series, extrapolated from climate model outputs assuming earlier emissions scenarios. This report presents an intercomparison of recent climate model projections for the same 32 regions based directly on the new IPCC emissions scenarios. Results are presented for mean seasonal temperature and precipitation changes between 1961-1990 and three time periods in the future centred on the 2020s, 2050s and 2080s. Uncertainties in the direction of change are portrayed, and the statistical significance of future changes evaluated. Such information may be of interest to readers wishing to gain an impression of recent projections of regional climate change. It may also be of assistance to researchers needing to select climate scenarios for use in impact and adaptation assessments.

The publication is also available on the internet
www.environment.fi/publications

ISBN 952-11-1463-0
ISBN 952-11-1464-9 (PDF)
ISSN 1238-7312

Edita Publishing Ltd
P.O.Box 800, FIN-00043 EDITA, Finland,
Phone + 358 20 450 00.
Mail orders:
phone + 358 20 450 05, fax + 358 20 450 2380.
EDITA-BOOKSHOP IN HELSINKI
Annankatu 44, phone 020 450 2566